BIOGEOCHEMISTRY OF BLUE CARBON IN COASTAL WETLANDS UNDER RISING SEAS: COMBINED LABORATORY AND FIELD EXPERIMENTS

by

Sean Fettrow

A dissertation submitted to the Faculty of the University of Delaware in partial fulfillment of the requirements for the degree of Doctor of Philosophy in Plant and Soil Sciences

Spring 2023

BIOGEOCHEMISTRY OF BLUE CARBON IN COASTAL WETLANDS UNDER RISING SEAS: COMBINED LABORATORY AND FIELD EXPERIMENTS

by

Sean Fettrow

Approved: _____

Erik H. Ervin, Ph.D.
Chair of the Department of Plant and Soil Sciences

Approved: _____

Calvin L. K. Keeler Jr., Ph.D
Interim Dean of the College of Agriculture and Natural Resources

Approved: _____

Louis F. Rossi, Ph.D.
Vice Provost for Graduate and Professional Education and
Dean of the Graduate College

I certify that I have read this dissertation and that in my opinion it meets the academic and professional standard required by the University as a dissertation for the degree of Doctor of Philosophy.

Signed: _____

Angelia L. Seyfferth, Ph.D
Professor in charge of dissertation

I certify that I have read this dissertation and that in my opinion it meets the academic and professional standard required by the University as a dissertation for the degree of Doctor of Philosophy.

Signed: _____

Rodrigo Vargas, Ph.D
Member of dissertation committee

I certify that I have read this dissertation and that in my opinion it meets the academic and professional standard required by the University as a dissertation for the degree of Doctor of Philosophy.

Signed: _____

Holly Michael, Ph.D
Member of dissertation committee

I certify that I have read this dissertation and that in my opinion it meets the academic and professional standard required by the University as a dissertation for the degree of Doctor of Philosophy.

Signed: _____

Andrew Wozniak, Ph.D
Member of dissertation committee

ACKNOWLEDGMENTS

This highly rewarding, challenging, and enriching PhD experience would not have been possible without my dedicated advisor, Angelia Seyfferth. She provided countless hours to my professional, intellectual, and academic growth, and I am forever grateful. I could never repay her for allowing me these life changing opportunities, but I will be sure to pass along the dedicated mentorship down the road. My committee members Rodrgio Vargas, Holly Michael and Andrew Wozniak also provided invaluable lessons and advice along the way, as well as their individual expertise which created an exciting and interdisciplinary research experience.

Thank you to my parents Ken and Sandy Fettrow who allowed me to play in the mud growing up, likely a reason why I still play in the mud, and for providing me the resources and support to pursue my true passion. Thank you to my grandmother Marie Fettrow, who sparked my curiosity in plants and soils at a young age by simply allowing me to help her landscape the backyard and our many conversations about plants and animals. Thank you to my wife Gabrielle Schusler for constant support and for proofreading my writing for the past 4 years. Thank you to my cats Bug and Bean for all the laughs.

The data collected for this dissertation was made possible by the Advanced Materials Characterization Lab (AMCL), the UD Soil Testing Lab, the National Synchrotron Light Source and the Seyfferth Lab. This work was also possible thanks to the DENIN Environmental Fellowship and the University of Delaware Unique

Strengths fellowship. This work was supported with funding from the National Science Foundation (Grant Nos. 1759879 and #2012484).

TABLE OF CONTENTS

LIST OF TABLES

LIST OF FIGURES

ABSTRACT

Blue carbon (C) stored in coastal wetland soils has recently been considered a natural climate change solution due to the high rate of soil C storage inherent in these ecosystems. However, coastal wetlands continue to be lost at a global rate of 1-2% each year and the specific lateral and vertical C fluxes in these ecosystems remain highly uncertain. In addition, sea level rise (SLR) adds another layer of complexity; SLR is expected to drastically alter soil chemistry and coastal ecosystem functions while also causing soil salinization and migration of marshes into upland forests and agricultural fields. To decrease uncertainty in salt marsh blue C dynamics under current and future climate scenarios, this dissertation investigated the spatial and temporal variability of lateral and vertical C flux, examined how SLR will alter these fluxes in tidal salt marshes, and further investigated how SLR induced marsh migration will alter the soil biogeochemistry of upland forests and farms. These studies comprised a variety of laboratory and field experiments to achieve several main objectives including to (1) determine the temporal and spatial variability of salt marsh soil C concentration and investigate soil biogeochemical mechanisms that explain this variability; (2) understand how SLR may alter C cycling and the lateral and vertical C fluxes; and (3) investigate how marsh migration will alter belowground biogeochemistry in forests and farms experiencing salinization due to SLR. Taken together, the results gathered throughout this dissertation improve our understanding

of blue C cycling. The results were obtained from four separate experiments, organized here into four main chapters.

The first experiment (Chapter 2) of this dissertation was designed to investigate the uncertainty surrounding salt marsh soil C concentration which causes wide ranges in soil storage rates (i.e., 18-1700 g C m^{-2} $year^{-1}$). While the range in storage values for these ecosystems is large, the reasons for such large uncertainty remain largely unknown, particularly at the marsh scale. We investigated soil C concentration across temporal and spatial scales to better understand variables controlling soil C concentration across the marsh platform. We hypothesized that soil C would change spatially between different vegetative zones across the marsh, as well as temporally between plant phenology phases. We further hypothesized that soil biogeochemical variables would explain some of the variance in soil C concentration. We found significant ($p<0.05$) spatial and temporal differences in soil C concentration and found increasing soil C with increasing soil sulfur and sulfide. These results indicate the importance of considering several site level factors that cause uncertainty in blue C estimates.

The second experiment (Chapter 3 of this dissertation) was designed to investigate the uncertainty in the salt marsh lateral C flux which is defined as the C being exported and imported via tidal channel surface water. The current estimated lateral flux in North America is 16±16 Tg C $year^{-1}$, indicating an uncertainty level of 100% of the estimated value. This again calls for additional research to determine the reasons causing such a large range in flux values. Rather than focusing on the lateral movement of C between tidal channels and adjacent estuaries like most studies have done, we took a different approach and examined the smaller scale horizonal exchange

of C between the marsh platform and the tidal creek. We hypothesized that Fe oxides stabilize dissolved organic carbon (DOC) during ebb tide when soils are oxic, but release DOC into the porewater during flood tide when the soils are sub to anoxic. We further hypothesized that the hydraulic gradient between the marsh platform groundwater and the tidal creek surface water drives changes in the concentration and source of C being exported or imported out of/ into the marsh. Our final hypothesis was that soil trace gases are physically pushed up and out of the creek bank soil with rising tides. We found evidence for a mechanism in which carbon-bearing Fe oxides reductively dissolve during flood tide and precipitate as soils oxidize during ebb tide, causing DOC mobility to change based on tidal cycle. We also found that the hydraulic gradient alters both the concentration and source of C in the tidal creek. Finally, we found that trace gas fluxes move horizontally out of the creek bank as the tide rises. The results indicate several physiochemical mechanisms at the tidal creek-marsh platform interface that may be causing uncertainty in the lateral C flux.

The third experiment (Chapter 4 of this dissertation) was designed to investigate how sea level rise (SLR) will alter the dynamics and fluxes discussed in the first two chapters. This was achieved by conducting a laboratory-controlled mesocosm experiment. We hypothesized that Fe oxides would increasingly dissolve under SLR conditions, causing DOC to be more mobile and be more readily fluxed laterally. We further hypothesized that mineral-associated DOC released under SLR conditions would be more easily accessed by soil microbes, thereby increasing respiration and the soil gas flux (vertical flux) from the soils. We found that Fe oxides increasingly dissolved under SLR conditions, releasing DOC into the porewater, and increasing the lateral C flux. We however did not see a significant increase in soil gas

flux under SLR conditions as we hypothesized. We observed the opposite; a decreased soil gas flux under SLR conditions, likely due to decreased oxygen levels under flooded conditions and decreased respiration rates. These results indicate that SLR may decrease the stability of mineral-associated C, thereby increasing the lateral flux, but decrease the soil respiration rate, thereby decreasing the vertical flux of soil greenhouse gases.

The fourth study (Chapter 5 of this dissertation) investigated how the soil biogeochemistry changes along transects from coastal marshes to upland farms or forests in the Delmarva peninsula, which is at the forefront of SLR. We hypothesized that carbon concentrations would increase while soil redox potential would decrease following the salinity gradient from upland sites to the marshes. There was more soil C found in the marsh than all upland sites, supporting our hypothesis. In addition, we observed a biogeochemical redox gradient that followed changes in salinity from upland to lowland, where sulfate was being reduced in the marsh, Fe was being reduced in the transitional areas, and oxygen was likely being reduced in the upland areas. These results highlight biogeochemical gradients over short distances from marshes to upland endmembers, some of which are already experiencing salinization and more reducing conditions with SLR, with consequent impacts on ecosystem function.

Taken together, our results help improve our understanding of coastal wetland blue C cycling under both current and future climate scenarios. These findings will be used to improve ecosystem vertical and lateral C flux estimates, better understand the underlying mechanisms controlling variability in C flux and C cycling and improve our understanding of how these ecosystems will function under increased inundation

with SLR. These results can be further incorporated into Earth System Models (ESMs) to increase the predictive capacity of C feedback cycles and may also be used to improve policy aimed at protecting and restoring these critical natural ecosystems.

Chapter 1

INTRODUCTION

1.1 Background

Tidal salt marshes sequester soil carbon (C) at similar rates to tropical rain forests each year, despite occupying at least 50 times less land area (Duarte et al. 2013). This disproportionately large C reservoir is what makes tidal salt marshes one of the most valuable ecosystems on the planet (Duarte et al. 2008) and why the term "blue carbon" was created a decade ago (Nellemann et al. 2009). This term is meant to distinguish coastal soil C from its terrestrial counterpart, green carbon. Coining this term has helped spark recent global interest in studying C that is cycled in coastal ecosystems (Alongi 2018). Much if this research has led to a consensus in the blue carbon community that preserving, restoring, and even artificially creating these ecosystems is an effective climate change mitigation strategy on practical timescales (Crooks et al. 2011; Pendleton et al. 2012; Mcleod et al. 2016; Duarte 2017). Climate change mitigation has become the greatest societal challenge of the 21st century as a recent IPCC report shows with "very high confidence" that climate affects have already taken a toll on human health, with far greater impacts expected in the future (IPCC 2022).

Even though the importance of salt marshes as C sinks is well established, the planet has lost up to 50% of salt marsh area since the 1800s (Bridgham et al. 2006; Crooks et al. 2011) and still today, 1-2% are lost each year (Duarte et al. 2008). This yearly loss of marsh area is not only associated with the diminished C storage, but also

with the emission of large quantities of potent greenhouses locked away in the soils (Seyfferth et al. 2020), further exacerbating climate change (Pendleton et al. 2012). To protect these ecosystems from further degradation and restore these high-capacity C sinks, better policy is required. Tidal wetlands could be incorporated into climate mitigation policy programs just as tropical forests are under "Reducing emissions from deforestation and forest degradation" (REDD+), but C budget estimates (specifically lateral and vertical C flux) in tidal wetlands remains highly uncertain (Cavallaro et al. 2018), leading to a major roadblock for better policy (Macreadie et al. 2019). Further research on salt marsh C dynamics is required to inform better policy that may ultimately help preserve and restore these valuable ecosystems.

In addition, sea level rise (SLR) is likely to add another layer of uncertainty. The rate of local SLR and sedimentation may determine whether a given salt marsh drowns or keeps pace with rising seas (Morris et al. 2002), while salt marsh area may expand upland if given enough accommodation space (Schuerch et al. 2018) through forests and abandoned agricultural fields. While some research has been done on predicting how coastal wetland C cycles may change with SLR (Mudd et al. 2009; Elsey-Quirk et al. 2011; Li et al. 2020; Guimond et al. 2020), the stability of existing salt marsh soil C stocks estimated at 6.5 Pg C (Duarte et al. 2013) is unknown. The affects SLR may have on this large soil C stock and how SLR will alter upland soil biogeochemistry must be investigated because major alterations to local and global C budgets and fluxes are expected to occur.

1.2 Soil Blue Carbon

The current global soil C stock is estimated at approximately 2500 Pg C (FAO & ITPS 2015). Blue carbon accounts for up to 25% of the total soil C pool (Roulet

2000; Mitra et al. 2005) while salt marshes account for up to 65% of the blue carbon pool (Duarte et al. 2013). In addition, salt marshes on average store 16% of their gross primary productivity compared to 1.5% from upland forests and 0.4% from the ocean (Duarte, 2017). Though salt marshes can store soil C better than most ecosystems, high uncertainty remains within ecosystem scale soil C sequestration rates. The current range in salt marshes is between 18-1713 g C m^{-2} $year^{-1}$ with an average closer to 210 g C m^{-2} $year^{-1}$ (Mcleod et al. 2016; Alongi 2018). In comparison, tropical forest soil C sequestration ranges between 1-8 g C m^{-2} $year^{-1}$ with an average of 4 g C m^{-2} $year^{-1}$. Tropical forests are among the most productive ecosystems on earth, yet salt marshes can store soil C up to 1000 times faster. This reflects the unique environmental characteristics that allow for rapid soil C sequestration in tidal salt marshes compared to upland ecosystems.

High primary productivity coupled with slow decomposition rates from sediment anoxia and high sedimentation rates from tidal creeks (Arias-Ortiz et al. 2018) make these ecosystems ideal for soil C sequestration. Additionally, the high sedimentation rates of coastal wetlands allow them to have the capacity for continuous soil C storage whereas upland systems eventually reach a plateau and begin to subside (Schlesinger and Lichter 2001). Sedimentation rates outpace terrestrial systems by up to 50-fold due to fluvial inputs (Mcleod et al. 2016). This enables rapid C burial and a sustained system for continuous soil C storage. While these environmental characteristics are common at most salt marshes, high uncertainty still exists in soil C storage rates, highlighting the fact that site level variables likely cause some level of uncertainty.

1.3 Lateral Blue Carbon Flux

The lateral C flux encompasses the import and export of dissolved organic and inorganic carbon (DOC/ DIC) and particulate OC (POC) via tidal channels. Most blue carbon studies focus on the vertical C flux, with far fewer studies focusing on the lateral C budget (Santos et al., 2021). This has likely led to an underestimation of the net carbon flux within coastal wetlands, particularly because some studies suggest that the lateral C flux may exceed the vertical flux (Bogard et al., 2020; Czapla et al., 2020; Wang et al., 2016). The long-term fate of this laterally transported salt marsh C is unknown, but there are several pathways. One pathway is biotic or abiotic breakdown and return to the atmosphere as CO_2 or CH_4. Another pathway is export to the bay or ocean, where long-term fates are unknown. A fraction of lateral C may be deposited and preserved outside the ecosystem of origin such as coastal shelf and deep-sea sediments (Duarte, 2017). While salt marshes occupy only 0.3% of the global ocean area, they contribute 6% and 4% of lateral DIC and DOC to the oceans, respectively (Bauer et al., 2013). While DOC may be quickly transformed and degraded in oligotrophic oceanic waters (Barrón & Duarte, 2015), some suggest oceanic DOC can have an average age of 4,000 to 6,000 years (Hansell et al., 2009). In addition, high concentrations of marsh derived DIC (Wang et al., 2016) exported to the oceans may persist over geologic timescales (Maher et al., 2018; Millero, 2007). Therefore, the lateral C flux in tidal salt marshes plays an important role in blue C storage and estimates.

Although it is becoming clearer that the lateral C flux is a major component of the net C flux in tidal wetlands, there remains high uncertainty. The North American tidal wetland lateral C flux uncertainty is 100% of the estimated value (Cavallaro et al., 2018). High uncertainty in the lateral C estimate stems from a variety of factors

including few long-term lateral flux studies (Chu et al., 2018; Santos et al., 2019; Wang et al., 2016; Wang & Cai, 2004), lack of incorporation of both DOC and DIC into estimates (Duarte, 2017; Santos et al., 2019), few studies on lateral GHG fluxes from tidal creeks (Trifunovic et al., 2020), and limited mechanistic understanding of lateral C flow between marsh soils and tidal creek. Most studies focus on large-scale surface water flux between the marsh, estuary, and ocean boundaries (Chu et al., 2018; Najjar et al., 2018; Osburn et al., 2015; Tzortziou et al., 2008; Wang & Cai, 2004; Winter et al., 1996), leaving out direct connections between C-rich porewater and the tidal channel. Therefore, having an improved mechanistic understanding of the small-scale chemical and physical controls on the horizontal flow of C between the tidal creek and marsh soils may help decrease uncertainty.

1.4 Sea Level Rise Impacts on Salt Marsh Carbon Cycling

Due to the proximity of tidal salt marshes to the coastline, these ecosystems are susceptible to sea-level rise (SLR). SLR is expected to drastically alter salt marsh ecosystem function, but there remains uncertainty around what effects may occur. Some evidence suggests marshes may be completely submerged if vertical accretion does not keep pace with SLR, decreasing soil C storage (Valiela et al., 2018). On the other hand, some evidence suggests that SLR increased the C storage potential and marshes kept pace with SLR (Gonneea et al., 2019). Other alternate scenarios under SLR conditions include marsh migration (Donnelly and Bertness, 2001; Schuerch et al., 2018; Elsey-Quirk et al., 2019) which is largely dependent on accommodation space (Schuerch et al., 2018). SLR is expected to drastically alter salt marsh C dynamics, but how is largely unresolved, highlighting the need for additional research.

In addition to changes in C cycling and alterations to the lateral and vertical C flux, SLR will alter upland biogeochemistry as marshes migrate. Coastal wetlands are migrating upland into forests (Raabe and Stumpf 2016; Langston et al. 2017, 2022) and agricultural land (Gedan and Fernández-Pascual 2019; Guimond and Michael 2021) due to a combination of fast processes associated with increased storm surge (Fagherazzi et al. 2019; Kearney et al. 2019) and slow processes associated with increased sea level rise (SLR) (Schieder et al. 2018) that are driving saltwater intrusion (Tully et al. 2019). How SLR will alter current marsh carbon stocks and change upland biogeochemical cycling of C remains unresolved and requires further research.

REFERENCES

Alongi DM (2018) Kelp Forests. In: Springer Briefs in Climate Studies. pp 53–57

Arias-Ortiz A, Masqué P, Garcia-Orellana J, et al (2018) Reviews and syntheses: ²¹⁰Pb-derived sediment and carbon accumulation rates in vegetated coastal ecosystems – setting the record straight. Biogeosciences 15:6791–6818. https://doi.org/10.5194/bg-15-6791-2018

Barrón C, Duarte CM (2015) Dissolved organic carbon pools and export from the coastal ocean. 1725–1738. https://doi.org/10.1002/2014GB005056.Received

Bauer JE, Cai WJ, Raymond PA, et al (2013) The changing carbon cycle of the coastal ocean. Nature

Bogard MJ, Bergamaschi BA, Butman DE, et al (2020) Hydrologic Export Is a Major Component of Coastal Wetland Carbon Budgets. Global Biogeochem Cycles 34:1–14. https://doi.org/10.1029/2019GB006430

Bridgham SD, Megonigal JP, Keller JK, et al (2006) The carbon balance of North American wetlands. Wetlands. https://doi.org/10.1672/0277-5212(2006)26[889:TCBONA]2.0.CO;2

Cavallaro N, Shrestha G, Birdsey R, et al (2018) Second State of the Carbon Cycle Report. Washington, DC

Chu SN, Wang ZA, Gonneea ME, et al (2018) Deciphering the dynamics of inorganic carbon export from intertidal salt marshes using high-frequency measurements. Mar Chem 206:7–18. https://doi.org/10.1016/j.marchem.2018.08.005

Crooks S, Herr D, Tamelander J, et al (2011) Mitigating Climate Change through Restoration and Management of Coastal Wetlands and Near-shore Marine Ecosystems: Challenges and Opportunities. Environment Department Papers 121:1–69

Czapla KM, Anderson IC, Currin CA (2020) Net Ecosystem Carbon Balance in a North Carolina, USA, Salt Marsh. J Geophys Res Biogeosci 125:1–16. https://doi.org/10.1029/2019JG005509

Donnelly JP, Bertness MD (2001) Rapid shoreward encroachment of salt marsh cordgrass in response to accelerated sea-level rise. Proc Natl Acad Sci U S A 98:14218–14223. https://doi.org/10.1073/pnas.251209298

Duarte CM (2017) Reviews and syntheses: Hidden forests, the role of vegetated coastal habitats in the ocean carbon budget. Biogeosciences 14:301–310. https://doi.org/10.5194/bg-14-301-2017

Duarte CM, Dennison WC, Orth RJW, Carruthers TJB (2008) The Charisma of Coastal Ecosystems: Addressing the Imbalance. Estuaries and Coasts 31:233–238. https://doi.org/10.1007/s12237-008-9038-7

Duarte CM, Losada IJ, Hendriks IE, et al (2013) The role of coastal plant communities for climate change mitigation and adaptation. Nat Clim Chang 3:961–968. https://doi.org/10.1038/nclimate1970

Elsey-Quirk T, Mariotti G, Valentine K, Raper K (2019) Retreating marsh shoreline creates hotspots of high-marsh plant diversity. Sci Rep 9:. https://doi.org/10.1038/s41598-019-42119-8

Elsey-Quirk T, Seliskar DM, Sommerfield CK, Gallagher JL (2011) Salt marsh carbon pool distribution in a mid-Atlantic Lagoon, USA: Sea level rise implications. Wetlands 31:87–99. https://doi.org/10.1007/s13157-010-0139-2

Fagherazzi S, Anisfeld SC, Blum LK, et al (2019) Sea level rise and the dynamics of the marsh-upland boundary. Front Environ Sci 7:1–18. https://doi.org/10.3389/fenvs.2019.00025

Fagherazzi S, Mariotti G, Leonardi N, et al (2020) Salt Marsh Dynamics in a Period of Accelerated Sea Level Rise. J Geophys Res Earth Surf. https://doi.org/10.1029/2019JF005200

Gedan KB, Fernández-Pascual E (2019) Salt marsh migration into salinized agricultural fields: A novel assembly of plant communities. Journal of Vegetation Science. https://doi.org/10.1111/jvs.12774

Gonneea ME, Maio C v., Kroeger KD, et al (2019) Salt marsh ecosystem restructuring enhances elevation resilience and carbon storage during accelerating relative sea-level rise. Estuar Coast Shelf Sci 217:56–68. https://doi.org/10.1016/j.ecss.2018.11.003

Guimond JA, Michael HA (2021) Effects of Marsh Migration on Flooding, Saltwater Intrusion, and Crop Yield in Coastal Agricultural Land Subject to Storm Surge Inundation. Water Resour Res 57:1–18. https://doi.org/10.1029/2020WR028326

Guimond JA, Yu X, Seyfferth AL, Michael HA (2020) Using Hydrological-Biogeochemical Linkages to Elucidate Carbon Dynamics in Coastal Marshes Subject to Relative Sea Level Rise. Water Resour Res 56:1–16. https://doi.org/10.1029/2019WR026302

IPCC (2014) Summary for policymakers. In: World in Transition 3. Routledge, pp 23–32

Jarraud M, Steiner A (2014) IPCC: Climate Change 2014

Kearney WS, Fernandes A, Fagherazzi S (2019) Sea-level rise and storm surges structure coastal forests into persistence and regeneration niches. PLoS One. https://doi.org/10.1371/journal.pone.0215977

Li YL, Guo HQ, Ge ZM, et al (2020) Sea-level rise will reduce net CO2 uptake in subtropical coastal marshes. Science of the Total Environment 747:141214. https://doi.org/10.1016/j.scitotenv.2020.141214

Macreadie PI, Anton A, Raven JA, et al (2019) The future of Blue Carbon science. Nat Commun 10:3998. https://doi.org/10.1038/s41467-019-11693-w

Maher DT, Call M, Santos IR, Sanders CJ (2018) Beyond burial: lateral exchange is a significant atmospheric carbon sink in mangrove forests. Biol Lett 14:20180200. https://doi.org/10.1098/rsbl.2018.0200

Mcleod E, Chmura GL, Bouillon S, et al (2016) A blueprint for blue carbon: toward an improved understanding of the role of vegetated coastal habitats in sequestering CO2. Front Ecol Environ 9:552–560. https://doi.org/https://www.jstor.org/stable/41479959

Mitra S, Wassmann R, Vlek PLG (2005) An appraisal of global wetland area and its organic carbon stock. Curr Sci 88:25–35

Morris JT, Sundareshwar P v, Nietch CT, et al (2002) Responses of Coastal Wetlands to Rising Sea Level Published by : Wiley Stable URL : http://www.jstor.org/stable/3072022 REFERENCES Linked references are available on JSTOR for this article : You may need to log in to JSTOR to access the linked references. Ecology 83:2869–2877

Mudd SM, Howell SM, Morris JT (2009) Impact of dynamic feedbacks between sedimentation, sea-level rise, and biomass production on near-surface marsh stratigraphy and carbon accumulation. Estuar Coast Shelf Sci 82:377–389. https://doi.org/10.1016/j.ecss.2009.01.028

Najjar RG, Herrmann M, Alexander R, et al (2018) Carbon Budget of Tidal Wetlands, Estuaries, and Shelf Waters of Eastern North America. Global Biogeochem Cycles 32:389–416. https://doi.org/10.1002/2017GB005790

Nellemann C, Corcoran E, Duarte CM, et al (2009) Blue Carbon - The Role of Healthy Oceans in Binding Carbon

Osburn CL, Mikan MP, Etheridge JR, et al (2015) Seasonal variation in the quality of dissolved and particulate organic matter exchanged between a salt marsh and its adjacent estuary. Journal of Geophysical Research G: Biogeosciences 120:1430–1449. https://doi.org/10.1002/2014JG002897

Pendleton L, Donato DC, Murray BC, et al (2012) Estimating Global "Blue Carbon" Emissions from Conversion and Degradation of Vegetated Coastal Ecosystems. PLoS One 7:e43542. https://doi.org/10.1371/journal.pone.0043542

Roulet NT (2000) Peatlands, carbon storage, greenhouse gases, and the kyoto protocol: Prospects and significance for Canada. Wetlands. https://doi.org/10.1672/0277-5212(2000)020[0605:PCSGGA]2.0.CO;2

Santos IR, Burdige DJ, Jennerjahn TC, et al (2021) The renaissance of Odum's outwelling hypothesis in "Blue Carbon" science. Estuar Coast Shelf Sci 255:107361. https://doi.org/10.1016/j.ecss.2021.107361

Santos IR, Maher DT, Larkin R, et al (2019) Carbon outwelling and outgassing vs. burial in an estuarine tidal creek surrounded by mangrove and saltmarsh wetlands. Limnol Oceanogr 64:996–1013

Schieder NW, Walters DC, Kirwan ML (2018) Massive Upland to Wetland Conversion Compensated for Historical Marsh Loss in Chesapeake Bay, USA. Estuaries and Coasts 41:940–951. https://doi.org/10.1007/s12237-017-0336-9

Schlesinger WH, Lichter J (2001) Limited carbon storage in soil and litter of experimental forest plots under increased atmospheric CO2. Nature. https://doi.org/10.1038/35078060

Schuerch M, Spencer T, Temmerman S, et al (2018a) Future response of global coastal wetlands to sea-level rise. Nature 561:231–234. https://doi.org/10.1038/s41586-018-0476-5

Schuerch M, Spencer T, Temmerman S, et al (2018b) Future response of global coastal wetlands to sea-level rise. Nature 561:231–234. https://doi.org/10.1038/s41586-018-0476-5

Seyfferth AL, Bothfeld F, Vargas R, et al (2020) Spatial and temporal heterogeneity of geochemical controls on carbon cycling in a tidal salt marsh. Geochim Cosmochim Acta 282:1–18. https://doi.org/10.1016/j.gca.2020.05.013

Trifunovic B, Vázquez-Lule A, Capooci M, et al (2020) Carbon Dioxide and Methane Emissions From A Temperate Salt Marsh Tidal Creek. J Geophys Res Biogeosci 125:. https://doi.org/10.1029/2019JG005558

Tully K, Gedan K, Epanchin-Niell R, et al (2019) The invisible flood: The chemistry, ecology, and social implications of coastal saltwater intrusion. Bioscience

Tzortziou M, Neale PJ, Osburn CL, et al (2008) Tidal marshes as a source of optically and chemically distinctive colored dissolved organic matter in the Chesapeake Bay. Limnol Oceanogr 53:148–159. https://doi.org/10.4319/lo.2008.53.1.0148

Valiela I, Lloret J, Bowyer T, et al (2018) Transient coastal landscapes: Rising sea level threatens salt marshes. Science of The Total Environment 640–641:1148–1156. https://doi.org/10.1016/j.scitotenv.2018.05.235

Wang ZA, Cai W (2004) Carbon Dioxide Degassing and Inorganic Carbon Export from a Marsh-Dominated Estuary(The Duplin River): A Marsh CO2 Pump. 49:341–354

Wang ZA, Kroeger KD, Ganju NK, et al (2016) Intertidal salt marshes as an important source of inorganic carbon to the coastal ocean. Limnol Oceanogr 61:1916–1931. https://doi.org/10.1002/lno.10347

Winter PED, Schlacher TA, Baird D (1996) Carbon flux between an estuary and the ocean: A case for outwelling. Hydrobiologia 337:123–132. https://doi.org/10.1007/BF00028513

Chapter 2

WHERE AND WHEN YOU SAMPLE MATTERS FOR SOIL C ESTIMATES IN TIDAL MARSH ECOSYSTEMS

Abstract

Tidal salt marshes are important contributors to soil carbon (C) stocks despite their relatively small land surface area. Although it is well understood that salt marshes have soil C burial rates orders of magnitude greater than those of terrestrial ecosystems, there is a wide range in storage rates among spatially distributed marshes. In addition, wide ranges in C storage rates also exist within a single marsh ecosystem. Tidal marshes often contain multiple grass species due to altered hydrology and soil biogeochemistry caused by microtopography and distance from tidal creeks, creating distinct subsites. Our overarching objective was to observe how soil C concentration changes across four plant phenology phases and across three subsites categorized by unique vegetation, hydrology, and biogeochemistry, while also investigating dominant biogeochemical controls on soil C concentration. We hypothesized that subsite biogeochemistry drives spatial heterogeneity in soil C concentration, and this causes variability in soil C concentration at the marsh scale. In addition, we hypothesized that soil C concentration and porewater biogeochemistry vary temporally across the four plant phenology phases (i.e., senescence, dormancy, green-up, maturity), causing further variation in marsh soil C that could lead to uncertainty. To test these hypotheses, we quantified soil C concentrations in 12 cm core sections of soil cores (0-48 cm depth) across time and space, alongside several porewater biogeochemical

variables including dissolved organic carbon (DOC), EEMs/ UV-VIS, redox potential, pH, salinity, reduced iron (Fe^{2+}), reduced sulfur (S^{2-}), and total porewater element (Fe, Ca) concentrations in three distinct subsites. Soil C concentration varied significantly ($p<0.05$) among the three subsites and was significantly greater during plant dormancy. Soil S, porewater sulfide, redox potential, and depth predicted 44% of the variability in soil C concentration. Our results show that soil C can vary spatially across a marsh ecosystem by as much as 63% and across plant phenology by as much as 26%. Therefore, it is critical to consider spatial and temporal heterogeneity in soil C concentration when conducting blue C assessments.

2.1 Introduction

Coastal blue carbon (C) cycled in tidal salt marshes is critically important for global soil C sequestration despite the small relative land area (Mcowen et al. 2017). High primary productivity coupled with high sedimentation rates and flooded anoxic soils and sediments allow salt marshes to rapidly accrete and preserve soil C (Arias-Ortiz et al. 2018). Soils in such ecosystems retain approximately 15% of their yearly primary productivity in soils compared to just 1% for tropical rainforests (Duarte 2017). Restoring, protecting, and artificially creating salt marshes can facilitate removal of CO_2 from the atmosphere and storage in soils on timescales conducive to climate change mitigation goals. These ecosystems should therefore be included in climate mitigation policy (Ewers Lewis et al. 2019; Serrano et al. 2019). However, a wide range of global salt marsh soil C sequestration rates of ~ 1 to >1100 g C m^{-2} $year^{-1}$ has been reported (Wang et al. 2021). The inclusion of salt marshes in improved climate mitigation policy is, in part, contingent upon improving our understanding of the environmental variables causing wide ranges in marsh soil C concentration and

thus soil sequestration rates (Saintilan et al. 2013; Macreadie et al. 2019). Understanding key controls on salt marsh soil C variability will also help decrease uncertainty in Earth System Models and inform new policy aimed at protecting these valuable ecosystems.

Soil C concentrations in salt marsh ecosystems vary spatially across the planet. Part of this variation is explained by regional environmental controls such as average annual air temperature (Chmura et al. 2003), geomorphic setting (van Ardenne et al. 2018), salinity gradients, inundation frequency (van de Broek et al. 2016; Baustian et al. 2017; Luo et al. 2019), rainfall patterns (Sanders et al. 2016; Negandhi et al. 2019), soil pH, soil moisture, and the dominant plant species and soils (Bai et al. 2016; Ford et al. 2019). Soil C accumulation rates also vary based on the age of the marsh and tend to be highest in newly expanding marsh edges (Miller et al. 2022). Other logistical factors contributing to salt marsh blue C estimate uncertainty include the type of corer used (Smeaton et al. 2020) and the depth of soil that is integrated into storage rates (Bai et al. 2016; Van De Broek et al. 2016; Mueller et al. 2019). While understanding global and regional controls on soil C is important for reducing uncertainty in C estimates, understanding site-level factors is also critical because ecosystem-level variability can be just as high as regional- to global-level variability (Ewers Lewis et al. 2018). Belowground biogeochemical heterogeneity is often noticeable in the aboveground vegetation due to striking zonation of marsh grass species across the marsh platform. This is often attributable to small spatial-scale changes in hydrologic patterns (Guimond et al. 2020b, a) based on proximity to the tidal channel that drives unique subsite biogeochemistry (Seyfferth et al. 2020) which also affects the type of vegetation that can survive within a certain tidal zone (Davy et

al. 2011). While tidal frame zonation alters vegetation and belowground biogeochemistry, it remains unclear if soil C concentrations are altered by these dynamics.

Primary production rates may partially control soil C concentration and may vary among vegetative zones. For example, the short form of *Spartina alterniflora* has a lower primary production rate than the tall form (Roman and Daiber 1984) and *Phragmites australis* has above and below ground production rates two times that of the shorter *Spartina patens* (Windham 2001). Belowground productivity includes root exudates (Luo et al. 2018) in the form of dissolved organic carbon (DOC), which could influence soil C concentration because belowground productivity often exceeds above ground productivity in these ecosystems (Frasco and Good 1982). Even though DOC exudates are considered to be labile (Yousefi Lalimi et al. 2018), they may contribute to soil C accumulation over time due to microbial transformation (Valle et al. 2018) and association with soil minerals such as Fe oxides (Chen et al. 2014; Chen and Sparks 2015; Sowers et al. 2018a, b, 2019), as well variability in the optical properties of chromophoric dissolved organic carbon (CDOM) that could affect degradability (Clark et al. 2014).

Subsites can also have unique biogeochemical signatures based on soil redox conditions and inundation extent and frequency. For example, high marsh areas and areas near tidal channels have soils are at least periodically oxic to sub-oxic and are dominated by iron (III) reduction, whereas low marsh areas have continuously inundated soils and are dominated by sulfate (SO_4^{2-}) reduction (Seyfferth et al. 2020). While these biogeochemical characteristics can directly influence vegetation (Moffett and Gorelick 2016) and thus indirectly influence soil C concentrations, they may also

directly affect soil C through the interactions of soil C with soil minerals. Fe oxides have an intimate role in the C cycle and C stabilization in soils experiencing dynamic redox fluctuation (Sodano et al. 2017), as previous work has shown that 99% of the dissolved Fe in the ocean is complexed with organic ligands (Whitby et al. 2020) and ~21% of all organic C in marine sediments has been found to be directly bound to reactive Fe species (Lalonde et al. 2012). Fe oxides may play an important role in C stabilization in soils experiencing dynamic redox fluctuation. Fe oxides can protect DOC against microbial degradation through physiochemical protection (Blair and Aller 2012; Chen and Sparks 2015; Sodano et al. 2017; Sowers et al. 2018a; Dorau et al. 2019; Wordofa et al. 2019), but these organo-mineral assemblages can be dissociated under reducing conditions (Riedel et al. 2013; Wordofa et al. 2019; Lacroix et al. 2022; Fettrow et al. 2023). Therefore, examining the spatial variability in soil biogeochemistry and relating those variables to soil C concentration may elucidate important mechanisms that cause the wide range in salt marsh soil C concentrations.

While it is critical to assess spatial heterogeneity in soil C concentration, it is also important to assess temporal variability. The temporal assessment of soil C in salt marshes often considers long-term trends of historic C burial rates (Cusack et al. 2018; McTigue et al. 2019; Breithaupt et al. 2020; Cuellar-Martinez et al. 2020), but variability of salt marsh soil C concentrations may also occur on shorter time scales such as across a single year. Several studies suggest salt marsh soil C does not significantly change across seasons throughout the year (Yu et al. 2014; Zhao et al. 2016), even though major changes in soil biogeochemical variables occur on this timescale (Koretsky et al. 2005; Negrin et al. 2011; Seyfferth et al. 2020; Trifunovic et

al. 2020; Zhu et al. 2021). While soil C concentration may be stable across seasons, it is unclear if soil C concentration changes based on site-specific plant phenology. The phenology of a marsh is associated with the greenness index of vegetation (Trifunovic et al. 2020) and is strongly associated with carbon dynamics in wetland systems (Desai 2010; Kang et al. 2016). Soil C concentration should be measured across plant phenology phases to determine if temporal changes in phenology alter soil C concentration and cause another source of uncertainty in ecosystem-scale C estimates.

To address these knowledge gaps, we conducted a year-long soil biogeochemical study of a temperate tidal salt marsh to assess how soil C concentration and porewater biogeochemistry change in space (subsite) and time (phenology). Our overarching research objectives were to understand how soil C concentration and soil biogeochemistry change across spatial and temporal scales, and to investigate key biogeochemical mechanisms influencing soil C concentration at the ecosystem level. We hypothesized that subsites would contain significantly different concentrations of soil C due to differences in soil biogeochemistry across the marsh platform. We further hypothesized that soil C concentration and associated biogeochemistry would significantly differ across plant phenology phases. Our results improve our understanding of mechanistic controls on salt marsh soil C with implications for reducing uncertainty in C sequestration estimates, while also adding to the body of literature that shows tidal salt marshes are critical reservoirs of sequestered C.

2.2 Methods and Materials

2.2.1 Field Site

This study was conducted at the St. Jones National Estuarine Research Reserve located in Dover, Delaware (Figure 2.1). The ecosystem is classified as a temperate mesohaline tidal salt marsh with a tidal creek salinity ranging between 5 to 18 ppt (Capooci et al. 2019). Three separate subsites were previously identified at this site, each with a different vegetation type and hydrology (Guimond et al. 2020a; Seyfferth et al. 2020). The subsite nearest the channel is primarily colonized by the tall form of *Spartina alterniflora* and has semidiurnal tidal oscillation. This subsite is hereafter referred to as Tall Spartina (TS). Farther from the tidal channel, the elevation is slightly higher due to a natural levee and flooding of the upper 25 cm of soil occurs only during spring tides; this location has the larger cordgrass *S. cynosuroides* and is hereafter referred to as Tall Cordgrass (TC). The third subsite is farthest from the tidal channel, lowest in elevation, and is primarily colonized by the short form of *S. alterniflora* due to near continuous inundation; this subsite is hereafter referred to as Short Spartina (SS). These subsites have distinct hydro-biogeochemistry and vegetation that varies across small spatial scales and thus provides an ideal setting to understand site-level uncertainty in soil C concentration and porewater biogeochemistry.

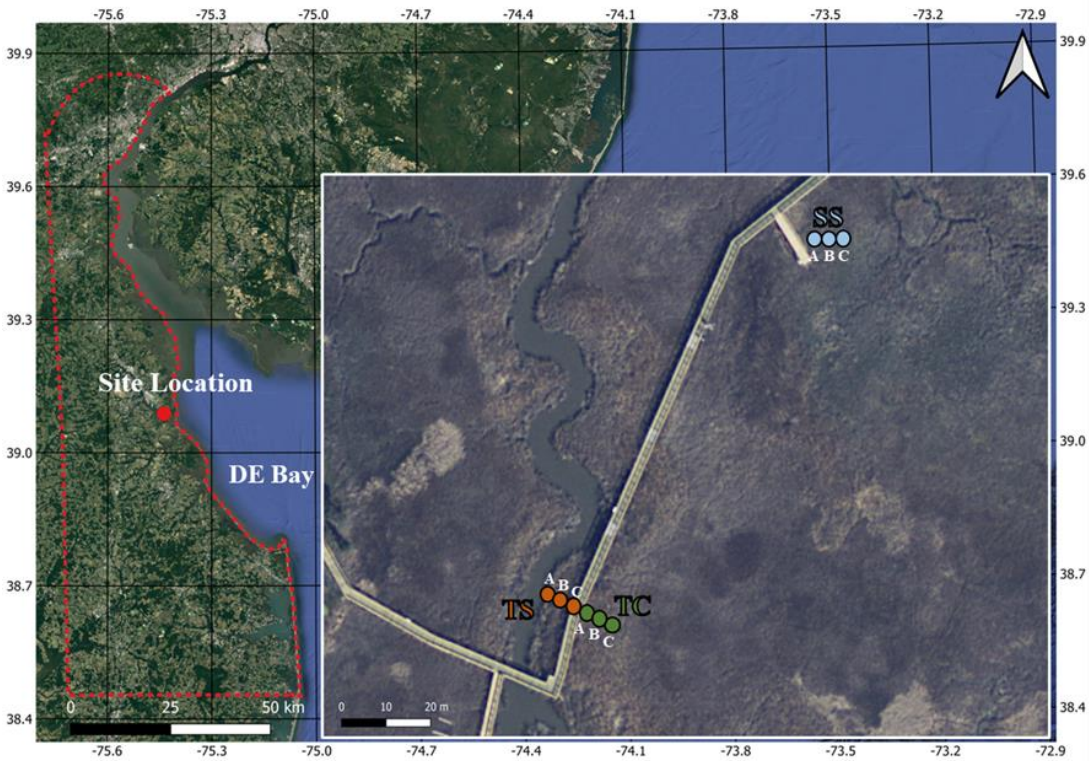

Figure 2.1 Map of the field site located at the St Jones Reserve in Dover, DE. Three unique subsites (TS, TC and SS) have been characterized based on previous studies at this field site showing subsite specific hydrology, vegetation and biogeochemistry based on distance from the tidal creek (Guimond et al. 2020a; Seyfferth et al. 2020). The coring locations were sampled in triplicate (Core A, B and C), with core A starting closest to the creek and each subsequent core in each subsite being ~30cm from one another.

2.2.2 Soil Sampling and Analysis

Soil cores were obtained from each of the three subsites (TS, TC, SS) in triplicate (n=3) during each sampling event. Replicates were taken approximately 30cm from one another and are labeled cores A, B, and C based on distance to the tidal channel with A being closest to the channel and C the farthest (Figure 2.1). Sampling events occurred at four separate times of the year to coincide with each of

the phenophases (i.e., senescence on 10/3/2019, dormancy on 12/3/2019, green-up on 4/29/2020, maturity on 8/13/2020), which were previously determined using the Greenness Index (Trifunovic et al. 2020). Soil cores (6 cm x 48 cm) were extracted using a gouge auger that has been shown to be an effective coring technique for reducing compaction in soft marsh soils (Smeaton et al. 2020). Soil cores were sectioned in the field into 12 cm increments (0-12cm, 12-24cm, 24-36cm and 36-48cm relative to the soil surface) and quickly preserved under anoxic conditions following previous methods (Seyfferth et al. 2020). For reference, the rooting zone of *Spartina* grasses is between 8-20cm (Muench and Elsey-Quirk 2019), so the upper two sections include C from root exudates. The 12cm increments were chosen because many soil C stock papers use increments between 10-15 cm and there tends to be little variation across the ~10 cm increment in a variety of wetland soils (Baustian et al. 2017). Briefly, the soil sections were placed into 250 ml HDPE bottles which were left uncapped in gas-impermeable bags that contained oxygen scrubbers (AneroPack-Anero, Mitsubishi), and the bags were vacuum-sealed in the field. The soil samples were placed on ice during transport back to the lab. Once back in the lab, the soil sections in the gas-impermeable bags were immediately placed inside an anoxic glove bag containing ~5% hydrogen and ~95% nitrogen. A subsample of soil was dried, ground, sieved (2mm), and powdered for analysis of total C and S (Vario EL Cube, Elementar). Soil C and S are reported as % C (= 100% * g C/g soil dry wt.) and % S (= 100% * g S/g soil dry wt.). The remaining field-moist soil was left inside the HDPE vial, capped inside the glove bag, and centrifuged for extraction of porewater using methods in the following section.

2.2.3 Porewater Extraction and Analysis

Porewater was extracted from each 12-cm soil section by centrifugation for 2 minutes at 2,500 rpm. A portion of the porewater was filtered with 0.45µm PTFE syringe filters while the rest was vacuum filtered using glass fiber filters (0.7µm). The 0.45µm PTFE filtered porewater was immediately analyzed for Fe^{2+} using the ferrozine colorimetric method (Stookey 1970), S^{2-} using the methylene blue method (Cline 1969), redox potential with a 220mV offset, pH, and conductivity using calibrated probes (Orion Ross Ultra pH/ATC Triode, Orion 9179E Triode, Orion DuraProbe Conductivity Cell), and the remaining sample was acidified to 2% HNO_3 for elemental analysis using an ICP-OES. The porewater filtered with glass fiber (0.7µm) was acidified with HCl and analyzed for DOC (Vario TOC Analayzer, Elementar). To characterize the DOC, unacidified DOC samples from the plant maturity sampling event were analyzed via ultraviolet-visible (UV-VIS)/ excitation-emission matrix spectroscopy (EEMs) (Aqualog Spectrophotometer, Horiba). The Aqualog was zeroed with double deionized water blanks, checked using the manufacturer's excitation check, corrected for inner filter effects, applied first and second order Rayleigh masking and data were normalized using the average Raman area (Gao et al. 2011; Clark et al. 2014). Measurements were taken over the wavelengths of 200-730nm with 2nm steps. Fluorescence and absorbance peaks and indices were calculated using previously established equations (Table S1).

2.2.4 Statistical Analysis

Statistical differences between subsites and phenology phases were analyzed using repeated measures analysis of variance (ANOVA) (α=0.05), with a post-hoc Tukey-HSD analysis to determine differences between individual subsites and

phenology phases. Correlations with depth were analyzed using linear regression and only the significant ($p<0.05$) relationships are reported. Relationships among all measured variables were assessed using principal components analysis. In addition, a stepwise regression model was built to determine variables that significantly predict soil C concentration. All statistical analyses were conducted in JMP (Version 16.2).

2.3 Results

2.3.1 Soil Carbon and Sulfur

To explore the spatiotemporal heterogeneity of soil carbon and sulfur at each subsite, subsamples of each collected soil increment were combusted for soil C and S concentration. Concentrations of soil C were highly variable between subsites, phenology, depth, and between replicate cores (Figure 2.2), indicating several possible sources of uncertainty in marsh soil C stock estimates. SS showed the highest soil C concentrations, as illustrated by darker colors in the heat map, compared to both TS and TC. Soil C was also higher at TS than TC, illustrated by relatively darker colors in the heat map. For all subsites, soil C concentrations changed throughout the year with the highest values during plant dormancy and the lowest during green-up. However, variability across individual replicates A, B, and C and with depth complicated generalities across time and space. For example, at subsite SS from 24-36 cm during senescence, core A is ~5% soil C while core C is ~10% soil C, a factor of 2 difference within replicates. Large ranges among replicates were also observed during green-up at TS from 12-24 cm and during maturity at TC from 36-48 cm. This exemplifies the heterogeneity inherent in soils, and a source of variation in marsh soil C estimates.

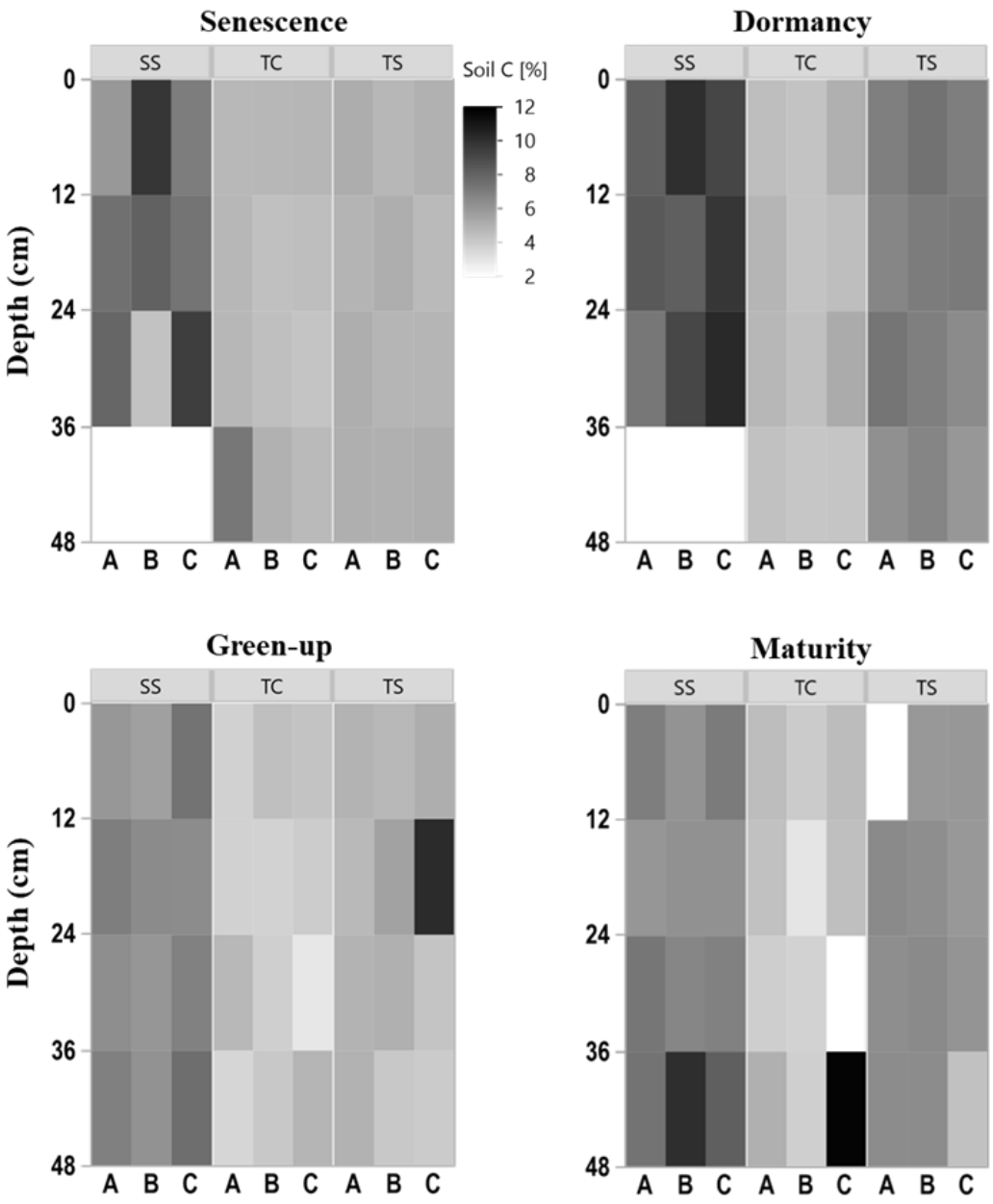

Figure 2.2 Heat maps of soil C concentration with depth at the three subsites (SS, TC, and TS), four phenology phases, and for each replicate core (A (closest to channel), B, and C (farthest from channel)). No measurement was able to be obtained for some 12-cm sections as shown by white rectangles.

There was also variability in soil C concentration with depth (Figure 2.3). Subsite SS had the highest mean soil C concentration at all four depths, as well as the largest range in values. TS had the second highest mean soil C values at all four depths as well as the second largest range in values. TC had the lowest mean soil C at all four depths as well as the smallest range in values at each depth. It is clear from this graph that SS contains higher overall concentrations of soil C, followed by TS and then TC. Soil C at TS during dormancy significantly decreased with depth (R^2=0.44, p=0.02) and soil C at SS during maturity significantly increased with depth (R^2=0.41, p=0.02). No other correlations between soil C existed with depth.

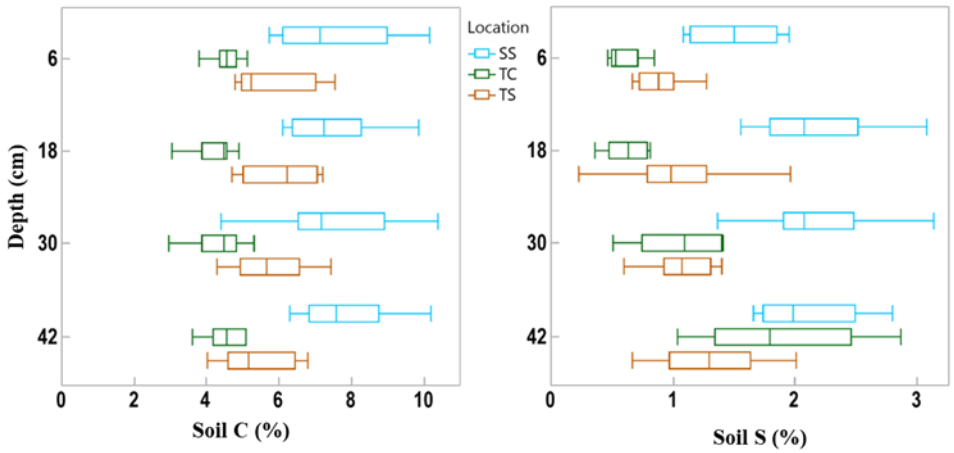

Figure 2.3 Box and whisker plot of soil C and S concentrations across the three subsites and separated by the four sampling depths. This indicates the difference in soil C and S variability between subsites and depth.

Soil S also varied across 12 cm sampling increment depths (Figure 3). SS had the highest mean soil S concentration at each depth, and the range of values initially

increased with depth. TS has a higher mean concentration than TC at all depths except at the bottom core section. The range of soil S values increased with depth at TC while the range was more consistent with depth at TS, except for the wide range of values measured at the 18cm depth interval. Soil S at SS during maturity significantly increased with depth (R^2=0.50, p=0.01), as did TC during dormancy (R^2=0.88, p<0.0001), green-up (R^2=0.51, p=0.01), and senescence (R^2=0.42, p=0.02). No other correlations between soil S existed with depth.

2.3.2 Porewater Data

2.3.2.1 Porewater DOC and Characterization

Porewater DOC was highly variable across subsites, phenology, depth, and replicate cores (Figure 2.4). Note that the data in Figure 4 have been log transformed (natural log) due to large ranges in values across the one-year sampling campaign. Unlike soil C, which was relatively consistent with depth, DOC concentrations were highly variable with depth and even more so between replicate cores. Some of the highest individual concentrations of DOC were detected nearest the surface and rooting zone, which can extend to 20 cm below the surface (Muench and Elsey-Quirk 2019), but also at depth at SS during senescence. DOC concentrations decreased with depth at SS during green-up (R^2=0.44, p=0.02) and maturity (R^2=0.37, p=0.03) and increased with depth at TC during dormancy (R^2=0.76, p=0.0002). These results indicate the highly variable nature of porewater DOC concentrations, possibly leading to additional uncertainty and complexity in marsh soil C estimates.

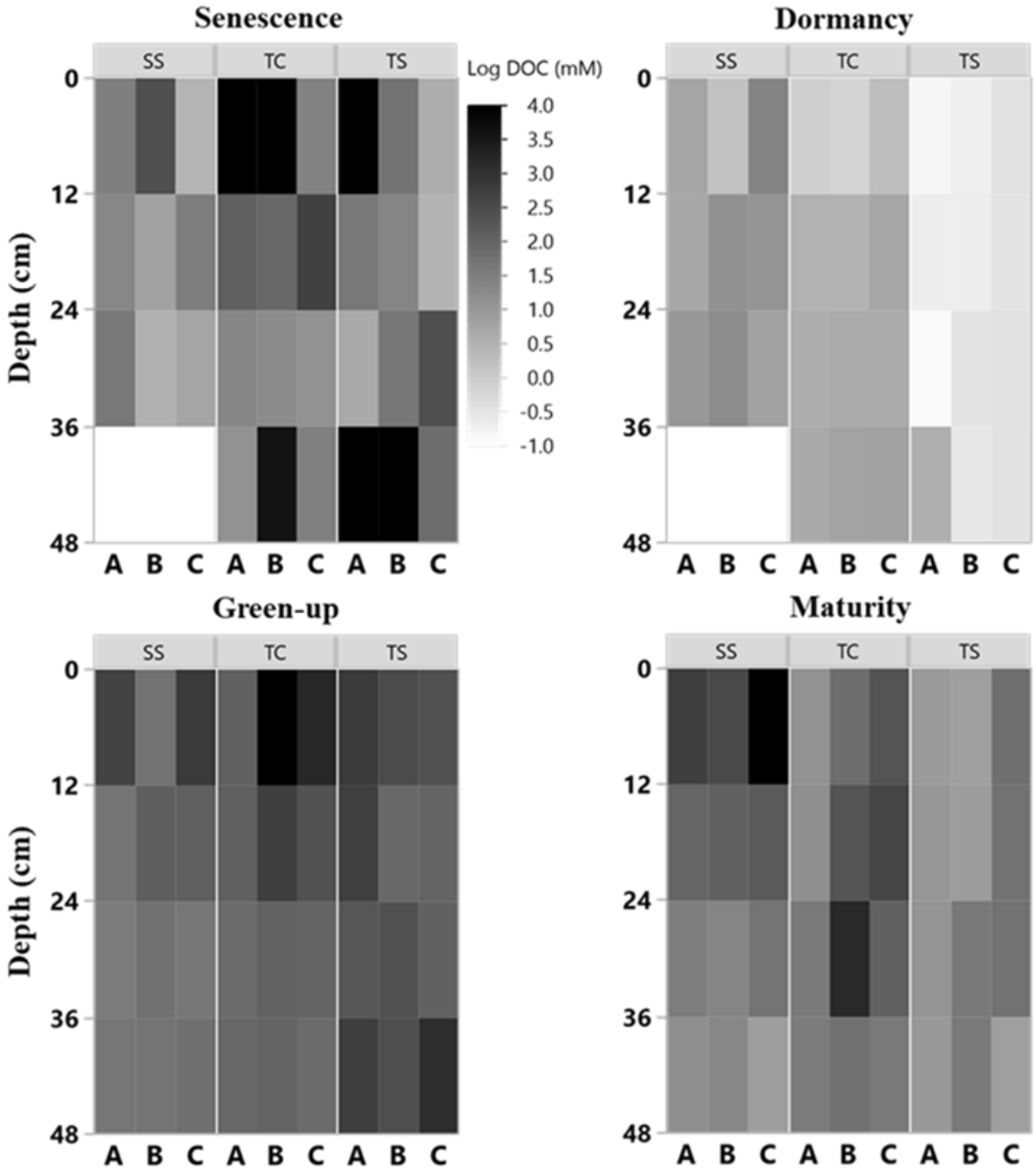

Figure 2.4 Heat maps of porewater DOC (natural log) concentration with depth at the three subsites (SS, TC, and TS), four phenology phases, and for each replicate core (A (closest to channel), B, and C (farthest from channel)). No measurement was able to be obtained for some 12-cm sections as shown by white rectangles.

Porewater ultraviolet-visible (UV-VIS) and excitation emission matrices (EEMs) data were collected only from the maturity sampling event to further characterize DOC molecular properties (Figure 2.5). Optical properties (i.e., peaks, indices) from spectroscopic data were calculated and interpreted following previous studies cited in the supplemental table (Table S1). These data show significant trends with depth at SS. At SS, coble peak intensities T (R^2=0.55, p=0.01), B (R^2=0.49, p=0.01), A (R^2=0.57, p=0.004), M (R^2=0.55, p=0.01) and C (R^2=0.49, p=0.01) all significantly decreased with depth, as did the fluorescence index (FI) (R^2=0.79, p=0.0001), the biological index (BIX) (R^2=0.50, p<0.01) and absorbance at 254nm (Abs_{254}) (R^2=0.36, p=0.04), indicating decreases in CDOM with depth. To ensure the coble peaks represented changes in CDOM properties and not DOC concentration, they were normalized to DOC concentration and the relationships remained significant (p<0.05), except for the Coble B peak (R^2=0.11, p=0.20). The E_2:E_3 (R^2=0.50, p=0.01) and $SUVA_{254}$ (R^2=0.53, p=0.007) significantly increased with depth at SS, indicating a decrease in molecular weight and an increase in aromaticity with depth. No significant trends with depth were present at TC or TS. Differences in DOC molecular properties between subsites are apparent for many of the calculated indices and peaks.

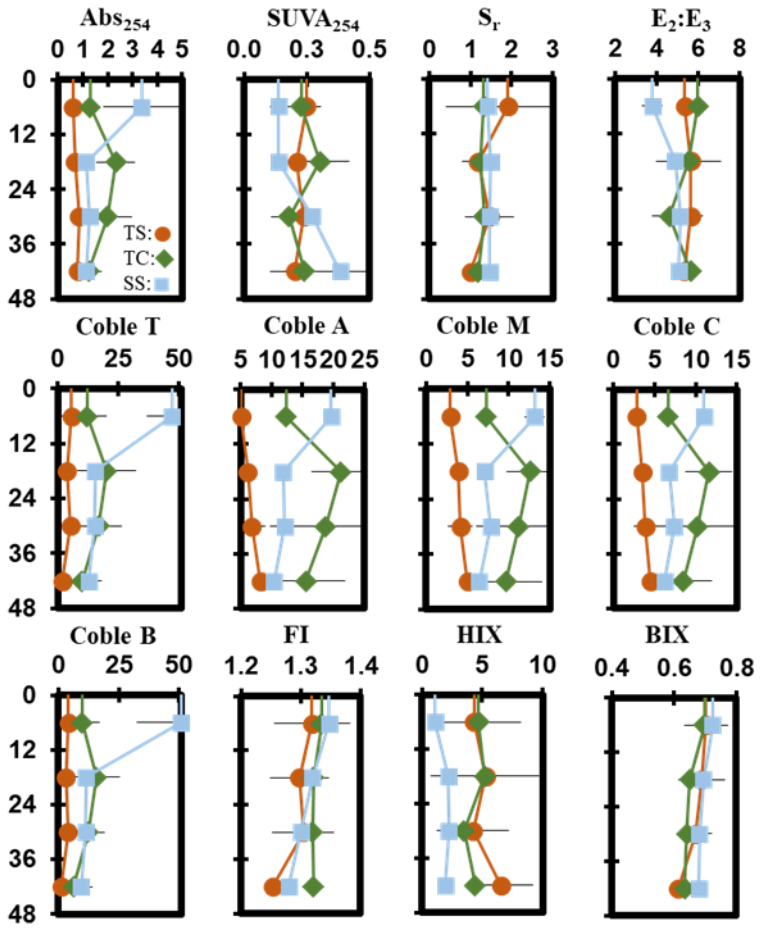

Figure 2.5 Depth profiles of porewater EEMs/ UV-VIS peaks and indices down to 48cm. Each point represents the mean between replicates (n=3) with error lines indicating the standard deviation (± 1 SD).

2.3.2.2 Porewater Chemistry

Measured porewater biogeochemistry was variable across subsites, phenology, and depth (Figure 2.6). Porewater redox potentials showed minimal trends with depth, except for a significant decrease with depth at SS during maturity (R^2=0.58, p=0.004). The pH was relatively consistent with depth, except for a significant increase with depth at TC during dormancy (R^2=0.42, p=0.02), and a significant decrease with depth

at TS during dormancy (R^2=0.56, p=0.005). Redox potential and pH formed a significant negative correlation (R^2=0.12, p<0.0001) across the entire 1-year dataset.

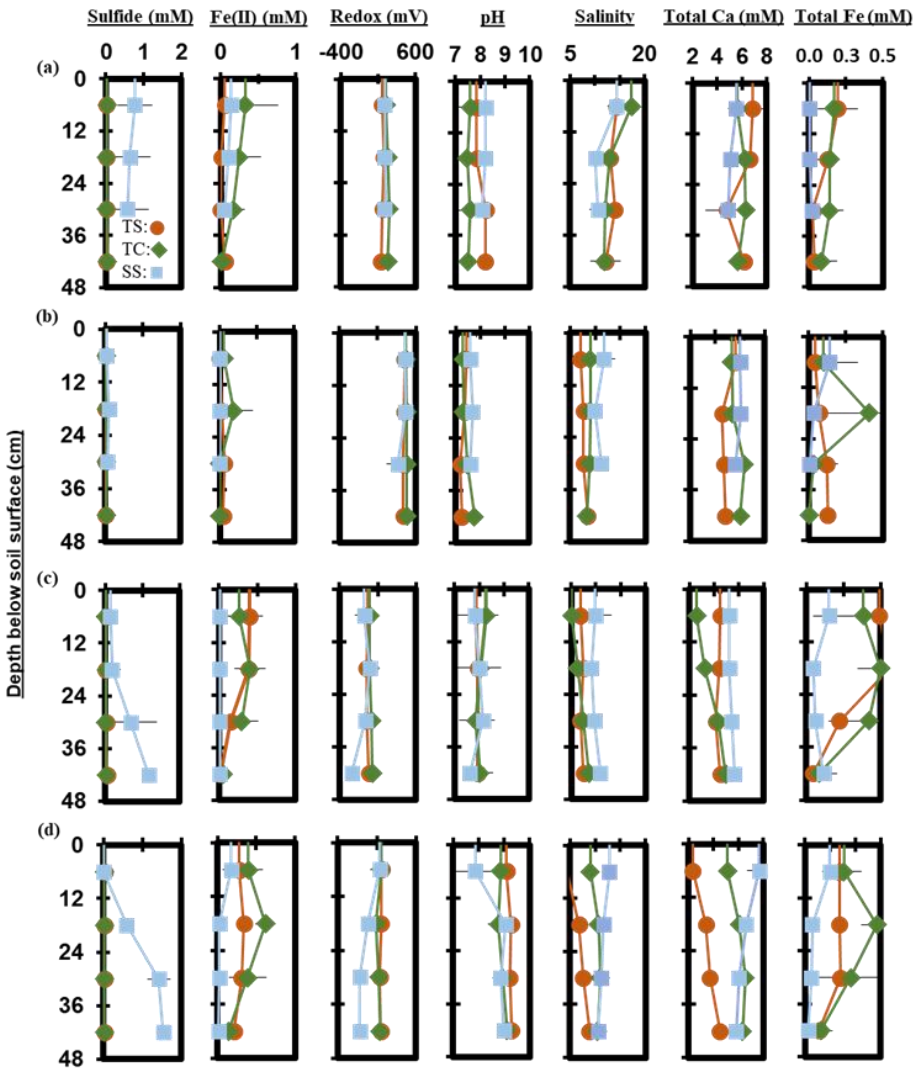

Figure 2.6 Depth profiles of porewater chemistry variables down to 48cm for sampling events that occurred during plant (a) senescence, (b) dormancy, (c) green-up and (d) maturity. Each point represents the mean between replicates (n=3) with error lines indicating the standard deviation (± 1 SD).

Porewater S^{2-} varied significantly with depth. S^{2-} increased significantly with depth across the entire 1-year dataset (R^2=0.04, p=0.03). S^{2-} increased significantly with depth at SS during green-up (R^2=0.51, p=0.01) and maturity (R^2=0.86, p<0.0001). TS S^{2-} increased significantly during green-up (R^2=0.46, p=0.02) while TC S^{2-} increased significantly during maturity (R^2=0.36, p=0.04). Porewater Fe^{2+} trended negatively with S^{2-} (R^2=0.06, p=0.004) and decreased with depth (p=0.01, R^2=0.05) across the entire 1-year dataset. Significant decreases were observed at TS during green-up (R^2=0.68, p=0.001), and at SS during maturity (R^2=0.41, p=0.02). Total Fe concentration followed similar depth trends to Fe^{2+}, with a significant decrease with depth across the entire 1-year experiment (R^2=0.06, p=0.01). Total Fe decreased with depth at TS during senescence (R^2=0.41, p=0.03) and green-up (R^2=0.58, p=0.004), and at SS during maturity (R^2=0.57, p=0.01).

Porewater salinity formed varying relationships with depth. Salinity significantly decreased with depth at TC during senescence (R^2=0.52, p=0.01), and at SS during maturity (R^2=0.62, p=0.002) while salinity significantly increased with depth at TC during green-up (R^2=0.69, p=0.001) and at TS during maturity (R^2=0.87, p<0.0001). Salinity and total Ca generally increased together (p>0.0001, R^2=0.42) across the entire 1-year experiment. Total Ca increased significantly with depth at TC during green-up (R^2=0.86, p<0.0001) and at TS (R^2=0.80, p<0.0001) and TC (R^2=0.47, p=0.01) during maturity. SS total Ca significantly decreased with depth during maturity (R^2=0.60, p=0.005).

2.3.3 Analysis of Variance (ANOVA) Between Subsite and Phenology

ANOVAs were run on subsite and phenology phase mean values that were obtained by averaging samples from all depths across all four phenology phases (for subsite comparisons) (Table 2.1) and all depths across all three subsites (for phenology phase comparisons) (Table 2.2). These results show significant spatial and temporal variability in many of our measured variables. All three subsites contain significantly different average concentrations of soil C, with SS having the highest average (7.5% C), followed by TS (5.8% C) and TC (4.6% C). This indicates that on average, subsite SS contains ~29% more soil C than TS and 63% more soil C than TC. In addition, plant dormancy contained significantly more soil C than plant green-up. While soil S did not significantly vary across phenology phases, soil S at SS was significantly higher in concentration by a factor of two than both TS and TC.

Table 2.1 One-way ANOVA results for all variables assessed based on subsite and averaged by depth and phenology. The mean is reported (± SD) along with a connecting letter report. Means with letters that do not connect are significantly ($p<0.05$) different.

Variable	Tall Spartina (TS)	Tall Cordgrass (TC)	Short Spartina (SS)
Soil C (%)	$5.8\pm(1.2)^{B}$	$4.6\pm(1.3)^{C}$	$7.5\pm(1.4)^{A}$
Soil S (%)	$1.1\pm(0.5)^{B}$	$1.0\pm(0.6)^{B}$	$2.0\pm(0.7)^{A}$
DOC (mM)	$11.9\pm(27)^{A}$	$13.6\pm(27)^{A}$	$7\pm(9)^{A}$
Redox (mV)	$179\pm(176)^{AB}$	$211\pm(185)^{A}$	$93\pm(235)^{B}$
pH	$8.12\pm(0.8)^{A}$	$7.99\pm(0.7)^{A}$	$8.13\pm(0.6)^{A}$
Fe^{2+} (mM)	$0.15\pm(0.1)^{A}$	$0.22\pm(0.3)^{A}$	$0.04\pm(0.1)^{B}$

Sulfide (mM)	0.02±(0.01)^{B}	0.02±(0.01)^{B}	0.6±(0.6)^{A}
Salinity (ppt)	8.8±(3.1)^{B}	9.7±(3)^{AB}	11±(2)^{A}
Total Fe (mM)	0.21±(0.2)^{A}	0.26±(0.3)^{A}	0.08±(0.1)^{B}
Total Ca (mM)	4.7±(1.3)^{B}	5.4±(1.2)^{A}	5.8±(0.8)^{A}

Table 2.2 One-way ANOVA results for all variables assessed based on phenology and averaged by depth and subsite. The mean is reported (± SD) along with a connecting letter report. Means with letters that do not connect are significantly ($p<0.05$) different.

Variable	Senescence	Dormancy	Green-up	Maturity
Soil C (%)	5.7±(1.5)^{AB}	6.7±(1.1)^{A}	5.3±(1.5)^{B}	6.1±(1.8)^{AB}
Soil S (%)	1.4±(0.7)^{A}	1.4±(0.9)^{A}	1.4±(0.7)^{A}	1.3±(0.7)^{A}
DOC (mM)	22.2±(42)^{A}	1.6±(1)^{B}	12.3±(14)^{AB}	7.9±(10)^{B}
Redox (mV)	193±(60)^{B}	453±(58)^{A}	-42±(98)^{D}	83±(111)^{C}
pH	7.89±(0.4)^{B}	7.45±(0.2)^{C}	7.96±(0.6)^{B}	8.94±(0.5)^{A}
Fe^{2+} (mM)	0.1±(0.2)^{BC}	0.03±(0.1)^{C}	0.2±(0.2)^{AB}	0.2±(0.2)^{A}
Sulfide (mM)	0.2±(0.4)^{AB}	0.04±(0.04)^{B}	0.2±(0.4)^{AB}	0.3±(0.6)^{A}
Salinity (ppt)	12.9±(2.4)^{A}	9.0±(1.8)^{BC}	8.0±(2.1)^{C}	9.6±(2.4)^{B}
Total Fe (mM)	0.1±(0.1)^{B}	0.1±(0.2)^{B}	0.3±(0.2)^{A}	0.3±(0.2)^{A}
Total Ca (mM)	5.8±(1.0)^{A}	5.5±(0.7)^{A}	4.5±(0.9)^{B}	5.3±(1.6)^{A}

DOC concentration also varied among subsites (Table 2.1) and phenology (Table 2.2). The average DOC concentration at SS was approximately half of that found at TS and TC, but these results are not statistically significant due to large variability and ranges in concentration observed across the 1-year experiment. This large variability is exemplified by standard deviations that are larger than the means. In addition, DOC also varied between the phenology phases. Dormancy had the lowest mean DOC concentration and was significantly lower than senescence by an order of magnitude. Maturity and green-up did not have statistically different DOC concentrations. The EEMs/ UV-VIS dataset from plant maturity was analyzed based on subsites (Table 2.3). There were significant differences in peaks and indices between subsites. Coble peaks T, A, M, C and Abs_{254} were significantly lower at TS than at both TC and SS by at least a factor of two which is in line with the lower DOC concentrations observed for TS at maturity (Fig. 4). Subsite SS had a significantly lower HIX and E_2:E_3 than both TS and TC. These results indicate significantly different DOC molecular characteristics across subsites. EEMs/ UV-VIS data could not be assessed across phenology since these data were collected only during plant maturity.

Table 2.3 ANOVA results for UV-VIS EMMs data during plant maturity. The mean is reported (± SD) along with a connecting letter report. Means with letters that do not connect are significantly ($p<0.05$) different.

Parameter	Tall Spartina (TS)	Tall Cordgrass (TC)	Short Spartina (SS)
Abs_{254}	$0.7\pm(0.2)^{B}$	$1.7\pm(0.9)^{A}$	$1.7\pm(1.3)^{A}$
$SUVA_{254}$	$0.2\pm(0.1)^{A}$	$0.2\pm(0.1)^{A}$	$0.2\pm(0.1)^{A}$

s_r	1.39±(0.95)^{A}	1.27±(0.33)^{A}	1.46±(0.28)^{A}
E_2:E_3	5.5(0.4)^{A}	5.4±(1.1)^{A}	4.7±(0.7)^{B}
Coble T	4.1±(3.8)^{B}	14.7±(10.3)^{A}	22.6±(16.2)^{A}
Coble A	6.6±(2.1)^{B}	16.9±(7.02)^{A}	13.5±(4.2)^{A}
Coble M	4.0±(1.4)^{B}	10.2±(4.4)^{A}	8.6±(3.1)^{A}
Coble C	3.7±(1.2)^{B}	9.2±(4.0)^{A}	7.8±(2.3)^{A}
FI	1.3±(0.6)^{A}	1.3±(0.02)^{A}	1.3±(0.03)^{A}
HIX	5.1±(3.0)^{A}	4.4±(3.1)^{A}	1.9±(0.6)^{B}
BIX	0.7±(0.7)^{A}	0.7±(0.03)^{A}	0.7±(0.02)^{A}

Differences in porewater chemistry among subsites (Table 2.1) and phenology (Table 2.2) were also significant. SS had the lowest average redox potential and was significantly different from TC which had the highest, while TS was not significantly different from either SS or TC. Redox potentials were even more variable between phenology phases where all four phases had significantly different means. The highest mean was measured during dormancy and decreased significantly in the order senescence, maturity and green-up. The pH was not significantly different across any of the subsites but did change significantly with phenology. Dormancy had the lowest pH which was significantly different from all other phenology phases. Senescence and green-up had a statistically similar mean pH values that were higher than dormancy, and the porewater pH during maturity was statistically higher than all other phenology phases.

S^{2-} also varied significantly among subsites. SS contained on average more than an order of magnitude greater S^{2-} than both TS and TC. S^{2-} is lowest during dormancy but is only significantly different than maturity which has the highest S^{2-} mean. Variability in Fe^{2+} between subsites was opposite of S^{2-}. While TS and TC had low concentrations of S^{2-}, they had high concentrations of Fe^{2+}, which were more than double and significantly higher than Fe^{2+} at SS. Fe^{2+} concentrations varied with phenology similar to S^{2-} where dormancy had the lowest mean which was significantly different only from maturity when the highest levels of Fe^{2+} were detected. Differences between subsite total Fe followed the same trend as Fe^{2+}, where SS was significantly lower than both TS and TC. Total Fe was lowest during dormancy and senescence, which were both statistically similar, but different from green-up and maturity.

SS had the highest mean salinity and was significantly different only from TS which had the lowest mean salinity. Green-up had a significantly lower mean salinity than all other phenology phases except dormancy. Dormancy was only significantly different from senescence, which had the highest mean salinity. Subsite differences in Ca were similar to salinity where SS had a significantly higher mean Ca concentration than TS, but not TC. Green-up had the lowest mean Ca concentration which was significantly different from all other phenology phases.

2.3.4 Relationships Among Variables

To examine the relationships among variables, principal components analysis (PCA) was conducted using mean parameter values categorized by subsite and phenology phase (Figure A.1). Soil C, soil S and sulfide generally trend in a similar direction in the PCAs, indicating that overall, soil C increases with soil S and sulfide

concentration. Redox potential and pH generally trend negatively. Salinity and Ca tend to trend together as would be expected in a saline system, while total Fe and Fe^{2+} trend together. It is important to consider that many of these trends between variables change based on phenology and subsite being considered (Figure A.1). For example, sulfide and soil S trend well with soil C particularly during plant senescence at TC and plant maturity at SS, while sulfide and soil S do not trend well with soil C during plant green-up at TS. The relationships among variables change depending on phenology and subsite and further demonstrates the complexity of salt marsh soil biogeochemistry across temporal and spatial scales. To determine the overall most important biogeochemical variables across phenology and subsites that lead to soil C storage, a stepwise regression was run to predict soil C concentration based on our measured variables.

A stepwise regression model was run across the entire 1-year experiment to determine the most important biogeochemical predictors of soil C concentration in our dataset (Table 2.4). The model results indicate that depth, redox potential, soil S, and sulfide are the best predictors of soil C concentration. The model R^2-value is 0.44, indicating that these variables explain 44% of the variability in our soil C concentration data and the model is highly significant ($p < 0.0001$). Sulfide, redox, and soil S each have positive estimates, meaning that these variables increase as soil C increases while depth had a negative estimate, meaning that soil C tends to decrease with depth across the entire dataset. Each individual predictor variable is also significant ($p<0.05$).

Table 2.4 Stepwise regression results.

Parameter	Estimate	P-Value	Model R^2	Model P-Value
Depth	-0.03	0.003	0.44	<0.0001
Sulfide	0.96	0.04		
Redox	0.002	0.002		
Soil S%	1.3	<0.0001		

2.3.5 Soil Carbon Accumulation Rates

Based on soil accretion rates obtained from a previous study near our core locations (Tucker 2016), bulk density at each of the three subsites previously obtained (Wilson and Smith 2015), and our mean soil C concentrations averaged across depth and phenology (Table 1), we calculated the soil C accumulation rates at each of the three subsites, as well as soil C stock estimates to 48 cm depth (Table 2.5). These results indicate that SS is indeed a hotspot for greater soil C accumulation and stock, with ~20 g C m^{-2} yr^{-2} more than and ~2000 g C m^{-2} higher stocks than the two near channel locations. Our accumulation rates are in range of previously reported values for mesohaline tidal salt marshes (Chmura et al. 2003; Lovelock et al. 2014; Ye et al. 2015; Mcleod et al. 2016; Macreadie et al. 2017, 2020), as are the soil C stock estimates (Zhao et al. 2016; Ewers Lewis et al. 2018; van Ardenne et al. 2018; Ouyang and Lee 2020; Gorham et al. 2021).

Table 2.5 Soil Carbon accumulation rate means for each subsite and soil C stock estimates for each subsite down to 48cm.

Variable	Tall Spartina (TS)	Tall Cordgrass (TC)	Short Spartina (SS)
Soil C Accumulation Rates (g C m^{-2} yr^{-1})	122	115	136
Soil C Stocks (g C m^{-2})	13641	12806	15120

2.4 Discussion

2.4.1 Subsite Differences in Soil C and Biogeochemistry

We hypothesized that soil C concentration and soil biogeochemistry would differ across our subsite locations. Our results support this hypothesis and suggest significant differences in both soil C concentration and porewater biogeochemistry among subsites. This finding illustrates the importance of considering multiple sampling locations when conducting blue C assessments to account for ecosystem-scale variability. At SS, soil C concentrations were 63% higher than at TC and 29% higher than at TS. Even though these subsites are only several meters from one another, they each had statistically different mean soil C concentrations which led to differences in both soil C accumulation rates and stocks. Higher soil C at SS does not seem to be related to higher primary productivity because the *Spartina alterniflora* at SS are stunted. The short form of *S. alterinflora* is generally less productive than the tall form (Roman and Daiber 1984) and likely exudes less DOC from the smaller root mass. This is supported by a lower average DOC concentration at SS. Also, the chromophoric dissolved organic matter (CDOM) properties at SS were different than at the other subsites. SS CDOM had a significantly lower E2:E3 than TS and TC, indicative of higher molecular weight DOC at SS. In addition, the humification index

(HIX) was significantly lower at SS indicating that the DOC at SS has been reworked by microbes less than it has been at TS and TC. Furthermore, SS consistently had lower porewater redox potentials than the other subsites. Redox potentials at SS were low enough to support sulfate reduction. This is confirmed by our elevated S^{2-} porewater concentrations measured at SS. Therefore, the greatest controls on soil C concentration at SS is likely a lower redox potential which decreases microbial oxidation of C, leading to CDOM which is less affected by microbial degradation (i.e., low HIX, high E_2:E_3) and a less energetically favorable metabolism (i.e., sulfate reduction), all resulting in more C storage. In addition, there is likely a much longer residence time of porewater and groundwater at SS because it is less hydraulically connected to the tidal creek, and there is less flushing of oxygenated surface water. This has important implications for soil C stock uncertainty because most of the St. Jones marsh area is composed of subsite SS (Seyfferth et al. 2020). Sampling only near the tidal creek (TS and TC) could significantly underestimate soil C stocks, while sampling only in the marsh interior could lead to an oversimplification of soil biogeochemistry and DOC molecular properties in salt marsh ecosystems.

In contrast to SS, soil redox potentials were significantly higher at TC and soil C was significantly lower. This is likely due to TC having a slightly higher elevation on a natural levee and less reducing surface soils (Seyfferth et al., 2020). The redox potential is not low enough to support sulfate reduction but is low enough to support Fe reduction. This is supported by the abundant amount of Fe^{2+} measured in the porewater at TC. A higher redox potential and more energetically favorable electron acceptor (Fe^{3+}) likely leads to higher rates of C mineralization and explains the lower soil C concentration at TC. On the other hand, we found some of the highest

concentrations of DOC at TC, particularly closer to the surface near the rooting zone. This can be explained by a greater root mass and correspondingly higher root exudation rate of the taller *S. cynosuroides*. A higher concentration of freshly produced DOC and a lower concentration of soil C is also consistent with the priming effect which posits that high concentrations of freshly produced and microbially labile DOC can stimulate microbial growth leading to the degradation of older, more stable soil C (Textor et al. 2019; Zhang et al. 2021). In addition, TC CDOM fluorescence peaks (Coble, A, M, C, T), were similar to SS, indicating that SS and TC have strong sources of fluorescent CDOM.

TS had a similar redox potential to TC and supported Fe reduction due to elevated levels of Fe^{2+}. Though TS and TC are biogeochemically similar, they had significantly different soil C concentrations and different dominant vegetation. While the average redox potentials are not statistically different, TS had a lower mean redox potential than TC. In addition, TS experiences diurnal flooding (i.e., flooding conditions twice daily) while TC experiences spring-tide flooding (i.e., flooding conditions once every two weeks). These differences in hydrology may cause soil C to accumulate more so under slightly stronger reducing conditions at TS compared to TC. Another unique attribute of subsite TS is the CDOM signature. The coble peaks (A, T, C, and M) and Abs_{254} were significantly lower at TS than both TC and SS, which indicates a decreased concentration of terrestrially-derived CDOM. This is likely because TS is nearest the tidal creek and therefore porewater solutes are exported to the tidal channel twice daily during ebb tide (Fettrow et al., 2023), decreasing the marsh grass derived terrestrial CDOM signature in the near-channel porewater.

2.4.2 Phenology Phase Differences in Soil and Biogeochemistry

We further hypothesized that soil C concentration and biogeochemistry would vary across plant phenology phases. Our data support this hypothesis. Soil C was greatest during plant dormancy and was on average 26% higher than green-up, 18% higher than senescence, and 10% higher than maturity. This highlights the importance of considering the time of year soil samples are taken when conducting a blue C assessment. Likewise, many of the biogeochemical variables also changed with phenology phase. The redox potential of all four phenology phases were significantly different from one another, with the highest average redox potential occurring during dormancy. Higher redox potentials during dormancy are associated with significantly lower porewater Fe^{2+} and S^{2-}, indicating that microbial reduction is likely suppressed during the winter months when labile DOC produced from root exudation is less available. Dormancy also had the highest soil C concentration. We suggest this may be related to a suppressed priming affect due to low porewater DOC concentrations and to Fe oxide formation during the high redox potential of dormancy, allowing any remaining porewater C to be pulled into the solid phase with oxidized Fe minerals (Riedel et al. 2013; Sodano et al. 2017; ThomasArrigo et al. 2019).

Belowground allocation of C in *S. alterniflora* has been shown to increase late into the growing season (Lytle and Hull 1980) while concentrations of soil organics have been shown to decrease during the summer months due to higher temperatures and higher rates of soil respiration (Caçador et al. 2004). This is supported by our data because DOC concentrations are higher during senescence and significantly lower during plant maturity. High porewater DOC during senescence agrees with previous work showing higher belowground allocation of biomass in *Spartina* before the winter (Crosby et al. 2015). Higher rates of belowground C allocation during senescence is

further supported by the previously reported higher rates of soil respiration during senescence (Vázquez-Lule and Vargas 2021) due to increased labile DOC availability and associated microbial activity.

2.4.3 Biogeochemical Controls on Soil C

Our data reveal important biogeochemical controls on soil C concentration across space and time. The results of the stepwise regression model suggest that soil C concentrations are most strongly controlled by sulfide, soil S, redox potential, and depth. Soil C increased significantly with increasing sulfide and soil S concentration, indicated by positive model estimate (Table 4). While this is likely associated with the lower elevation and redox potential at SS and subsequent higher sulfate input from the flooded conditions, the increased S concentration with increased C concentration may also be a result of sulfurization where inorganic sulfur, namely sulfide, may interact with organic matter via abiotic reactions (Alperin et al. 1994). Evidence suggests that this interaction can help preserve and stabilize soil C (Tegelaar et al. 1989), though spectroscopic evidence would be required to determine if this is an important process at this study site.

Depth also has an important control on soil C concentration and the estimate was negative, indicating that soil C decreases with depth. This is consistent with the literature suggesting higher soil C concentration at the surface and decreasing with depth in coastal salt marshes (Bai et al. 2016). While depth was an important predictor of soil C from the stepwise regression model, our depth profiles (Figure 4) indicate only small changes with depth. This may be a result of only sampling to 48 cm and integrating across 12 cm increments, or it may be a result of our method design of extracting porewater from the soils and running porewater DOC as a separate fraction

of C from the solid phase soil C. Because our porewater DOC results indicate higher concentrations near the surface, the removal of porewater DOC prior to soil C analysis may lead to lower concentrations of soil C at the surface because in most studies, porewater DOC is typically incorporated into the bulk soil C measurements upon soil drying and not extracted as a separate fraction of C. We suggest future studies consider porewater DOC as a separate component of the overall soil C concentration, particularly because the variability with depth is much higher for porewater DOC than soil C and porewater DOC is highly labile. Therefore, when porewater is extracted from the soil, the measured soil C concentration may appear relatively stable with depth and time leading to more consistent marsh soil C estimates.

Redox potential was the final significant predictor in the stepwise regression model and increased significantly with soil C. We expected to see a negative relationship between soil C and redox potential due to higher C preservation under reducing conditions, but an overall positive relationship between redox potential and soil C indicates an additional and possibly more important mechanism. We suspect that this is related to elevated soil C concentrations and increased redox potential during plant dormancy, possibly a result of Fe oxides forming under more oxidizing winter conditions, thereby increasing soil C concentration by incorporating remaining solution phase C into the solid phase. While there is an abundance of evidence showing the importance of Fe oxides in soil C storage (Lalonde et al. 2012; Riedel et al. 2013; Sowers et al. 2018a, b, 2019; Adhikari et al. 2019), recent studies have shown the important role of Fe oxides in carbon cycling in tidal salt marshes (Seyfferth et al. 2020; Fettrow et al. 2023). Variations in Fe oxide complexation with

C due to phenological phase should be further investigated using spectroscopic analyses.

2.5 Conclusion

Our results highlight the variability in soil C in time and space at the site-level. We found that some level of uncertainty in estimates of stocks and accumulation rates is likely related to spatial and temporal variability of soil C and biogeochemistry at the marsh scale. Subsites that were only a few meters from one another contained significantly different soil C concentrations, likely used different metabolic pathways for C mineralization, and contained significantly different porewater CDOM molecular properties. The biogeochemical controls that were best correlated with soil C concentration were redox potential, soil S, sulfide, and depth, indicating that the redox potential and sulfur content of the soils are critical in controlling how much soil C accumulates in coastal marsh ecosystems. We also found that soil C concentration varies significantly across the phenology phases of the marsh grasses. Plant dormancy contained the highest mean soil C concentration, possibly a result of high redox potential during winter months that causes remaining porewater DOC to be incorporated into the solid phase with oxidized minerals such as Fe oxides. These results demonstrate the importance of considering marsh scale spatial and temporal heterogeneity when conducting a blue C assessment. Based on these results, we suggest taking soil cores from multiple locations within a marsh and in replicate, particularly if multiple types of marsh grass are present, and at different seasons to account for both spatial and temporal variability.

REFERENCES

Adhikari D, Sowers T, Stuckey JW, et al (2019) Formation and redox reactivity of ferrihydrite-organic carbon-calcium co-precipitates. Geochim Cosmochim Acta 244:86–98. https://doi.org/10.1016/j.gca.2018.09.026

Alperin MJ, Albert DB, Martens CS (1994) Seasonal variations in production and consumption rates of dissolved organic carbon in an organic-rich coastal sediment. Geochim Cosmochim Acta 58:4909–4930. https://doi.org/10.1016/0016-7037(94)90221-6

Arias-Ortiz A, Masqué P, Garcia-Orellana J, et al (2018) Reviews and syntheses:210Pb-derived sediment and carbon accumulation rates in vegetated coastal ecosystems – setting the record straight. Biogeosciences 15:6791–6818. https://doi.org/10.5194/bg-15-6791-2018

Bai J, Zhang G, Zhao Q, et al (2016) Depth-distribution patterns and control of soil organic carbon in coastal salt marshes with different plant covers. Sci Rep 6:. https://doi.org/10.1038/srep34835

Baustian MM, Stagg CL, Perry CL, et al (2017) Relationships Between Salinity and Short-Term Soil Carbon Accumulation Rates from Marsh Types Across a Landscape in the Mississippi River Delta. Wetlands 37:313–324. https://doi.org/10.1007/s13157-016-0871-3

Blair NE, Aller RC (2012) The fate of terrestrial organic carbon in the Marine environment. Ann Rev Mar Sci 4:401–423. https://doi.org/10.1146/annurev-marine-120709-142717

Breithaupt JL, Smoak JM, Bianchi TS, et al (2020) Increasing Rates of Carbon Burial in Southwest Florida Coastal Wetlands. J Geophys Res Biogeosci 125:1–25. https://doi.org/10.1029/2019JG005349

Caçador I, Costa AL, Vale C (2004) Carbon storage in tagus salt marsh sediments. Water, Air, and Soil Pollution: Focus 4:701–714. https://doi.org/10.1023/B:WAFO.0000028388.84544.ce

Capooci M, Barba J, Seyfferth AL, Vargas R (2019) Experimental influence of storm-surge salinity on soil greenhouse gas emissions from a tidal salt marsh. Science of the Total Environment 686:1164–1172. https://doi.org/10.1016/j.scitotenv.2019.06.032

Chen C, Dynes JJ, Wang J, Sparks DL (2014) Properties of Fe-organic matter associations via coprecipitation versus adsorption. Environ Sci Technol 48:13751–13759. https://doi.org/10.1021/es503669u

Chen C, Sparks DL (2015) Multi-elemental scanning transmission X-ray microscopy-near edge X-ray absorption fine structure spectroscopy assessment of organo-mineral associations in soils from reduced environments. Environmental Chemistry 12:64–73. https://doi.org/10.1071/EN14042

Chmura GL, Anisfeld SC, Cahoon DR, Lynch JC (2003) Global carbon sequestration in tidal, saline wetland soils. Global Biogeochem Cycles 17:1111. https://doi.org/10.1029/2002GB001917

Clark CD, Aiona P, Keller JK, de Bruyn WJ (2014) Optical characterization and distribution of chromophoric dissolved organic matter (CDOM) in soil porewater from a salt marsh ecosystem. Mar Ecol Prog Ser 516:71–83. https://doi.org/10.3354/meps10833

Cline JD (1969) SPECTROPHOTOMETRIC DETERMINATION OF HYDROGEN SULFIDE IN NATURAL WATERS1. Limnol Oceanogr 14:454–458. https://doi.org/10.4319/lo.1969.14.3.0454

Crosby SC, Ivens-Duran M, Bertness MD, et al (2015) Flowering and biomass allocation in U.S. Atlantic coast Spartina alterniflora. Am J Bot 102:669–676. https://doi.org/10.3732/ajb.1400534

Cuellar-Martinez T, Ruiz-Fernández AC, Sanchez-Cabeza JA, et al (2020) Temporal records of organic carbon stocks and burial rates in Mexican blue carbon coastal ecosystems throughout the Anthropocene. Glob Planet Change 192:103215. https://doi.org/10.1016/j.gloplacha.2020.103215

Cusack M, Saderne V, Arias-Ortiz A, et al (2018) Organic carbon sequestration and storage in vegetated coastal habitats along the western coast of the Arabian Gulf. Environmental Research Letters 13:074007. https://doi.org/10.1088/1748-9326/aac899

Davy AJ, Brown MJH, Mossman HL, Grant A (2011) Colonization of a newly developing salt marsh: disentangling independent effects of elevation and redox potential on halophytes. Journal of Ecology 99:1350–1357. https://doi.org/10.1111/j.1365-2745.2011.01870.x

Desai AR (2010) Climatic and phenological controls on coherent regional interannual variability of carbon dioxide flux in a heterogeneous landscape. J Geophys Res 115:G00J02. https://doi.org/10.1029/2010JG001423

Dorau K, Pohl L, Just C, et al (2019) Soil Organic Matter and Phosphate Sorption on Natural and Synthetic Fe Oxides under in Situ Conditions. Environ Sci Technol 53:13081–13087. https://doi.org/10.1021/acs.est.9b03260

Duarte CM (2017) Reviews and syntheses: Hidden forests, the role of vegetated coastal habitats in the ocean carbon budget. Biogeosciences 14:301–310. https://doi.org/10.5194/bg-14-301-2017

Ewers Lewis CJ, Baldock JA, Hawke B, et al (2019) Impacts of land reclamation on tidal marsh 'blue carbon' stocks. Science of the Total Environment 672:427–437. https://doi.org/10.1016/j.scitotenv.2019.03.345

Ewers Lewis CJ, Carnell PE, Sanderman J, et al (2018) Variability and Vulnerability of Coastal 'Blue Carbon' Stocks: A Case Study from Southeast Australia. Ecosystems 21:263–279. https://doi.org/10.1007/s10021-017-0150-z

Fettrow S, Vargas R, Seyfferth AL (2023) Experimentally simulated sea level rise destabilizes carbon-mineral associations in temperate tidal marsh soil. Biogeochemistry. https://doi.org/10.1007/s10533-023-01024-z

Ford H, Garbutt A, Duggan-Edwards M, et al (2019) Large-scale predictions of salt-marsh carbon stock based on simple observations of plant community and soil type. Biogeosciences 16:425–436. https://doi.org/10.5194/bg-16-425-2019

Frasco BA, Good RE (1982) Decomposition Dynamics of Spartina alterniflora and Spartina patens in a New Jersey Salt Marsh. Am J Bot 69:402. https://doi.org/10.2307/2443145

Gao L, Fan D, Sun C, et al (2011) Optical characterization of CDOM in a marsh-influenced environment in the Changjiang (Yangtze River) Estuary. Environ Earth Sci 64:643–658. https://doi.org/10.1007/s12665-010-0885-8

Gorham C, Lavery P, Kelleway JJ, et al (2021) Soil Carbon Stocks Vary Across Geomorphic Settings in Australian Temperate Tidal Marsh Ecosystems. Ecosystems 24:319–334. https://doi.org/10.1007/s10021-020-00520-9

Guimond JA, Seyfferth AL, Moffett KB, Michael HA (2020a) A physical-biogeochemical mechanism for negative feedback between marsh crabs and carbon storage. Environmental Research Letters 15:034024. https://doi.org/10.1088/1748-9326/ab60e2

Guimond JA, Yu X, Seyfferth AL, Michael HA (2020b) Using Hydrological-Biogeochemical Linkages to Elucidate Carbon Dynamics in Coastal Marshes Subject to Relative Sea Level Rise. Water Resour Res 56:1–16. https://doi.org/10.1029/2019WR026302

Kang X, Hao Y, Cui X, et al (2016) Variability and Changes in Climate, Phenology, and Gross Primary Production of an Alpine Wetland Ecosystem. Remote Sens (Basel) 8:391. https://doi.org/10.3390/rs8050391

Koretsky CM, Van Cappellen P, Dichristina TJ, et al (2005) Salt marsh pore water geochemistry does not correlate with microbial community structure. Estuar Coast Shelf Sci 62:233–251. https://doi.org/10.1016/j.ecss.2004.09.001

Lacroix EM, Mendillo J, Gomes A, et al (2022) Contributions of anoxic microsites to soil carbon protection across soil textures. Geoderma 425:. https://doi.org/10.1016/j.geoderma.2022.116050

Lalonde K, Mucci A, Ouellet A, Gélinas Y (2012) Preservation of organic matter in sediments promoted by iron. Nature 483:198–200. https://doi.org/10.1038/nature10855

Lovelock CE, Adame MF, Bennion V, et al (2014) Contemporary rates of carbon sequestration through vertical accretion of sediments in mangrove forests and saltmarshes of South East Queensland, Australia. Estuaries and Coasts. https://doi.org/10.1007/s12237-013-9702-4

Luo M, Huang J-F, Zhu W-F, Tong C (2019) Impacts of increasing salinity and inundation on rates and pathways of organic carbon mineralization in tidal wetlands: a review. Hydrobiologia 827:31–49. https://doi.org/10.1007/s10750-017-3416-8

Luo M, Liu Y, Huang J, et al (2018) Rhizosphere processes induce changes in dissimilatory iron reduction in a tidal marsh soil: a rhizobox study. Plant Soil 433:83–100. https://doi.org/10.1007/s11104-018-3827-y

Lytle RW, Hull RJ (1980) Annual Carbohydrate Variation in Culms and Rhizomes of Smooth Cordgrass (Spartina alterniflora Loisel.) 1 . Agron J 72:942–946. https://doi.org/10.2134/agronj1980.00021962007200060019x

Macreadie PI, Anton A, Raven JA, et al (2019) The future of Blue Carbon science. Nat Commun 10:3998. https://doi.org/10.1038/s41467-019-11693-w

Macreadie PI, Nielsen DA, Kelleway JJ, et al (2020) Can we manage coastal ecosystems to sequestor more blue carbon? 15:206–213

Macreadie PI, Ollivier QR, Kelleway JJ, et al (2017) Carbon sequestration by Australian tidal marshes. Sci Rep 7:44071. https://doi.org/10.1038/srep44071

Mcleod E, Chmura GL, Bouillon S, et al (2016) A blueprint for blue carbon: toward an improved understanding of the role of vegetated coastal habitats in sequestering CO2. Front Ecol Environ 9:552–560. https://doi.org/https://www.jstor.org/stable/41479959

Mcowen C, Weatherdon L, Bochove J-W, et al (2017) A global map of saltmarshes. Biodivers Data J 5:e11764. https://doi.org/10.3897/BDJ.5.e11764

McTigue N, Davis J, Rodriguez AB, et al (2019) Sea Level Rise Explains Changing Carbon Accumulation Rates in a Salt Marsh Over the Past Two Millennia. J Geophys Res Biogeosci 124:2945–2957. https://doi.org/10.1029/2019JG005207

Miller CB, Rodriguez AB, Bost MC, et al (2022) Carbon accumulation rates are highest at young and expanding salt marsh edges. Commun Earth Environ 3:. https://doi.org/10.1038/s43247-022-00501-x

Moffett K, Gorlick S (2016) Relating salt marsh pore water geochemistry patterns to vegetation zones and hydrologic influences. J Am Water Resour Assoc 52:1729–1745. https://doi.org/10.1111/j.1752-1688.1969.tb04897.x

Mueller P, Ladiges N, Jack A, et al (2019) Assessing the long-term carbon-sequestration potential of the semi-natural salt marshes in the European Wadden Sea. Ecosphere 10:. https://doi.org/10.1002/ecs2.2556

Muench A, Elsey-Quirk T (2019) Competitive reversal between plant species is driven by species-specific tolerance to flooding stress and nutrient acquisition during early marsh succession. Journal of Applied Ecology 56:2236–2247. https://doi.org/10.1111/1365-2664.13458

Negandhi K, Edwards G, Kelleway JJ, et al (2019) Blue carbon potential of coastal wetland restoration varies with inundation and rainfall. Sci Rep 9:4368. https://doi.org/10.1038/s41598-019-40763-8

Negrin VL, Spetter C V., Asteasuain RO, et al (2011) Influence of flooding and vegetation on carbon, nitrogen, and phosphorus dynamics in the pore water of a Spartina alterniflora salt marsh. Journal of Environmental Sciences 23:212–221. https://doi.org/10.1016/S1001-0742(10)60395-6

Ouyang X, Lee SY (2020) Improved estimates on global carbon stock and carbon pools in tidal wetlands. Nat Commun 11

Riedel T, Zak D, Biester H, Dittmar T (2013) Iron traps terrestrially derived dissolved organic matter at redox interfaces. Proceedings of the National Academy of Sciences 110:10101–10105. https://doi.org/10.1073/pnas.1221487110

Roman CT, Daiber FC (1984) Aboveground and Belowground Primary Production Dynamics of Two Delaware Bay Tidal Marshes. Torrey Botanical Society 111:34–41. https://doi.org/https://www.jstor.org/stable/2996208

Saintilan N, Rogers K, Mazumder D, Woodroffe C (2013) Allochthonous and autochthonous contributions to carbon accumulation and carbon store in southeastern Australian coastal wetlands. Estuar Coast Shelf Sci 128:84–92. https://doi.org/10.1016/j.ecss.2013.05.010

Sanders CJ, Maher DT, Tait DR, et al (2016) Are global mangrove carbon stocks driven by rainfall? J Geophys Res Biogeosci 121:2600–2609. https://doi.org/10.1002/2016JG003510

Serrano O, Lovelock CE, B. Atwood T, et al (2019) Australian vegetated coastal ecosystems as global hotspots for climate change mitigation. Nat Commun 10:4313. https://doi.org/10.1038/s41467-019-12176-8

Seyfferth AL, Bothfeld F, Vargas R, et al (2020) Spatial and temporal heterogeneity of geochemical controls on carbon cycling in a tidal salt marsh. Geochim Cosmochim Acta 282:1–18. https://doi.org/10.1016/j.gca.2020.05.013

Smeaton C, Barlow NLM, Austin WEN (2020) Coring and compaction: Best practice in blue carbon stock and burial estimations. Geoderma 364:114180. https://doi.org/10.1016/j.geoderma.2020.114180

Sodano M, Lerda C, Nisticò R, et al (2017) Dissolved organic carbon retention by coprecipitation during the oxidation of ferrous iron. Geoderma 307:19–29. https://doi.org/10.1016/j.geoderma.2017.07.022

Sowers TD, Adhikari D, Wang J, et al (2018a) Spatial Associations and Chemical Composition of Organic Carbon Sequestered in Fe, Ca, and Organic Carbon Ternary Systems. Environ Sci Technol 52:6936–6944. https://doi.org/10.1021/acs.est.8b01158

Sowers TD, Holden KL, Coward EK, Sparks DL (2019) Dissolved Organic Matter Sorption and Molecular Fractionation by Naturally Occurring Bacteriogenic Iron (Oxyhydr)oxides. Environ Sci Technol 53:4295–4304. https://doi.org/10.1021/acs.est.9b00540

Sowers TD, Stuckey JW, Sparks DL (2018b) The synergistic effect of calcium on organic carbon sequestration to ferrihydrite. Geochem Trans 19:22–26. https://doi.org/10.1186/s12932-018-0049-4

Stookey LL (1970) Ferrozine-A New Spectrophotometric Reagent for Iron. Anal Chem 42:779–781. https://doi.org/10.1021/ac60289a016

Tegelaar EW, de Leeuw JW, Derenne S, Largeau C (1989) A reappraisal of kerogen formation. Geochim Cosmochim Acta 53:3103–3106. https://doi.org/10.1016/0016-7037(89)90191-9

Textor SR, Wickland KP, Podgorski DC, et al (2019) Dissolved Organic Carbon Turnover in Permafrost-Influenced Watersheds of Interior Alaska: Molecular Insights and the Priming Effect. Front Earth Sci (Lausanne) 7:. https://doi.org/10.3389/feart.2019.00275

ThomasArrigo LK, Kaegi R, Kretzschmar R (2019) Ferrihydrite Growth and Transformation in the Presence of Ferrous Iron and Model Organic Ligands. Environ Sci Technol 53:13636–13647. https://doi.org/10.1021/acs.est.9b03952

Trifunovic B, Vázquez-Lule A, Capooci M, et al (2020) Carbon Dioxide and Methane Emissions From A Temperate Salt Marsh Tidal Creek. J Geophys Res Biogeosci 125:. https://doi.org/10.1029/2019JG005558

Tucker KJ (2016) VARIABILITY OF ORGANIC CARBON ACCUMULATION ON A TIDAL WETLAND COAST. University of Delaware

Valle J, Gonsior M, Harir M, et al (2018) Extensive processing of sediment pore water dissolved organic matter during anoxic incubation as observed by high-field mass spectrometry (FTICR-MS). Water Res 129:. https://doi.org/10.1016/j.watres.2017.11.015

van Ardenne LB, Jolicouer S, Bérubé D, et al (2018) The importance of geomorphic context for estimating the carbon stock of salt marshes. Geoderma 330:264–275. https://doi.org/10.1016/j.geoderma.2018.06.003

van de Broek M, Temmerman S, Merckx R, Govers G (2016) Controls on soil organic carbon stocks in tidal marshes along an estuarine salinity gradient. Biogeosciences 13:6611–6624. https://doi.org/10.5194/bg-13-6611-2016

Van De Broek M, Temmerman S, Merckx R, Govers G (2016) Controls on soil organic carbon stocks in tidal marshes along an estuarine salinity gradient. Biogeosciences 13:6611–6624. https://doi.org/10.5194/bg-13-6611-2016

Vázquez-Lule A, Vargas R (2021) Biophysical drivers of net ecosystem and methane exchange across phenological phases in a tidal salt marsh. Agric For Meteorol 300:108309. https://doi.org/10.1016/j.agrformet.2020.108309

Wang F, Sanders CJ, Santos IR, et al (2021) Global blue carbon accumulation in tidal wetlands increases with climate change. Natl Sci Rev 8:. https://doi.org/10.1093/nsr/nwaa296

Whitby H, Planquette H, Cassar N, et al (2020) A call for refining the role of humic-like substances in the oceanic iron cycle. Sci Rep 10:6144. https://doi.org/10.1038/s41598-020-62266-7

Wilson K, Smith E (2015) Marsh Carbon Storage in the National Estuarine Research Reserves, USA. 67

Windham L (2001) Comparison of biomass production and decomposition between Phragmites australis (common reed) and spartina patens (salt hay grass) in brackish tidal marshes of New Jersey, USA. Wetlands 21:179–188. https://doi.org/10.1672/0277-5212(2001)021[0179:COBPAD]2.0.CO;2

Wordofa DN, Adhikari D, Dunham-Cheatham SM, et al (2019) Biogeochemical fate of ferrihydrite-model organic compound complexes during anaerobic microbial reduction. Science of the Total Environment 668:216–223. https://doi.org/10.1016/j.scitotenv.2019.02.441

Ye S, Laws EA, Yuknis N, et al (2015) Carbon Sequestration and Soil Accretion in Coastal Wetland Communities of the Yellow River Delta and Liaohe Delta, China. Estuaries and Coasts. https://doi.org/10.1007/s12237-014-9927-x

Yousefi Lalimi F, Silvestri S, D'Alpaos A, et al (2018) The Spatial Variability of Organic Matter and Decomposition Processes at the Marsh Scale. J Geophys Res Biogeosci 123:3713–3727. https://doi.org/10.1029/2017JG004211

Yu J, Dong H, Li Y, et al (2014) Spatiotemporal Distribution Characteristics of Soil Organic Carbon in Newborn Coastal Wetlands of the Yellow River Delta Estuary. Clean (Weinh) 42:311–318. https://doi.org/10.1002/clen.201100511

Zhang D, Gong C, Zhang W, et al (2021) Labile carbon addition alters soil organic carbon mineralization but not its temperature sensitivity in a freshwater marsh of Northeast China. Applied Soil Ecology 160:. https://doi.org/10.1016/j.apsoil.2020.103844

Zhao Q, Bai J, Liu Q, et al (2016) Spatial and Seasonal Variations of Soil Carbon and Nitrogen Content and Stock in a Tidal Salt Marsh with Tamarix chinensis, China. Wetlands 36:145–152. https://doi.org/10.1007/s13157-015-0647-1

Zhu Q, Cochran JK, Heilbrun C, et al (2021) Small-Scale Geochemical Heterogeneities and Seasonal Variation of Iron and Sulfide in Salt Marshes Revealed by Two-Dimensional Sensors. Front Earth Sci (Lausanne) 9:. https://doi.org/10.3389/feart.2021.653698

Chapter 3

PHYSIOCHEMICAL CONTROLS ON THE HORIZONTAL EXCHANGE OF BLUE CARBON ACROSS THE SALT MARSH-TIDAL CHANNEL INTERFACE

This chapter contains a manuscript in review in the journal JGR Biogeosciences. The complete author list is Sean Fettrow, Virginia Jeppi (University of Delaware), Andrew Wozniak (University of Delaware), Rodrgio Vargas (University of Delaware), and Angelia Seyfferth (university of Delaware).

Abstract

Tidal channels are biogeochemical hotspots that horizontally exchange carbon (C) with marsh platforms, but the physiochemical drivers controlling these dynamics are not well understood. We hypothesized that C-bearing iron (Fe) oxides precipitate and immobilize dissolved organic carbon (DOC) during ebb tide as the soils oxygenate, and dissolve into the porewater during flood tide, promoting transport to the channel. The hydraulic gradient is a physical control of how these solutes are horizontally exchanged across the marsh platform-tidal channel interface; we hypothesized that this gradient alters the concentration and source of C being exchanged. We further hypothesized that trace soil gases (i.e., CO_2, CH_4, dimethyl sulfide) are pushed out of the channel bank as the groundwater rises. To test these hypotheses, we measured porewater, surface water, and soil trace gases over two 24-hour monitoring campaigns (i.e., summer and spring) in a mesohaline tidal marsh. We

found that Fe^{2+} and DOC were positively related during flood tide but not during ebb tide. This finding shows the formation and dissolution of C-bearing Fe oxides across a tidal cycle. In addition, the tidal channel contained significantly ($p<0.05$) more terrestrial-like DOC when the hydraulic gradient was driving flow toward the channel. In comparison, the channel water was saltier and contained significantly ($p<0.05$) more marine-like DOC when the hydraulic gradient reversed direction. Trace gas fluxes generally increased with rising groundwater levels, particularly dimethyl sulfide. These findings suggest multiple physiochemical mechanisms controlling the horizontal exchange of C at the marsh platform-tidal channel interface.

3.1 Introduction

Tidal salt marshes sequester soil carbon (C) at rates similar to tropical rain forests despite occupying at least 50 times less land area (Chmura et al., 2003; Duarte et al., 2013). This disproportionately large soil C reservoir results in tidal salt marshes being considered natural climate solutions (Duarte et al., 2008) to help offset climate change (IPCC, 2022). The potential of tidal salt marshes as a natural climate solution has gained much attention recently (Howard et al., 2017; Macreadie et al., 2021; Serrano et al., 2019), especially since the term blue C was coined a decade ago to describe the C held within these high-capacity C sinks (Nellemann et al., 2009). Most blue C studies focus on the distribution of C in the soil profile (Berthelin et al., 2022; van de Broek et al., 2016a, 2016b; Chmura et al., 2003; Gorham et al., 2021; Hinson et al., 2017; Spivak et al., 2019; Sun et al., 2019; Yu et al., 2014)or vertical trace gas fluxes (Abdul-Aziz et al., 2018; Capooci et al., 2019; Capooci & Vargas, 2022; Diefenderfer et al., 2018; O'Connor et al., 2020; Tong et al., 2020; Vázquez-Lule & Vargas, 2021; Wollenberg et al., 2018). Few studies focus on the lateral C flux, which

is the inorganic and organic C imported and exported via tidal channels (Santos et al., 2021; Trifunovic et al., 2020). This limited attention to lateral C flux has likely led to an underestimation of the net C flux within coastal wetlands. Some studies suggest that lateral C loss may be similar to or even exceed blue C burial rates (Bogard et al., 2020; Czapla et al., 2020; Z. A. Wang et al., 2016). For example, one study suggested that 17% of the total salt marsh primary productivity is preserved in the soils, while 19% is displaced laterally (Mcleod et al., 2016). This agrees with another study that suggests marsh-derived C is more likely to be laterally exported than it is to be stored within the marsh (Santos et al., 2019). While salt marshes occupy only 0.3% of the global ocean area, they contribute 6% and 4% of lateral dissolved inorganic carbon (DIC) and dissolved organic carbon (DOC), respectively, to the oceans (Bauer et al., 2013). These studies suggest the importance of the lateral C flux, but much uncertainty exists as the range in global salt marsh lateral flux is 31-78 Tg C year^{-1}, and there are limited studies indicating why the range is so large (Duarte, 2017). Further study is required to reduce uncertainty and better understand how tidal salt marshes can be managed as a natural climate solution.

Although it is increasingly recognized that the lateral C flux may represent a substantial component of the net C budget in tidal wetlands, there remains high uncertainty. The uncertainty of lateral C flux in North American tidal wetlands is 100% of the estimated value (Hayes et al., 2018), which illustrates that there is much to learn about lateral C fluxes from these ecosystems. High uncertainty in the lateral C flux stems from a variety of factors, including 1) only a limited amount of studies examining lateral C transport (Chu et al., 2018; Santos et al., 2019; Z. A. Wang et al., 2016; Z. A. Wang & Cai, 2004), 2) lack of incorporation of both DOC and DIC into

estimates (Duarte, 2017; Santos et al., 2019), 3) few studies on lateral trace gas C fluxes from tidal channels (Trifunovic et al., 2020), and 4) limited mechanistic understanding of horizontal C exchange between the salt marsh soil platform and tidal channel interface. In addition, most studies focus on large-scale surface water flux between the marsh, estuary, and ocean boundaries (Chu et al., 2018; Najjar et al., 2018; Osburn et al., 2015; Tzortziou et al., 2008; Z. A. Wang & Cai, 2004; Winter et al., 1996), whereas only a few address the horizontal exchange of C-rich porewater between marsh soils and surface water in tidal channels (Guimond, Seyfferth, et al., 2020). Therefore, having an improved mechanistic understanding of the chemical and physical controls on horizontal C exchange between the tidal channel and adjacent marsh soil could help decrease uncertainty in the lateral C flux.

The chemical mobility of DOC in soils near tidal channels may be controlled by Fe oxides, which offer mineral protection from microbial degradation and decrease the mobility of C (Zak & Gelbrecht, 2007). The role of Fe oxides in stabilizing DOC has been well established in controlled laboratory experiments, and upland terrestrial field settings (Adhikari et al., 2019; Chen & Sparks, 2015; Sowers, Adhikari, et al., 2018; Sowers et al., 2019; Sowers, Stuckey, et al., 2018), but the importance of Fe oxides in coastal settings is less clear. Previous work has shown that reactive Fe oxide species, including ferrihydrite, exist near tidal salt marsh channels alongside high quantities of DOC (Seyfferth et al., 2020). These soils are inundated and drain every 6 hours due to semidiurnal tides, causing rapid and large changes in soil redox potential over short periods (Guimond, Seyfferth, et al., 2020). Due to the redox sensitivity of Fe oxides (Schwertmann, 1991), reducing and oxidizing conditions in tidally influenced soils may allow coprecipitates of Fe and DOC to form and dissolve

between ebb and flood tides, as has been shown for other fluctuating redox environments. (Chen et al., 2014; Sodano et al., 2017). Thus, precipitation and dissolution of Fe-DOC coprecipitates across ebb-flood tides may be an important process controlling the transport of marsh soil DOC to and from tidal channels. The presence of Fe-DOC coprecipitates in marsh soils has previously been confirmed, as has their sensitivity to redox conditions under simulated sea level rise conditions (Fettrow et al., 2023).

While Fe oxides may partially control the chemical mobility of horizontally transported C, the physical transport of porewater solutes is governed by the hydraulic gradient between the near-channel groundwater and the tidal channel surface water (Guimond, Yu, et al., 2020). The hydraulic gradient likely changes rapidly in semi-diurnal systems, where a falling tide leads to groundwater/ porewater discharge into the tidal channel, and a rising tide leads to surface water seepage into the pore space (Xin et al., 2011). Changes in hydraulic gradient direction will likely alter the source and concentration of C being exchanged and laterally fluxed, such as light-reactive chromophoric dissolved organic carbon (CDOM). The proportion of marsh-derived, terrestrial-like CDOM has been shown to increase in tidal channels during ebb tide, while the proportion of marine-derived CDOM increases during flood tide (Osburn et al., 2015; Tzortziou et al., 2008). This is likely a result of C-rich marsh porewater flowing into the tidal channel during ebb tide and estuarine bay waters flowing into the tidal channel during flood tide. Still, to our knowledge, a direct connection between the magnitude and composition of C in the tidal channel and the horizontal exchange of water between the marsh platform and tidal channel is yet to be made over a complete tidal cycle and across seasons.

In addition to understanding the physical and chemical controls on horizontal C transport, it is also essential to know how soil trace gas emissions change across tidal cycles (Capooci & Vargas, 2022). Fluxes of soil greenhouse gases (e.g., CO_2, CH_4) offset the global cooling effect of stored C in soil. Therefore, assessing the horizontal fluxes of gases is critical to constraining the total ecosystem C flux (Santos et al., 2019; Trifunovic et al., 2020). In addition to CO_2 and CH_4, dimethyl sulfide (DMS) is a common C-containing gas produced in salt marshes, particularly those dominated by Spartina grasses (J. Wang & Wang, 2017). DMS is a climate-cooling gas due to its oxidation to SO_4 in the atmosphere (Charlson et al., 1987). Few studies have investigated horizontal trace gas fluxes from tidal channels, but evidence suggests these sites could represent biogeochemical hotspots in salt marshes (Trifunovic et al., 2020). Assessing soil trace gas emissions coupled to porewater and surface water near tidal channels may help constrain the magnitude and mechanisms of lateral C fluxes in tidally influenced ecosystems.

We postulate several interrelated hypotheses to investigate patterns and mechanisms of horizontal C flux between the marsh platform and tidal channel. First, we hypothesize that Fe oxides stabilize DOC during high soil redox conditions (i.e., ebb tide, while they dissolve and enter the porewater together as Fe^{2+} and DOC during low soil redox conditions (i.e., flood tide). Second, we hypothesize that the hydraulic gradient controls the physical exchange of solutes between the marsh porewater and the tidal channel, and drives changes in the concentration and source of lateral C. Finally, we hypothesized that soil trace gases are horizontally fluxed from channel bank soils to tidal channels due to tidal forces and the upward movement of groundwater. These hypotheses were tested by performing two 24-hr field campaigns

in the summer and spring in a mesohaline temperate salt marsh. Porewater, surface water, and soil trace gas fluxes were simultaneously measured in and alongside a tidal channel at a temperate tidal salt marsh every hour for 24 hours during each campaign. Our data highlight how interactions between physiochemical processes control the horizontal flow of C between marsh soils and adjacent tidal channels, with implications for improving our understanding of the lateral C flux between salt marshes and the coastal ocean.

3.2 Method and Materials

3.2.1 Field Site

The measurements were performed in and adjacent to the tidal channel of a temperate salt marsh located at the St Jones Estuarine Research Reserve in Dover, DE (Figure B.1). This field site has been described extensively in previous work (Capooci et al., 2019; Capooci & Vargas, 2022; Guimond, Seyfferth, et al., 2020; Guimond, Yu, et al., 2020; Seyfferth et al., 2020; Trifunovic et al., 2020). Tidal channel salinity ranges from 8 to 15ppt (Capooci et al., 2019) and flows into the nearby St Jones River that is connected to the Delaware Bay. Vegetation near the tidal channel consists primarily of Spartina alterniflora, with patches of both *S. patens* and *S. cynosuroides.* The soil was previously classified as a silty clay loam (Capooci et al., 2019) with an abundance of Fe oxide minerals, ~40% being poorly crystalline ferrihydrite (Seyfferth et al., 2020). Semidiurnal tides inundate soils near the tidal channel twice daily and drain as the tides go out, causing redox conditions to change drastically (-100mv to 500mV) and rapidly across a single tidal cycle (Guimond, Seyfferth, et al., 2020), particularly during spring tides when the tidal amplitude is at its maximum (Seyfferth

et al., 2020). To capture seasonal variability, 24-hour sampling campaigns were conducted once in the summer of 2020 during plant maturity and again in the spring of 2021 during plant green-up (Hill et al., 2021), hereafter referred to as summer and spring sampling events. The summer sampling event occurred during a new moon spring tide, while the spring sampling event occurred during a full moon spring tide. Spring tides were targeted to capture a wide range in tidal and redox amplitude over each tidal cycle.

3.2.2 In-Situ Measurements

3.2.2.1 Multi-level *in situ* redox sensor

To capture rapid changes in redox with tidal oscillation, a platinum electrode redox sensor (Paleo Terra, Amsterdam, Netherlands) was inserted vertically into the soil 1m from the tidal channel following previous methods (Guimond, Seyfferth, et al., 2020). The sensor was connected to a data logger (Campbell Scientific, CR1000), which recorded a data point every 15 minutes. A reference potential was established by connecting a Calomel reference electrode (Fisher Scientific) to the data logger. The reference electrode was encased in a KCl salt bridge solution to establish a connection to the surrounding soil. The redox system was calibrated in the lab with check standards before deployment. A correction factor of +245mV was added to the raw data to account for the difference in redox potential between the reference probe and the standard hydrogen electrode.

3.2.2.2 Hydrological Measurements

A groundwater well was previously installed approximately 1m from the tidal channel (Seyfferth et al., 2020). A pressure transducer (Aqua TROLL 200 Data

Logger) was inserted into the well, which collected a measurement every 15 minutes. In addition, an atmospheric pressure transducer (Baro-Driver) was installed aboveground near the well and was used to correct for atmospheric pressure to calculate water level elevation using software specifically designed for our transducers (Levelogger Version 4.5). Groundwater head is reported as elevation above (positive) or below (negative) ground surface.

Continuous surface water data was also collected in the tidal channel. The St. Jones Reserve manages a tidal channel sonde that records water level, salinity, water temperature, conductivity, pH, turbidity, and dissolved oxygen every 15 minutes. The surface water elevation data is reported as depth above (positive) or below (negative) the ground surface. Surface and groundwater level data were also used to calculate the hydraulic gradient between the channel bank groundwater and tidal channel surface water as the difference in head divided by the distance from the well to the channel bank, ~1m. Water level elevations were referenced to NAVD83.

3.2.3 Surface Water and Porewater Collection

Surface water from the tidal channel and soil porewater from the adjacent tidal channel bank were collected each hour simultaneously for 24 hours to connect porewater and surface water processes directly. Surface water was collected by rinsing an acid-washed 15mL falcon tube with tidal channel surface water three times before collection. Porewater was collected from four rhizon samplers (Rhizosphere Research Products) fitted with ceramic filters (1.2 µm pore size). Rhizons were inserted into the soil at various depths 72 hours before sampling to allow equilibration before sample collection. Three rhizons were inserted horizontally into the channel bank at -6, -18, and -30cm depth relative to the channel bank surface (hereafter referred to as R-6, R-

18, and R-30. In addition, one rhizon was inserted vertically downward into the soil surface approximately 1m from the channel bank toward the marsh interior and near the groundwater well (hereafter referred to as R-Int) (Figure B.2). Following previous methods, vacuum syringes were used to extract porewater from soil rhizons (Limmer et al., 2018). We used data from all rhizons, but R-30 had the most complete 24-hour dataset for summer and spring campaigns. Consequently, information from R-30 was used in statistical analyses to interpret diel patterns.

The water samples (i.e., surface water and porewater) were split and used for various chemical analyses. One portion was analyzed in the field with a calibrated electrode probe for pH (Orion Ross Ultra pH/ATC Triode). In addition, a subset of the sample was filtered in the field using 0.45µm PTFE syringe filters. This field-filtered sample was split and used for colorimetric analysis of S^{2-} and Fe^{2+} using the Cline and Stookey methods, respectively (Cline, 1969; Stookey, 1970). DOC samples were prepared in the lab by filtering 3mL of the sample through Whatman GF/F filters (0.7µm). Most of the sample was analyzed for DOC, DIC, and total N (Vario TOC Cube, Elementar,) while a subsample was used for Excitation Emission Matrices (EEMs) and Ultraviolet-Visible (UV-VIS) analysis on a fluorescence spectrophotometer (Aqualog, Horiba) to observe DOC source and composition. The Aqualog was calibrated using Double Deionized (DDI) blanks and data were normalized to the instrument's Raman Area. Wavelengths measured were between 230nm and 700nm with a measurement step of 2nm. Fluorescence peak intensities (Coble A, C) and indices (HIX, BIX) were determined, as well as absorbance indices (Abs254, Sr, SUVA254, E2: E3). Previously established methods were followed for calculating these peaks and indices (Table B.1).

3.2.4 Soil Trace Gas Flux Analysis

Soil trace gas measurements (i.e., CO_2, CH_4 DMS) were collected every hour to determine how the tidal cycle affects gas exchange from the channel bank. We also measured N_2O, but fluxes were very low and potentially under the detection limit, thus were not reported in this study. Two PVC collars were inserted 10cm and 30cm down the side of the channel bank (Figure B.2) approximately 72 hours before the start of the experiment to allow for soil equilibration before gas flux measurements. Flux measurements were taken every hour by fitting the soil collars with a PVC closed-loop chamber connected to a gas analyzer (DX4040, Gasmet Technologies, Finland) via gas impermeable tubing. A small fan was attached to the inside of the chamber to allow the air to mix during measurements (Pearson et al., 2016). Measurements were taken every 5 seconds for approximately 3 minutes. Fluxes were calculated using the following equation:

$$Soil\ Gas\ Flux = \frac{\Delta c}{\Delta t}\frac{V}{S}\frac{Pa}{RT}$$

where c is the mole fraction of CO2, CH4, or DMS in µmol mol-1, t is the observation time of 180 seconds, V is the total volume of the closed system, S is the surface area of the soil chamber, Pa is the atmospheric pressure, R is the universal gas constant, T is the surface soil temperature. We followed standardized protocols, and a linear fit was applied to calculate $\Delta c/\Delta t$ (Limmer et al., 2018). We kept measurements for all gases if the changes in CO_2 concentrations had an R^2 value of ≥ 0.90, assuming that the collars' micrometeorological conditions were stable enough to calculate all gas fluxes following established protocols (Capooci & Vargas, 2022; Petrakis et al., 2017). We could not make measurements when the collars were inundated by the highest tides,

resulting in 16 summer and 15 spring measurements. All 16 measurements passed the data quality threshold during the summer, but 7 of the 15 measurements obtained during the spring were below our threshold and, therefore, not included.

3.2.5 Statistical Analysis

Relationships between any two variables were assessed using bivariate linear regression (α=0.05). In addition, repeated measures analysis of variance (ANOVA) was performed to determine differences in tidal channel surface water and porewater biogeochemistry between data grouped in a variety of ways, including by hydraulic gradient direction (i.e., toward the channel or toward the channel bank soil) and groundwater direction (i.e., rising or falling). Significant differences between data groups were defined as having a p-value <0.05 and are represented with a p-value when only two groups are being assessed. When more than two data groups were evaluated, a repeated measures ANOVA was performed with a post hoc Tukey HSD test with significant differences between groups shown as different letters. All statistical analyses were performed using JMP Pro 16 (Version 16.2).

3.3 Results

3.3.1 Surface Water and Groundwater Hydrology

Two high tides and two low tides were studied across the two 24-hr monitoring periods (Figure 3.1). The water elevations are reported as depth above (+) or below (-) the near channel soil surface in the summer and spring. Even though both summer and spring sampling events occurred during spring tides, the average height of the groundwater and surface water were significantly ($p<0.0001$) different between events. The summer mean groundwater level was higher (20.1cm±16.9) than the

spring (-7.3cm±11.9). The tidal channel mean level was also higher in the summer (37.4cm±44.8) than in the spring (13.3cm±48.4). The tidal channel amplitude in the summer was 137cm (-87cm to 50cm), while in the spring, it was 126cm (-86cm to 40cm). The groundwater amplitude in the summer was 53cm (-2cm to 51cm), while in the spring, it was 36cm (-23cm to 13cm). Notably, the groundwater level dropped minimally below the marsh surface (-2cm) and only for a short period in the summer, while the drop in groundwater level in the spring was more substantial (-23cm) and for hours at a time (Figure 3.1). While there were significant differences in surface water and groundwater amplitudes and ranges between summer and spring sampling campaigns, there were also differences in the hydraulic gradient between sampling events.

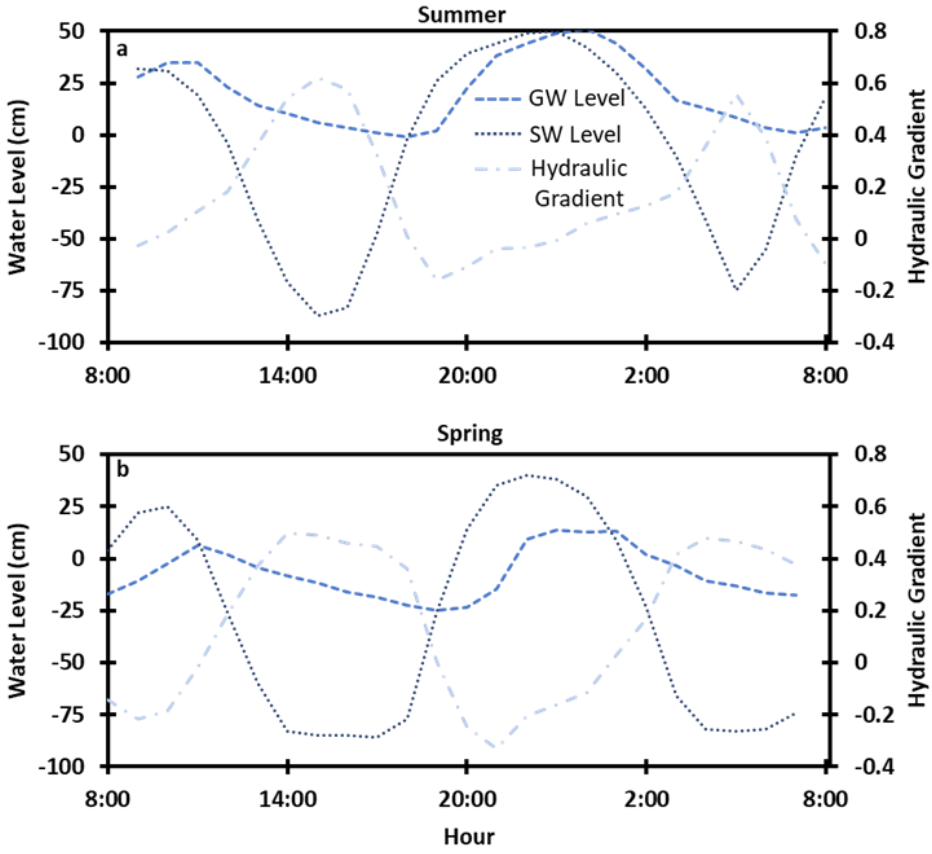

Figure 3.1 Groundwater (GW) in the channel bank, surface water (SW) in the tidal channel, and the hydraulic gradient between GW and SW across the 24-hour monitoring periods in the summer (a) and the spring (b). Water levels (GW and SW) are reported as depth above (+) or below (-) the near-channel soil surface.

Hydraulic gradients were derived from the groundwater and surface water elevations and varied over the 24-hour sampling events (Figure 3.2). The hydraulic gradient changed rapidly with tidal oscillation from negative gradients toward the channel bank soil to positive gradients toward the tidal channel. The mean hydraulic gradient in the summer (0.17±0.30) was not significantly different (p=0.51) from the mean hydraulic gradient in the spring (0.15±0.25). Both means were positive, which

indicates that, on average, the hydraulic gradient was driving flow toward the tidal channel during both summer and spring sampling events. In the spring, the mean hydraulic gradient was significantly ($p<0.0001$) higher during ebb tide (0.27±0.24) than during flood tide (-0.01±0.29). The summer hydraulic gradients were also significantly ($p=0.002$) different between ebb (0.23±0.21) and flood tides (0.09±0.24). Differences in surface water and groundwater hydrology between and within summer and spring sampling events affected porewater biogeochemistry.

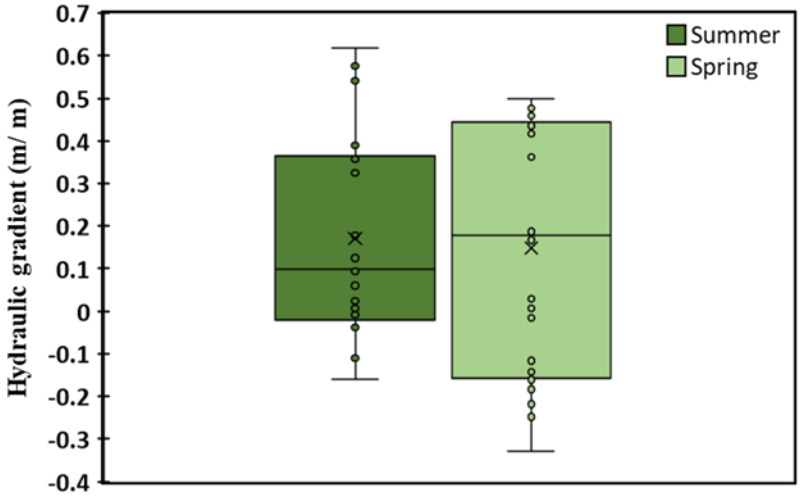

Figure 3.2 Box and whisker plot representing the large variation in hydraulic gradients during the summer and spring sampling events. Positive gradients indicate flow driven towards the tidal channel, while negative gradients indicate flow driven towards channel bank soils.

3.3.2 Porewater Biogeochemistry

Hydrologic tidal oscillation during the two sampling events altered porewater biogeochemistry. In-situ redox potentials from the continuous datalogger were lowest when the groundwater levels were highest, but differences existed between spring and

summer sampling events (Figure 3.3). The mean summer redox potential (-194.7mV±0.8) was significantly lower ($p<0.0001$) than the spring redox potential (220.7mV±255.5). In addition, the range of porewater redox potentials in the summer (-197mV to -193mV) was much lower than the range in the spring (-60mV to 557mV). Although the soil redox potential was significantly correlated to groundwater level in both seasons, the relationship was weaker in the summer ($R = 0.11$, $p<0.0001$) than in the spring ($R^2 = 0.40$, $p<0.0001$). In the summer, the groundwater level only dropped to 2cm below the ground surface, resulting in strongly reducing conditions throughout the entire 24-hour monitoring period. In the spring, the groundwater level dropped well below the surface (-23cm), causing spikes in soil redox potential during each low tide. These hydrologically driven redox oscillations affected redox-sensitive solutes.

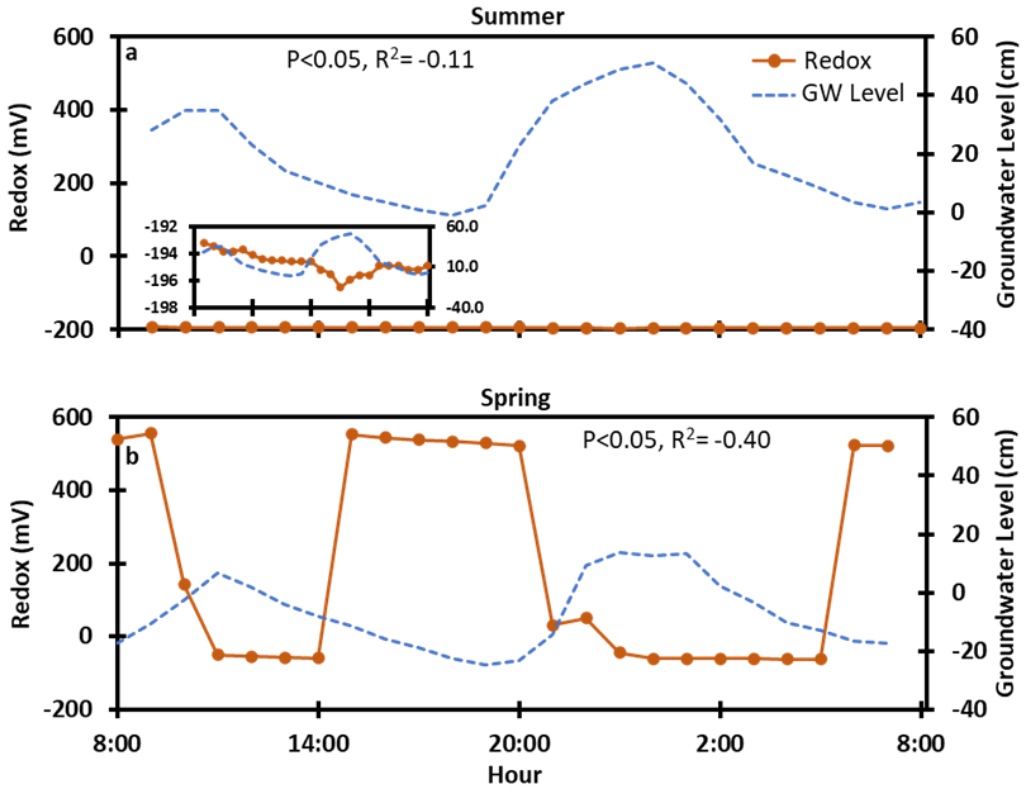

Figure 3.3 Redox conditions of soils were different between sampling events due to groundwater (GW) hydrology. In-situ redox at 18cm below ground surface plotted against groundwater level for summer (a) and spring (b). P-value and R2 result from a bivariate linear regression between groundwater and redox. The inset in (a) has a y-axis range of only 6mV to stress how little variation in redox there was during the summer sampling event when the groundwater level was higher.

Porewater data were assessed based on whether the groundwater level rose or fell during sampling (Table 3.1). In the spring, reduced Fe (Fe^{2+}) had a significantly higher mean when the groundwater level was rising (0.04mM±0.04) compared to when the groundwater level was falling (0.02mM±0.02). Summer Fe^{2+} concentrations did not change between falling (0.03mM±0.02) and rising (0.03mM±0.02) groundwater levels, consistent with minimal redox oscillation in the summer. In the

spring, DOC was significantly higher during rising groundwater (1.4mM±1.5) compared to falling groundwater (0.88±0.28), while in the summer, there was no significant difference in DOC concentrations between falling (2.1mM±0.8) and rising (2.0mM±0.6) groundwater. Furthermore, Fe^{2+} and DOC form a positive and significant relationship during both flood and ebb tide in the summer while only forming a significant relationship in the spring during flood tide (Figure 3.4). While porewater Fe^{2+} and DOC were affected by the tidal oscillation and thus redox state of the soils, porewater biogeochemistry also changed with depth.

Table 3.1 Results of repeated measures ANOVA from averaged porewater data between periods when the groundwater was either rising or falling in the summer and spring. Numbers are the means among all four rhizons (± SD). Significant differences ($p<0.05$) are indicated in bold.

Variable	Summer			Spring		
	Falling Groundwater	Rising Groundwater	P-Value	Falling Groundwater	Rising Groundwater	P-Value
Fe^{2+} (mM)	0.03(0.02)	0.03(0.02)	0.98	0.02(0.02)	0.04(0.04)	**0.002**
Sulfide (mM)	0.002(0.003)	0.003(0.001)	**0.02**	0.004(0.01)	0.004(0.0004)	0.89
pH	8.19(0.50)	8.32(0.59)	0.40	7.50(0.32)	7.42(0.18)	0.20
Salinity (ppt)	7.39(0.67)	7.24(0.90)	0.66	8.64(1.06)	9.26(1.63)	0.11
Sr	0.97(0.24)	0.95(0.16)	0.51	1.09(0.47)	0.95(0.37)	0.18
ABS_{254}	0.87(0.27)	0.93(0.39)	0.43	0.21(0.07)	0.21(0.08)	0.92
Coble A	7.37(1.68)	7.45(2.03)	0.84	2.14(0.57)	2.21(0.64)	0.57
Coble C	3.89(0.92)	4.00(1.21)	0.62	1.11(0.31)	1.13(0.35)	0.79
HIX	8.35(2.59)	8.37(2.92)	0.97	4.13(1.30)	3.73(1.66)	0.24

BIX	0.58(0.02)	0.57(0.02)	0.24	0.69(0.02)	0.69(0.03)	0.39
DOC (mM)	2.06(0.82)	2.04(0.61)	0.92	0.88(0.28)	1.44(1.54)	**0.05**
DIC (mM)	5.30(1.74)	5.19(2.02)	0.78	2.49(0.70)	2.58(0.79)	0.61
TC (mM)	7.36(2.12)	7.23(2.21)	0.79	3.37(0.67)	4.01(1.32)	**0.01**
TN (mM)	0.09(0.03)	0.10(0.04)	0.10	0.07(0.07)	0.13(0.11)	**0.004**
OC:N	31.02(28.54)	24.20(14.31)	0.14	20.97(18.74)	14.91(13.60)	0.10
SUVA254	0.38(0.20	0.40(0.15)	0.67	0.25(0.08)	0.21(0.09)	0.07
E2:E3	5.72(1.63)	5.69(1.13)	0.93	11.04(16.66)	13.87(14.67)	0.43

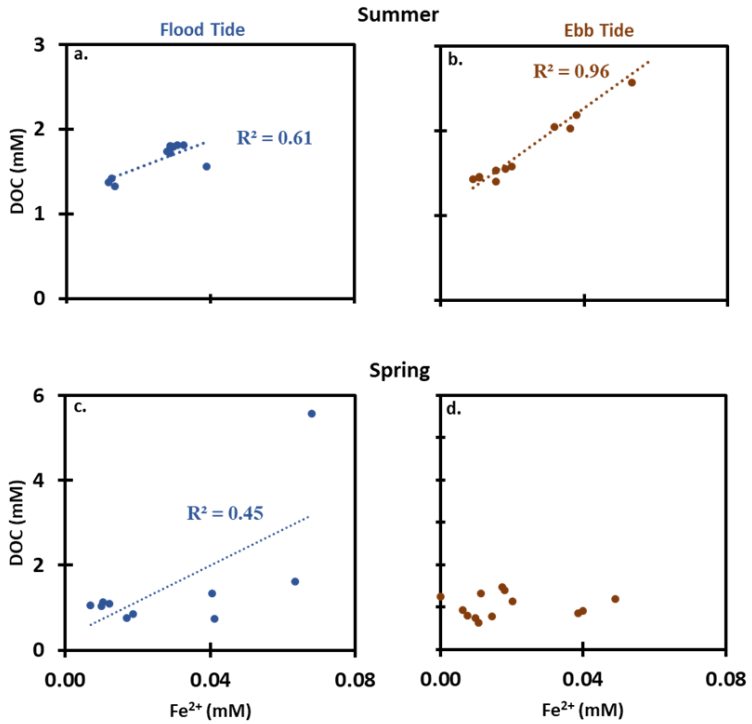

Figure 3.4 Linear correlations between DOC and Fe^{2+} for the summer (a-b) and the spring (c-d) from porewater samples at the 30cm channel bank rhizon (R-30). The data has been split up based on periods of ebb and flood tides. R^2 values result from a bivariate linear regression where $p<0.05$ for a-c, but not d.

Porewater variables changed with depth and proximity from the channel and differed between spring and summer sampling campaigns (Figure 5). In the summer, porewater pH increased with depth and was highest at R-Int. Fe^{2+} decreased with depth and distance from the tidal channel and was lowest at the interior rhizon, while DOC did not change with depth but was highest at R-Int. DIC increased with depth and was highest at R-Int, while TN did not change with depth and was lowest at R-Int. The DOC:TN ratio was approximately three times greater at R-Int than channel bank rhizons (R-6, R-18, R-30). R-Int had a stronger terrestrial C signal than the other three rhizons. Abs_{254}, a proxy for aromatic DOC, increased with depth but was greatest at R-Int. E_2:E_3, inverse to molecular weight, was greatest at the surface and decreased with depth. This indicates that DOC aromaticity and molecular weight increase with depth and distance from the tidal channel. Terrestrial C signals derived from EEMs indices (Coble A and C) also increased with depth and distance from the tidal channel, while the Biological Index (BIX) did not change with the rhizon location.

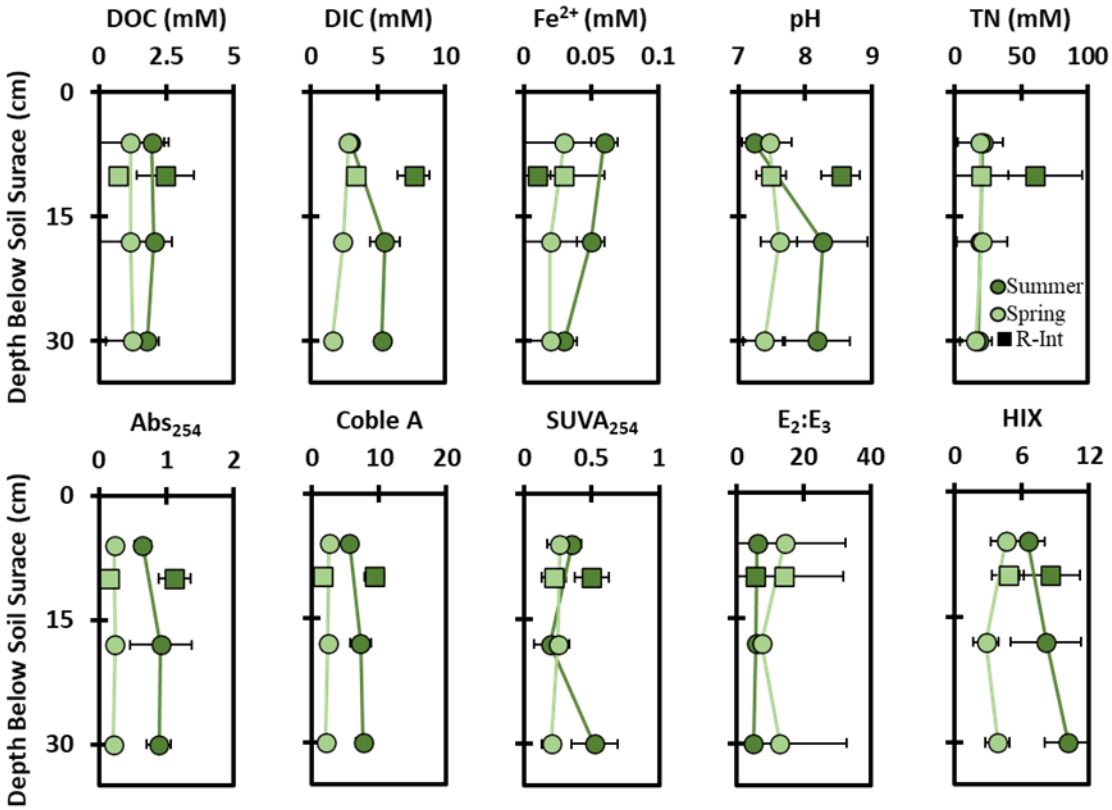

Figure 3.5 Depth profiles for rhizons placed horizontally in the channel bank at -6cm (R-6), -18cm (R-18), and -30cm (R-30) relative to the channel bank soil surface. The interior rhizon (R-Int) placed vertically into the soil approximately 1m from the channel bank is plotted as its own point at 10cm. The points represent the average across the 24-hour sampling (±SD).

The porewater results from the spring and summer sampling events differed. In the spring, concentrations of Fe^{2+} did not change with depth, nor did DOC. Unlike the summer, spring DIC concentrations decreased with depth, but R-Int still had the highest mean DIC value. There was no change in the DOC:TN ratio with depth in spring. Spring UV-VIS data had different patterns with depth and distance from the channel than in the summer. Abs_{254} did not change with depth and was lowest at R-Int.

Coble A decreased with depth and was lowest at R-Int during spring, opposite from what was observed in the summer. This indicates that terrestrial C decreased with depth and with distance from the tidal channel in the spring. The BIX remained consistent with depth and distance from the channel in spring.

In the spring, porewater concentrations of Fe^{2+} were lower than in the summer, though this difference was not significant (Table 3.2). DOC concentrations were significantly lower in the spring than in the summer, as was the DOC:N ratio. The pH was higher in the summer, while the salinity was lower. The spring Abs_{254} mean was approximately three times lower than in the summer, while the E_2:E_3 ratio was about twice as high in the spring. This indicates that spring DOC was less aromatic with a lower molecular weight than summer DOC. Coble A and C peaks were approximately three times lower in the spring. The BIX was significantly higher in the spring than in the summer, indicating that spring DOC has a higher microbial source.

Table 3.2 Results of repeated measures ANOVA of porewater data between spring and summer sampling events. Numbers are the means across the 24hr sampling events (± SD). Significant differences ($p<0.05$) are indicated in bold.

Variable	Spring	Summer	P-value
Fe^{2+} (mM)	0.02(0.03)	0.03(0.02)	0.14
Sulfide (mM)	0.004(0.006)	0.003(0.001)	0.37
pH	7.47(0.28)	8.23(0.54)	**<0.0001**
Salinity (ppt)	8.85(1.30)	7.33(0.76)	**<0.0001**
Sr	1.04(0.44)	0.96(0.21)	0.16
ABS_{254}	0.21(0.07)	0.89(0.32)	**<0.0001**

Coble A	2.16(0.59)	7.40(1.82)	**<0.0001**
Coble C	1.12(0.32)	3.93(1.03)	**<0.0001**
HIX	3.99(1.44)	8.36(2.71)	**<0.0001**
BIX	0.69(0.03)	0.58(0.02)	**<0.0001**
DOC (mM)	1.07(0.97)	2.05(0.74)	**<0.0001**
DIC (mM)	2.52(0.73)	5.25(1.84)	**<0.0001**
TC (mM)	3.59(0.99)	7.31(2.14)	**<0.0001**
TN (mM)	0.09(0.09)	0.09(0.03)	0.81
OC:N	18.70(17.16)	28.37(24.16)	**0.003**
SUVA254	0.23(0.08)	0.39(0.19)	**<0.0001**
E2:E3	12.02(15.97)	5.70(1.45)	**0.001**

3.3.3 Surface Water Biogeochemistry

Seasonal differences in the biogeochemistry of the tidal channel surface water were apparent, as most measured variables significantly differed across summer and spring sampling events (Table 3.3). Tidal channel DOC levels and the terrestrial signal (Coble A & C) were about twice as high in the summer than in the spring. Abs_{254} was significantly higher in the summer, indicating that summer surface water DOC was more aromatic than in the spring. TN levels were significantly higher in the spring than in the summer by an order of magnitude. The BIX was higher in the spring, indicating that spring surface water DOC had an increased marine-like signature. Continuous water quality data (salinity, pH, redox, temperature, dissolved oxygen, turbidity) was also collected in the tidal channel. All continuously measured variables were significantly different ($p<0.05$) between seasons (Figure B.3). Salinity (12.4 ppt±4.7) was higher in spring than in summer (7.5ppt±3.9) and, for both seasons,

tended to increase with the rising tide. The pH was higher in the spring (7.2±0.4) than in the summer (7.0±0.3), while redox potential was lower in the spring (-30.5mV±21.8) than in the summer (-2.1mV±15.5), though both seasons on average had reducing surface water. Spring surface water temperatures (23.6°C±2.5) were cooler than in the summer (25.2°C ±1.2), leading to higher dissolved oxygen levels in the spring (5.7mg L-1 ±5.3) than in the summer (2.7mg L-1 ±1.9). Turbidity values were almost twice as high in the spring (73.7NTU±32.11) than in the summer (41.0NTU±21.4).

Table 3.3 Results of repeated measures ANOVA from tidal channel surface water data between summer and spring sampling events. Numbers are the means across the 24hr sampling events (± SD). Significant differences ($p<0.05$) are indicated in bold.

Variable	Spring	Summer	P-value
Fe^{2+} (mM)	0.01(0.01)	0.01(0.01)	0.21
Sulfide (mM)	0.01(0.003)	0.002(0.001)	**<0.0001**
pH	7.10(0.10)	6.65(0.10)	**0.002**
Salinity (ppt)	9.15(3.22)	7.00(3.38)	**0.03**
Sr	1.14(0.71)	0.86(0.11)	0.07
ABS_{254}	0.22(0.07)	0.38(0.12)	**<0.0001**
Coble A	1.72(0.75)	2.96(1.04)	**<0.0001**
Coble C	0.88(0.42)	1.57(0.47)	**<0.0001**
HIX	4.27(1.89)	6.36(1.79)	**0.0003**
BIX	0.70(0.06)	0.62(0.04)	**<0.0001**
DOC (mM)	0.66(0.17)	0.96(0.23)	**<0.0001**
DIC (mM)	1.35(0.43)	1.28(0.67)	0.64

TC (mM)	2.02(0.57)	2.24(0.73)	0.25
TN (mM)	0.17(0.13)	0.04(0.02)	**<0.0001**
OC:N	9.27(16.01)	29.41(18.49)	**0.0002**
SUVA254	0.34(0.10)	0.39(0.08)	**0.03**
E2:E3	5.0(1.14)	5.36(0.70)	0.20

Surface water data was further assessed based on the hydraulic gradient between surface and groundwater. Positive gradients drive flow toward the channel, while negative gradients drive the flow into the channel bank. Tidal channel Fe^{2+} concentration increased significantly with the hydraulic gradient during spring and summer (Figure 6). DOC and the Coble peaks (A & C) also increased significantly with hydraulic gradient, but only in the spring. In contrast, BIX (R2=0.31), S_r (R^2=0.19), and salinity (R^2=0.29) formed significant negative relationships with the hydraulic gradient in the spring only. In the summer, BIX, S_r, and salinity did not include significant relationships with hydraulic gradient.

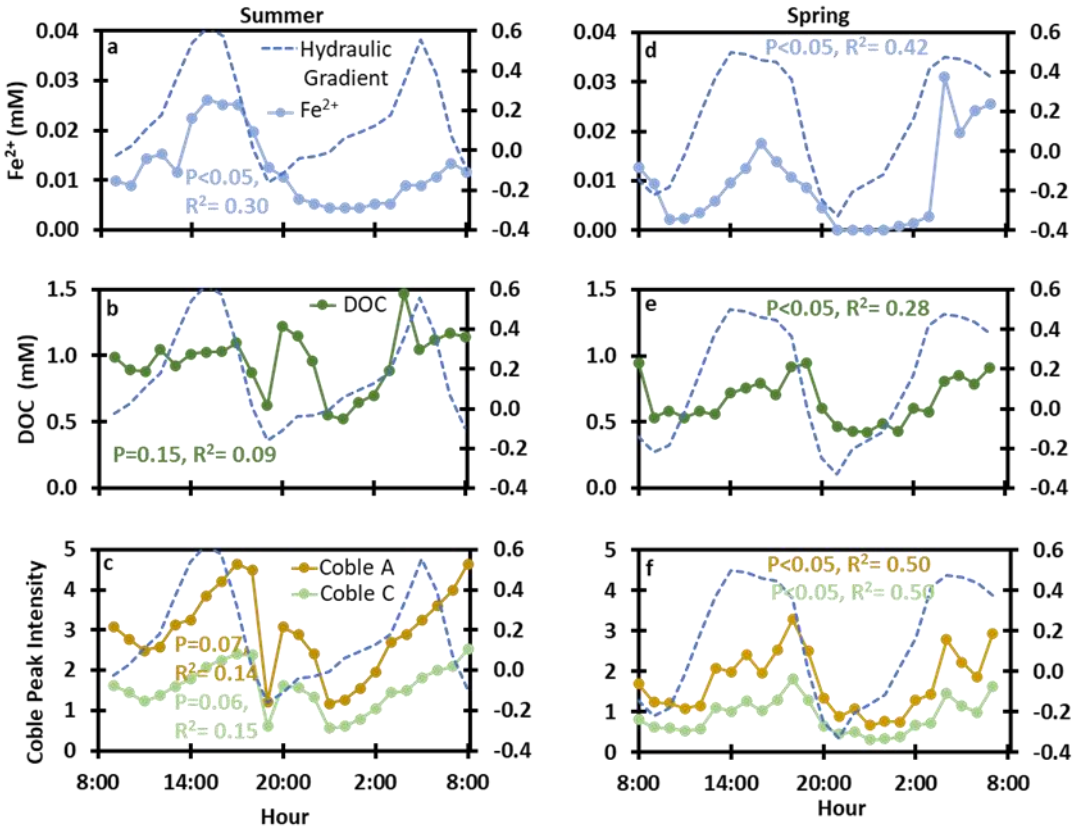

Figure 3.6 Plots of the hydraulic gradient with biogeochemical variables from tidal channel surface water samples. Plots a-c are from the summer, while d-f are from the spring. P-values and R^2 values result from bivariate linear regression between biogeochemical variables and the gradient.

Significant differences in means of many of the measured biogeochemical variables between times of positive and negative hydraulic gradients were observed in the spring (Table 3.4). During the spring sampling event, there were significantly higher Fe^{2+}, DOC, DIC, Coble A & C peaks, HIX, and Abs_{254} in the channel when the hydraulic gradient was driving flow toward the channel than when the flow was into the channel bank. In contrast, when the gradient drove into toward the bank, surface

water BIX, S_r, and salinity were significantly higher. This was not the case during the summer sampling event, as there were no significant differences in biogeochemistry between hydraulic gradient directions (Table 3.4), except for total nitrogen (TN). These results indicate differences in the source and concentration of solutes in the channel based on the flow direction between the marsh platform groundwater and tidal channel surface water, but these patterns changed between summer and spring sampling events.

Table 3.4 Results of repeated measures ANOVA from tidal channel surface water data between periods when the hydraulic gradient was either towards the channel (+) or the channel bank soil in the summer and spring. Note. Numbers are the means (± SD). Significant differences ($p<0.05$) are indicated in bold.

	Summer			**Spring**		
Variable	Towards Channel	Towards Soil	P-Value	Towards Channel	Towards Soil	P-Value
Fe^{2+} (mM)	0.01(0.01)	0.01(0.00)	0.12	0.01(0.01)	0.004(0.00)	**0.01**
Sulfide (mM)	0.002(0.00)	0.002(0.00)	0.65	0.01(0.00)	0.01(0.00)	0.30
pH	6.62(0.69)	6.72(0.34)	0.71	7.17(0.27)	6.99(0.28)	0.14
Salinity (ppt)	7.28(3.11)	6.31(4.16)	0.53	7.93(2.68)	11.18(3.12)	**0.01**
Sr	0.88(0.11)	0.83(0.09)	0.33	0.92(0.20)	1.50(1.07)	**0.04**
ABS_{254}	0.38(0.11)	0.36(0.16)	0.70	0.25(0.07)	0.17(0.05)	**0.007**
Coble A	3.09(0.97)	2.63(1.21)	0.34	2.08(0.70)	1.11(0.32)	**0.001**
Coble C	1.64(0.54)	1.40(0.68)	0.38	1.09(0.39)	0.54(0.16)	**0.001**
HIX	6.60(1.76)	5.76(1.89)	0.31	4.91(2.00)	3.19(1.11)	**0.03**
BIX	0.62(0.04)	0.62(0.06)	0.93	0.67(0.05)	0.75(0.05)	**0.003**
DOC (mM)	0.96(0.22)	0.95(0.26)	0.90	0.73(0.15)	0.56(0.16)	**0.02**

DIC (mM)	1.41(0.74)	0.95(0.26)	0.13	1.51(0.47)	1.09(0.14)	**0.02**
TC (mM)	2.38(0.81)	1.90(0.35)	0.15	2.24(0.59)	1.65(0.29)	**0.01**
TN (mM)	0.04(0.01)	0.05(0.03)	**0.04**	0.16(0.15)	0.18(0.12)	0.73
OC:N	32.90(20.23)	20.94(10.00)	0.15	11.66(19.83)	5.57(6.34)	0.39
SUVA254	0.40(0.08)	0.37(0.09)	0.38	0.34(0.06)	0.33(0.15)	0.72
E2:E3	5.33(0.68)	5.44(0.81)	0.73	5.12(0.78)	4.81(1.61)	0.54

3.3.4 Soil Trace Gas Fluxes

Soil trace gases from the channel bank were measured to assess horizontal gas movement seasonally and with hydrologic oscillation (Figure 3.7). In the summer, CO_2 flux from the 10cm collar was significantly ($p<0.0001$) higher (0.08µmol m^{-2} s^{-1} ±0.06) than in the spring (0.02µmol m^{-2} s^{-1} ±0.02) but this trend was opposite for the 30cm collar where CO_2 flux was higher in the spring (0.12µmol m^{-2} s^{-1} ±0.16) than in the summer (0.08µmol m^{-2} s^{-1} ±0.03), but these means were not significantly different ($p=0.12$). The CH_4 flux from the 10cm collar was significantly ($p<0.0001$) higher in the summer (0.47nmol m^{-2} s^{-1} ±0.61) than in the spring (0.02nmol m^{-2} s^{-1} ±0.04), while the 30cm collar was not significantly ($p=0.36$) different between spring (1.18nmol m^{-2} s^{-1} ±2.73) and summer (1.63nmol m^{-2} s^{-1} ±1.38). DMS from the 10cm collar was significantly ($p<0.0001$) higher in the summer (0.38nmol m^{-2} s^{-1} ±0.26) than in the spring (0.10nmol m^{-2} s^{-1} ±0.09), while the 30cm collar was also significantly ($p<0.0001$) higher in the summer (0.45nmol m^{-2} s^{-1} ±0.24) than in the spring (0.14nmol m^{-2} s^{-1} ±0.11). Variability in the gas flux data is not only apparent between sampling events but also between the depths, particularly for CH_4. When spring and summer datasets are combined, the 30cm collar (1.90nmol m^{-2} s^{-1} 3±2.71) emitted significantly more CH_4 than the 10cm collar (0.27nmol m^{-2} s^{-1} ±0.52), while there was

no significant difference between depths for CO_2 and DMS. Trace gas fluxes changed not only with seasonality and depth but also with groundwater level oscillation.

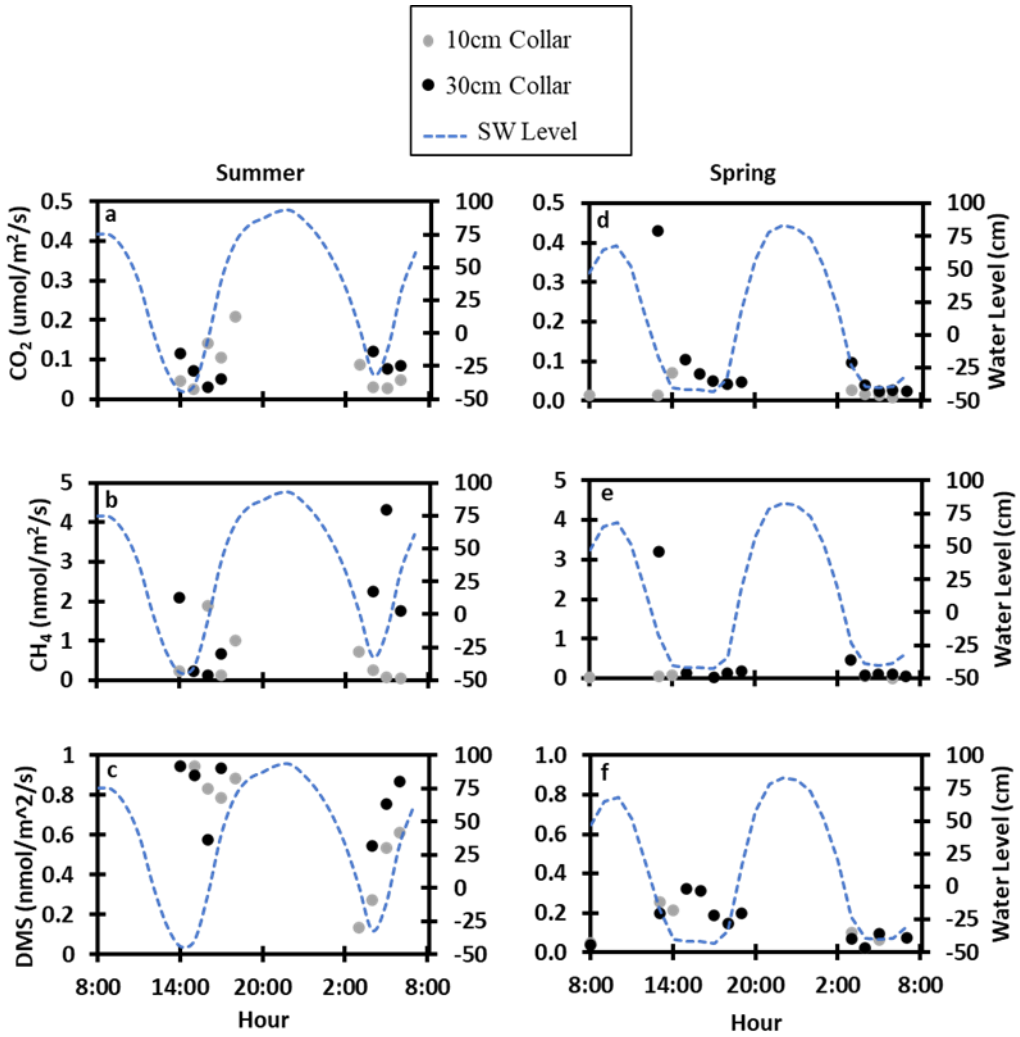

Figure 3.7 Plots of soil gas (CO_2, CH_4, DMS) fluxes with tidal channel surface water (SW) oscillation. Plots a-c are from the summer, while d-f are from the spring. Fluxes are represented as points instead of lines due to being unable to sample across the entire tidal cycle since the flux collars were underwater at higher tidal stages.

We observed several significant relationships between the groundwater level and trace gas fluxes. In the spring, DMS flux at the 10cm collar increased significantly (R^2=0.52, p<0.0001) with the groundwater table elevation. A similar positive relationship with groundwater level exists with CO_2 at the 30cm collar in the summer (R^2=0.51, p<0.0001). When spring and summer datasets are combined, DMS is significantly and positively correlated with groundwater level at both the 10cm collar (R^2=0.27) and the 30cm collar (R^2=0.51). CH_4 did not form any significant relationship with groundwater level. These positive relationships between groundwater level and DMS and CO_2 flux suggest a mechanism in which these gases are likely pushed upward and outward from the channel bank with the tides.

3.4 Discussion

3.4.1 Variability of CDOM Across Seasons

The spring and summer sampling events had significantly different chromophoric dissolved organic carbon (CDOM) concentrations and properties in both the porewater and tidal channel surface water, indicating high seasonal variability of CDOM concentration, source, and processing. These peaks correlate well with soil humics and terrestrially derived C (Baker et al., 2008; Cory et al., 2010). Indices such as S_r and the BIX correlate well with marine-derived microbial C, such as phytoplankton from the adjacent bay (Helms et al., 2008; Huguet et al., 2009). In the spring, the CDOM signature observed in both the porewater and surface water from the tidal channel indicates more algal contributions, as reflected by a higher BIX and Sr than in summer. This could be caused by benthic microalgae growing on the marsh platform surface because the soil surface would be fully shaded from the cordgrass in

summer. In addition, the OC:N ratio in the spring (18.70) is much closer to a marine algal source of ~7 than in the summer (28.37), indicating that spring CDOM is a mixture of both algal and terrestrial materials. By the summer, Spartina is well established and likely exudes high amounts of C into the porewaters. This is reflected in the much higher average porewater DOC concentration and OC:N ratio in the summer and the higher DOC concentration in the channel. Fresh inputs of C will stimulate soil microbial processing of CDOM, yielding an increased humic-like signature. The data reflects these observations because the summer CDOM signature is more terrestrial, humic, and aromatic. These data demonstrate changes in the characteristics of the porewater CDOM with potential implications for the microbial communities in marsh porewaters and for tidal channel waters to which they may be laterally exported. It is essential to consider the temporal variability of lateral and horizontally- fluxed C because the source, characteristics, and concentration change significantly between seasons. While these changes in CDOM seem to be related to primary productivity and seasonality, our sampling design represents only one time point in each season. Therefore, we cannot rule out alternative explanations, such as changes in hydraulic gradients and tidal flooding regimes. We suggest future studies link porewater and surface water horizontal exchange over extended periods.

3.4.2 Fe Oxides Affect DOC Mobility

We hypothesized that Fe oxides stabilize DOC in the solid phase during periods of soil oxidation (ebb tide), while these Fe-DOC associations dissolve during periods of soil reduction (flood tide). Our data support this hypothesis and provide insight into these tidally driven chemical processes affecting the horizontal transport of DOC. During flood tide in both the spring and summer events, porewater DOC and

Fe^{2+} form significant positive linear relationships. This can be interpreted as the destabilization of Fe-DOC solid-phase assemblages as Fe-reducing bacteria reductively dissolve C-bearing Fe oxides under reducing conditions during flood ties, causing Fe and DOC to enter the solution phase together (Hagedorn et al., 2000; Wordofa et al., 2019). The positive relationship between Fe^{2+} and DOC was expected during periods of flood tide when tidal inundation causes several hours of reducing soil conditions. The summer sampling event experienced flooded conditions and strongly reducing soil conditions throughout the entire 24-hr monitoring period due to the higher tide. Because the strongly reducing redox potential of the soils did not change between flood and ebb tide during the summer sampling event, the Fe and DOC likely remained in solution throughout the entire 24-hr monitoring period, as evidenced by the significant relationships between Fe^{2+} and DOC concentrations for both flood and ebb tide in the summer (Figure 3.4).

As the tide receded and ebb tide persisted, oxygen flowed into the soil pore spaces, causing an increase in soil redox potential. This was evident in the spring during ebb tide and was the point at which the relationship between porewater Fe^{2+} and DOC did not form a significant positive relationship. Previously dissolved Fe^{2+} may have reacted with oxygen, causing Fe^{2+} and DOC to coprecipitate and thus lower concentration in the solution phase. Coprecipitation can occur in less than 30 minutes of oxygen exposure and tends to occur readily in environments that experience periodic flooding and drying (Sodano et al., 2017). The conditions necessary for this reaction were exhibited during the spring sampling event when the groundwater level dropped well below the surface (-23cm) and allowed the soil redox to increase to ~550 mV. In contrast, these conditions were not detected during the summer sampling event

when groundwater levels remained near or above the surface during the 24-hour monitoring period. These results highlight hydrologic control on Fe-oxide retention mechanisms of DOC in variably flooded environments, and the differences between seasons and tidal patterns likely contribute to the high uncertainty of lateral C movement from coastal environments (Cavallaro et al., 2018). Our evidence suggests that coprecipitation and dissolution between ebb and flood tides partially control the horizontal flux of DOC to the tidal channel. In addition, because Fe oxides are sensitive to flood duration and thus soil redox, sea level rise may decrease the coprecipitation rate by limiting marsh soil oxygen exposure.

3.4.3 Horizontal Exchange of Solutes Between the Marsh Platform and the Tidal Channel

Our data support the hypothesis that the hydraulic gradient controls the physical exchange of solutes between the channel bank groundwater and the surface water of the tidal channel, regulating the concentration and source of C horizontally fluxed to tidal channels. We observed significant relationships between the concentration and source of C in the tidal channel and the direction and magnitude of solute flow driven by the hydraulic gradient. In the spring, DOC, DIC, and Fe^{2+} were significantly higher in the tidal channel when the hydraulic gradient drove flow toward the channel (Table 3.4). Our porewater data show that the groundwater is a substantial source of these solutes. In addition, tidal channel solute concentrations increased as the hydraulic gradient increased (Figure 3.6), consistent with an increased flux of solute-rich groundwater to the channel. Groundwater flowing into the tidal channel during positive gradients results in increased CDOM in the surface water. Our EEMs UV-VIS data support this interpretation as Coble A and C peaks were twice as high in

the channel during periods of positive gradients compared to negative gradients and correlated significantly with the hydraulic gradient (R^2=0.50, R^2=0.50). While positive gradients increased channel solutes, including C, that had more of a terrestrial CDOM signature, negative gradients led to an increase of marine-like C in the tidal channel.

Periods of negative gradients corresponded with periods when surface water was significantly saltier and higher in Sr and BIX intensities than periods of positive gradients. Therefore, water infiltrating the marsh platform when the flow is driven into the channel bank soils has more of a marine component. While the marine signatures (i.e., higher BIX, higher S_r) are more intense during negative gradients, terrestrial signatures (i.e., HIX, Coble Peaks) are still appreciable during these periods. Therefore, the tidal channel is a mixture of allochthonous marine-derived C and autochthonous marsh-derived C, but the relative contributions of each source (marine vs. terrestrial) change with tidal oscillation.

While the spring channel solutes showed clear differences and relationships with the hydraulic gradient, the summer data set did not. Porewater solute concentrations in the tidal channel did not form significant relationships with hydraulic gradient and were not significantly different between positive and negative gradients, nor were the characterization properties (Coble A & C, S_r, BIX) (Table 3.4). While the hydraulic gradient in the summer was similar in range to the spring, the groundwater level rarely dropped below the soil surface. This indicates that although the sampling events took place on the same tidal cycle event (i.e., spring tide), the hydrologic processes involved in horizontal exchange likely differed. In the summer, higher high tides caused overtopping of the bank soils and overland flow, causing the marsh platform to remain fully saturated with flooded conditions above it, even as the

channel receded, taking much longer to drain than in the spring. In the overtopping case, groundwater would flow into the channel during the ebb and low tide, driven by the flooded conditions and higher groundwater heads, but would be replenished by vertical infiltration of floodwater into the marsh sediments. Thus, a more expansive zone of groundwater adjacent to the channel would be flushed with channel water, reducing the influence of groundwater discharge on channel water quality due to greater similarity in solute concentrations. This could explain the weaker relationships between hydraulic gradient and tidal channel solutes in the summer because the horizontal exchange would be composed of higher amounts of infiltrated channel water rather than porewater-derived solutes. This could be another source of uncertainty because the horizontal exchange of laterally fluxed C may differ even during the same tidal events.

Based on discharge values from the marsh platform to the tidal creek calculated from a previous study at the field site (Guimond et al., 2020) and the average porewater concentrations during gradients driving flow towards the creek in this study, we estimate per meter of tidal channel that 0.12±0.03 g DOC day^{-1} and 0.31±0.11 g DIC day^{-1} are horizontally exported into the tidal channel in the summer, while 0.01±0.002 g DOC day^{-1} and 0.02±0.004 g DIC day^{-1} are horizontally exported into the tidal channel in the spring. Differences in flux rates are attributable to seasonal C concentrations and hydraulic conductivity differences between summer and spring which are partially driven by crab burrow activity (Guimond et al., 2020). These findings indicate that the horizontal exchange of solutes at the marsh-tidal channel interface partially drives variability in lateral C flux.

3.4.4 Trace Gas Fluxes are Influenced by Groundwater Oscillations

Lateral C fluxes tended to focus on particulate and dissolved C, often leaving out the assessment of trace gas fluxes which ultimately decrease the global cooling effect of stored C in coastal ecosystems (Santos et al., 2019). Trace gas fluxes from tidal channels may exceed vertical soil fluxes and require more attention because the mechanisms controlling emissions near channel banks are not fully understood (Trifunovic et al., 2020). We hypothesized that fluxes of horizontal gases from the channel bank are partially controlled by the rising and falling tides, whereby rising groundwater pushes gases up and outward from the channel bank. We found that several soil gases (CO_2, CH_4, DMS) were emitted from the channel bank and positively correlated with groundwater oscillation during certain tidal stages. DMS was strongly related to groundwater levels, suggesting a strong physical control of groundwater mainly during the spring at the 10cm collar (R^2=0.52), but it is known the temporal variability of this trace gas could be very large (Cappooci and Vargas 2022). Soil CO_2 fluxes also had an apparent positive relationship with groundwater level at 30cm collar in the summer (R^2=0.51). These findings indicate that the movement of soil trace gases out of the channel bank can be incorporated into future modeling efforts, although long-term (e.g., seasonal) patterns are likely a combination of hydrological patterns, temperature dependence and phenological stages of the ecosystem (Vázquez-Lule & Vargas, 2021). Because we could not measure trace gas fluxes during high water levels and only at discrete times, future studies should focus on automated measurements over longer-time periods to identify patterns and controls at multiple temporal scales (Capooci & Vargas, 2022).

3.5 Conclusion

The lateral C fluxes in tidal salt marshes may account for a substantial fraction of the net C flux, though current estimates remain highly uncertain. We propose several mechanisms that control the exchange of horizontal C between the tidal channel surface water and soil porewater interface that may help understand sources of uncertainty in lateral C flux. First, our porewater data show evidence of tidally driven chemical processes in which Fe oxides immobilize DOC during ebb tide and remobilize DOC during flood tide. Second, the concentration and source of C found in the tidal channel changed based on the hydraulic gradient (i.e., flow direction) between the tidal channel and the marsh platform. Third, CO_2, CH_4, and DMS flux horizontally from the channel bank, and fluxes tend to increase with rising groundwater. These physical and chemical processes show the importance of considering the horizontal transport of C on small spatial scales to better constrain large-scale lateral C budgets. The mechanisms highlighted here may help to improve and inform biogeochemical lateral C flux models.

REFERENCES

Abdul-Aziz, O. I., Ishtiaq, K. S., Tang, J., Moseman-Valtierra, S., Kroeger, K. D., Gonneea, M. E., et al. (2018). Environmental Controls, Emergent Scaling, and Predictions of Greenhouse Gas (GHG) Fluxes in Coastal Salt Marshes. Journal of Geophysical Research: Biogeosciences, 123(7), 2234–2256. https://doi.org/10.1029/2018JG004556

Adhikari, D., Sowers, T., Stuckey, J. W., Wang, X., Sparks, D. L., & Yang, Y. (2019). Formation and redox reactivity of ferrihydrite-organic carbon-calcium co-precipitates. Geochimica et Cosmochimica Acta, 244, 86–98. https://doi.org/10.1016/j.gca.2018.09.026

Baker, A., Bolton, L., Newson, M., & Spencer, R. G. M. (2008). Spectrophotometric properties of surface water dissolved organic matter in an afforested upland peat catchment. Hydrological Processes. https://doi.org/10.1002/hyp.6827

Bauer, J. E., Cai, W. J., Raymond, P. A., Bianchi, T. S., Hopkinson, C. S., & Regnier, P. A. G. (2013). The changing carbon cycle of the coastal ocean. Nature. https://doi.org/10.1038/nature12857

Berthelin, J., Laba, M., Lemaire, G., Powlson, D., Tessier, D., Wander, M., & Baveye, P. C. (2022). Soil carbon sequestration for climate change mitigation: Mineralization kinetics of organic inputs as an overlooked limitation. European Journal of Soil Science. https://doi.org/10.1111/ejss.13221

Bogard, M. J., Bergamaschi, B. A., Butman, D. E., Anderson, F., Knox, S. H., & Windham-Myers, L. (2020). Hydrologic Export Is a Major Component of Coastal Wetland Carbon Budgets. Global Biogeochemical Cycles, 34(8), 1–14. https://doi.org/10.1029/2019GB006430

van de Broek, M., Temmerman, S., Merckx, R., & Govers, G. (2016a). Controls on soil organic carbon stocks in tidal marshes along an estuarine salinity gradient. Biogeosciences, 13(24), 6611–6624. https://doi.org/10.5194/bg-13-6611-2016

van de Broek, M., Temmerman, S., Merckx, R., & Govers, G. (2016b). Controls on soil organic carbon stocks in tidal marshes along an estuarine salinity gradient. Biogeosciences, 13(24), 6611–6624. https://doi.org/10.5194/bg-13-6611-2016

Capooci, M., & Vargas, R. (2022). Diel and seasonal patterns of soil CO2 efflux in a temperate tidal marsh. Science of The Total Environment, 802, 149715. https://doi.org/10.1016/j.scitotenv.2021.149715

Capooci, M., Barba, J., Seyfferth, A. L., & Vargas, R. (2019). Experimental influence of storm-surge salinity on soil greenhouse gas emissions from a tidal salt marsh. Science of the Total Environment, 686, 1164–1172. https://doi.org/10.1016/j.scitotenv.2019.06.032

Cavallaro, N., Shrestha, G., Birdsey, R., Mayes, M. A., Najjar, R. G., Reed, S. C., et al. (2018). Second State of the Carbon Cycle Report. (N. Cavallaro, G. Shrestha, R. Birdsey, M. A. Mayes, R. G. Najjar, S. C. Reed, et al., Eds.), Usgcrp. Washington, DC. https://doi.org/10.7930/Soccr2.2018

Charlson, R. J., Lovelock, J. E., Andreae, M. O., & Warren, S. G. (1987). Oceanic phytoplankton, atmospheric sulphur, cloud albedo and climate. Nature, 326(6114). https://doi.org/10.1038/326655a0

Chen, C., & Sparks, D. L. (2015). Multi-elemental scanning transmission X-ray microscopy-near edge X-ray absorption fine structure spectroscopy assessment of organo-mineral associations in soils from reduced environments. Environmental Chemistry, 12(1), 64–73. https://doi.org/10.1071/EN14042

Chen, C., Dynes, J. J., Wang, J., & Sparks, D. L. (2014). Properties of Fe-organic matter associations via coprecipitation versus adsorption. Environmental Science and Technology, 48(23), 13751–13759. https://doi.org/10.1021/es503669u

Chmura, G. L., Anisfeld, S. C., Cahoon, D. R., & Lynch, J. C. (2003). Global carbon sequestration in tidal, saline wetland soils. Global Biogeochemical Cycles, 17(4), 1111. https://doi.org/10.1029/2002GB001917

Chu, S. N., Wang, Z. A., Gonneea, M. E., Kroeger, K. D., & Ganju, N. K. (2018). Deciphering the dynamics of inorganic carbon export from intertidal salt marshes using high-frequency measurements. Marine Chemistry, 206(August), 7–18. https://doi.org/10.1016/j.marchem.2018.08.005

Cline, J. D. (1969). SPECTROPHOTOMETRIC DETERMINATION OF HYDROGEN SULFIDE IN NATURAL WATERS1. Limnology and Oceanography, 14(3), 454–458. https://doi.org/10.4319/lo.1969.14.3.0454

Cory, R. M., McNeill, K., Cotner, J. P., Amado, A., Purcell, J. M., & Marshall, A. G. (2010). Singlet oxygen in the coupled photochemical and biochemical oxidation of dissolved organic matter. Environmental Science and Technology. https://doi.org/10.1021/es902989y

Czapla, K. M., Anderson, I. C., & Currin, C. A. (2020). Net Ecosystem Carbon Balance in a North Carolina, USA, Salt Marsh. Journal of Geophysical Research: Biogeosciences, 125(10), 1–16. https://doi.org/10.1029/2019JG005509

Diefenderfer, H. L., Cullinan, V. I., Borde, A. B., Gunn, C. M., & Thom, R. M. (2018). High-frequency greenhouse gas flux measurement system detects winter storm surge effects on salt marsh. Global Change Biology, 24(12), 5961–5971. https://doi.org/10.1111/gcb.14430

Duarte, C. M. (2017). Reviews and syntheses: Hidden forests, the role of vegetated coastal habitats in the ocean carbon budget. Biogeosciences, 14(2), 301–310. https://doi.org/10.5194/bg-14-301-2017

Duarte, C. M., Dennison, W. C., Orth, R. J. W., & Carruthers, T. J. B. (2008). The charisma of coastal ecosystems: Addressing the imbalance. Estuaries and Coasts, 31(2), 233–238. https://doi.org/10.1007/s12237-008-9038-7

Duarte, C. M., Losada, I. J., Hendriks, I. E., Mazarrasa, I., & Marbà, N. (2013). The role of coastal plant communities for climate change mitigation and adaptation. Nature Climate Change, 3(11), 961–968. https://doi.org/10.1038/nclimate1970

Fettrow, S., Vargas, R., Seyfferth A. (2023) Experimentally simulated sea level rise destabilizes carbon-mineral associations in temperate tidal marsh soil. Biogeochemistry. https://doi.org/10.1007/s10533-023-01024-z

Gorham, C., Lavery, P., Kelleway, J. J., Salinas, C., & Serrano, O. (2021). Soil Carbon Stocks Vary Across Geomorphic Settings in Australian Temperate Tidal Marsh Ecosystems. Ecosystems, 24(2), 319–334. https://doi.org/10.1007/s10021-020-00520-9

Guimond, J. A., Seyfferth, A. L., Moffett, K. B., & Michael, H. A. (2020). A physical-biogeochemical mechanism for negative feedback between marsh crabs and carbon storage. Environmental Research Letters, 15(3), 034024. https://doi.org/10.1088/1748-9326/ab60e2

Guimond, J. A., Yu, X., Seyfferth, A. L., & Michael, H. A. (2020). Using Hydrological-Biogeochemical Linkages to Elucidate Carbon Dynamics in Coastal Marshes Subject to Relative Sea Level Rise. Water Resources Research, 56(2), 1–16. https://doi.org/10.1029/2019WR026302

Hagedorn, F., Kaiser, K., Feyen, H., & Schleppi, P. (2000). Effects of Redox Conditions and Flow Processes on the Mobility of Dissolved Organic Carbon and Nitrogen in a Forest Soil. Journal of Environmental Quality, 29(1), 288–297. https://doi.org/10.2134/jeq2000.00472425002900010036x

Hayes, D. J., Vargas, R., Alin, S., Conant, R. T., Hutyra, L. R., Jacobson, A. R., et al. (2018). The North American Carbon Budget. Second State of the Carbon Cycle Report. Second State of the Carbon Cycle Report (SOCCR2): A Sustained Assessment Report.

Helms, J. R., Stubbins, A., Ritchie, J. D., Minor, E. C., Kieber, D. J., & Mopper, K. (2008). Absorption spectral slopes and slope ratios as indicators of molecular weight, source, and photobleaching of chromophoric dissolved organic matter. Limnology and Oceanography. https://doi.org/10.4319/lo.2008.53.3.0955

Hill, A. C., Vázquez-Lule, A., & Vargas, R. (2021). Linking vegetation spectral reflectance with ecosystem carbon phenology in a temperate salt marsh. Agricultural and Forest Meteorology, 307. https://doi.org/10.1016/j.agrformet.2021.108481

Hinson, A. L., Feagin, R. A., Eriksson, M., Najjar, R. G., Herrmann, M., Bianchi, T. S., et al. (2017). The spatial distribution of soil organic carbon in tidal wetland soils of the continental United States. Global Change Biology, 23(12), 5468–5480. https://doi.org/10.1111/gcb.13811

Howard, J., Sutton-Grier, A., Herr, D., Kleypas, J., Landis, E., Mcleod, E., et al. (2017). Clarifying the role of coastal and marine systems in climate mitigation. Frontiers in Ecology and the Environment, 15(1), 42–50. https://doi.org/10.1002/fee.1451

Huguet, A., Vacher, L., Relexans, S., Saubusse, S., Froidefond, J. M., & Parlanti, E. (2009). Organic Geochemistry Properties of fluorescent dissolved organic matter in the Gironde Estuary. Organic Geochemistry, 40(6), 706–719. https://doi.org/10.1016/j.orggeochem.2009.03.002

IPCC. (2022). Climate Change: Impacts, Adaptation and Vulnerability. IPCC, xxiii–xxxiii. https://doi.org/10.4324/9781315071961-11

Limmer, M. A., Mann, J., Amaral, D. C., Vargas, R., & Seyfferth, A. L. (2018). Silicon-rich amendments in rice paddies: Effects on arsenic uptake and biogeochemistry. Science of The Total Environment, 624, 1360–1368. https://doi.org/10.1016/j.scitotenv.2017.12.207

Macreadie, P. I., Costa, M. D. P., Atwood, T. B., Friess, D. A., Kelleway, J. J., Kennedy, H., et al. (2021). Blue carbon as a natural climate solution. Nature Reviews Earth and Environment. https://doi.org/10.1038/s43017-021-00224-1

Mcleod, E., Chmura, G. L., Bouillon, S., Salm, R., Björk, M., Duarte, C. M., et al. (2016). A blueprint for blue carbon: toward an improved understanding of the role of vegetated coastal habitats in sequestering CO2. Frontiers in Ecology and the Environment, 9, 552–560. https://doi.org/https://www.jstor.org/stable/41479959

Najjar, R. G., Herrmann, M., Alexander, R., Boyer, E. W., Burdige, D. J., Butman, D., et al. (2018). Carbon Budget of Tidal Wetlands, Estuaries, and Shelf Waters of Eastern North America. Global Biogeochemical Cycles, 32(3), 389–416. https://doi.org/10.1002/2017GB005790

Nellemann, C., Corcoran, E., Duarte, C. M., Valdés, L., De Young, C., Fonseca, L., & Grimsditch, G. (2009). Blue Carbon - The Role of Healthy Oceans in Binding Carbon. https://doi.org/978-82-7701-060-1

O'Connor, J. J., Fest, B. J., Sievers, M., & Swearer, S. E. (2020). Impacts of land management practices on blue carbon stocks and greenhouse gas fluxes in coastal ecosystems—A meta-analysis. Global Change Biology, 26(3), 1354–1366. https://doi.org/10.1111/gcb.14946

Osburn, C. L., Mikan, M. P., Etheridge, J. R., Burchell, M. R., & Birgand, F. (2015). Seasonal variation in the quality of dissolved and particulate organic matter exchanged between a salt marsh and its adjacent estuary. Journal of Geophysical Research G: Biogeosciences, 120(7), 1430–1449. https://doi.org/10.1002/2014JG002897

Pearson, A. J., Pizzuto, J. E., & Vargas, R. (2016). Influence of run of river dams on floodplain sediments and carbon dynamics. Geoderma, 272. https://doi.org/10.1016/j.geoderma.2016.02.029

Petrakis, S., Seyfferth, A., Kan, J., Inamdar, S., & Vargas, R. (2017). Influence of experimental extreme water pulses on greenhouse gas emissions from soils. Biogeochemistry, 133(2), 147–164. https://doi.org/10.1007/s10533-017-0320-2

Santos, I. R., Maher, D. T., Larkin, R., Webb, J. R., & Sanders, C. J. (2019). Carbon outwelling and outgassing vs. burial in an estuarine tidal creek surrounded by mangrove and saltmarsh wetlands. Limnology and Oceanography. https://doi.org/10.1002/lno.11090

Santos, I. R., Burdige, D. J., Jennerjahn, T. C., Bouillon, S., Cabral, A., Serrano, O., et al. (2021). The renaissance of Odum's outwelling hypothesis in "Blue Carbon" science. Estuarine, Coastal and Shelf Science, 255(April), 107361. https://doi.org/10.1016/j.ecss.2021.107361

Schwertmann. (2020). Solubility and dissolution of iron oxides Author, 130(1), 1–25.

Serrano, O., Lovelock, C. E., B. Atwood, T., Macreadie, P. I., Canto, R., Phinn, S., et al. (2019). Australian vegetated coastal ecosystems as global hotspots for climate change mitigation. Nature Communications, 10(1). https://doi.org/10.1038/s41467-019-12176-8

Seyfferth, A. L., Bothfeld, F., Vargas, R., Stuckey, J. W., Wang, J., Kearns, K., et al. (2020). Spatial and temporal heterogeneity of geochemical controls on carbon cycling in a tidal salt marsh. Geochimica et Cosmochimica Acta, 282, 1–18. https://doi.org/10.1016/j.gca.2020.05.013

Sodano, M., Lerda, C., Nisticò, R., Martin, M., Magnacca, G., Celi, L., & Said-Pullicino, D. (2017). Dissolved organic carbon retention by coprecipitation during the oxidation of ferrous iron. Geoderma, 307(June), 19–29. https://doi.org/10.1016/j.geoderma.2017.07.022

Sowers, T. D., Adhikari, D., Wang, J., Yang, Y., & Sparks, D. L. (2018). Spatial Associations and Chemical Composition of Organic Carbon Sequestered in Fe, Ca, and Organic Carbon Ternary Systems. Environmental Science and Technology, 52(12), 6936–6944. research-article. https://doi.org/10.1021/acs.est.8b01158

Sowers, T. D., Stuckey, J. W., & Sparks, D. L. (2018). The synergistic effect of calcium on organic carbon sequestration to ferrihydrite. Geochemical Transactions, 19(1), 22–26. https://doi.org/10.1186/s12932-018-0049-4

Sowers, T. D., Holden, K. L., Coward, E. K., & Sparks, D. L. (2019). Dissolved Organic Matter Sorption and Molecular Fractionation by Naturally Occurring Bacteriogenic Iron (Oxyhydr)oxides. Environmental Science and Technology, 53(8), 4295–4304. research-article. https://doi.org/10.1021/acs.est.9b00540

Spivak, A. C., Sanderman, J., Bowen, J. L., Canuel, E. A., & Hopkinson, C. S. (2019). Global-change controls on soil-carbon accumulation and loss in coastal vegetated ecosystems. Nature Geoscience, 12(9), 685–692. https://doi.org/10.1038/s41561-019-0435-2

Stookey, L. L. (1970). Ferrozine-A New Spectrophotometric Reagent for Iron. Analytical Chemistry, 42(7), 779–781. https://doi.org/10.1021/ac60289a016

Sun, H., Jiang, J., Cui, L., Feng, W., Wang, Y., & Zhang, J. (2019). Soil organic carbon stabilization mechanisms in a subtropical mangrove and salt marsh ecosystems. Science of The Total Environment, 673, 502–510. https://doi.org/10.1016/j.scitotenv.2019.04.122

Tong, C., Luo, M., Huang, J., She, C., Li, Y., & Ren, P. (2020). Greenhouse gas fluxes and porewater geochemistry following short-term pulses of saltwater and Fe(III) in a subtropical tidal freshwater estuarine marsh. Geoderma, 369(March), 114340. https://doi.org/10.1016/j.geoderma.2020.114340

Trifunovic, B., Vázquez-Lule, A., Capooci, M., Seyfferth, A. L., Moffat, C., & Vargas, R. (2020). Carbon Dioxide and Methane Emissions From A Temperate Salt Marsh Tidal Creek. Journal of Geophysical Research: Biogeosciences, 125(8). https://doi.org/10.1029/2019JG005558

Tzortziou, M., Neale, P. J., Osburn, C. L., Megonigal, J. P., Maie, N., & Jaffé, R. (2008). Tidal marshes as a source of optically and chemically distinctive colored dissolved organic matter in the Chesapeake Bay. Limnology and Oceanography, 53(1), 148–159. https://doi.org/10.4319/lo.2008.53.1.0148

Vázquez-Lule, A., & Vargas, R. (2021). Biophysical drivers of net ecosystem and methane exchange across phenological phases in a tidal salt marsh. Agricultural and Forest Meteorology, 300, 108309. https://doi.org/10.1016/j.agrformet.2020.108309

Wang, J., & Wang, J. (2017). Spartina alterniflora alters ecosystem DMS and CH4 emissions and their relationship along interacting tidal and vegetation gradients within a coastal salt marsh in Eastern China. Atmospheric Environment, 167, 346–359. https://doi.org/10.1016/j.atmosenv.2017.08.041

Wang, Z. A., & Cai, W. (2004). Carbon Dioxide Degassing and Inorganic Carbon Export from a Marsh-Dominated Estuary(The Duplin River): A Marsh CO2 Pump, 49(2), 341–354.

Wang, Z. A., Kroeger, K. D., Ganju, N. K., Gonneea, M. E., & Chu, S. N. (2016). Intertidal salt marshes as an important source of inorganic carbon to the coastal ocean. Limnology and Oceanography, 61(5), 1916–1931. https://doi.org/10.1002/lno.10347

Winter, P. E. D., Schlacher, T. A., & Baird, D. (1996). Carbon flux between an estuary and the ocean: A case for outwelling. Hydrobiologia, 337(1–3), 123–132. https://doi.org/10.1007/BF00028513

Wollenberg, J. T., Biswas, A., & Chmura, G. L. (2018). Greenhouse gas flux with reflooding of a drained salt marsh soil. PeerJ, 2018(11), 1–21. https://doi.org/10.7717/peerj.5659

Wordofa, D. N., Adhikari, D., Dunham-Cheatham, S. M., Zhao, Q., Poulson, S. R., Tang, Y., & Yang, Y. (2019). Biogeochemical fate of ferrihydrite-model organic compound complexes during anaerobic microbial reduction. Science of the Total Environment, 668, 216–223. https://doi.org/10.1016/j.scitotenv.2019.02.441

Xin, P., Yuan, L.-R., Li, L., & Barry, D. A. (2011). Tidally driven multiscale pore water flow in a creek-marsh system. Water Resources Research, 47(7). https://doi.org/10.1029/2010WR010110

Yu, J., Dong, H., Li, Y., Wu, H., Guan, B., Gao, Y., et al. (2014). Spatiotemporal Distribution Characteristics of Soil Organic Carbon in Newborn Coastal Wetlands of the Yellow River Delta Estuary. CLEAN - Soil, Air, Water, 42(3), 311–318. https://doi.org/10.1002/clen.201100511

Zak, D., & Gelbrecht, J. (2007). The mobilisation of phosphorus , organic carbon and ammonium in the initial stage of fen rewetting (a case study from NE Germany). Biogeochemistry, 85, 141–151. https://doi.org/10.1007/s10533-007-9122-2

Chapter 4

EXPERIMENTALLY SIMULATED SEA LEVEL RISE DESTABILIZES CARBON-MINERAL ASSOCIATIONS IN TEMPERATE TIDAL MARSH SOIL

This chapter contains a manuscript published in *Biogeochemistry* available at https://doi.org/10.1007/s10533-023-01024-z. The complete author list is Sean Fettrow, Rodrigo Vargas (University of Delaware), and Angelia Seyfferth (University of Delaware).

Abstract

How sea level rise (SLR) alters carbon (C) dynamics in tidal salt marsh soils is unresolved. Changes in hydrodynamics could influence organo-mineral associations, influencing dissolved organic carbon (DOC) fluxes. As SLR increases the duration of inundation, we hypothesize that lateral DOC export will increase due to reductive dissolution of C-bearing iron (Fe) oxides, destabilizing soil C stocks and influencing greenhouse gas (GHG) emissions. To test this, soil cores (0-8 cm depth) were collected from the high marsh of a temperate salt marsh that currently experiences changes in water level and soil redox oscillation due to spring-neap tides. Mesocosms experimentally simulated SLR by continuously inundating high marsh soils and were compared to mesocosms with Control conditions, where the water level oscillated on a spring-neap cycle. Porewater DOC, lateral DOC, and porewater reduced Fe (Fe^{2+}) concentrations were significantly higher in SLR treatments (1.7±0.5 mM, 0.63±0.14

mM, and 0.15±0.11 mM, respectively) than Control treatments (1.2±0.35 mM, 0.56±0.15 mM, and 0.08±01 mM, respectively Solid phase analysis with Fe Extended X-Ray Absorption Fine-Structure Spectroscopy (EXAFS) further revealed that SLR led to >3 times less Fe oxide-C coprecipitates than Control conditions In addition, the overall global warming potential (GWP) decreased under SLR due to suppressed CO2 emissions. Our data suggest that SLR may increase lateral C export of current C stocks by dissolving C-bearing Fe oxides but decrease the overall GWP from emissions of soil trace gases. These findings have implications for understanding the fate of soil C dynamics under future SLR scenarios.

4.1 Introduction

Tidal salt marshes are important carbon (C) reservoirs at the terrestrial-aquatic interface, but the fate of these "Blue C" stocks may be affected by sea level rise (SLR). Blue C ecosystems have soil C sequestration rates orders of magnitude greater than inland forests (Chmura et al. 2003; Mcleod et al. 2016). High plant productivity, slow decomposition, and high sedimentation rates (Arias-Ortiz et al. 2018) make tidal salt marshes an ideal C storage sink (Alongi 2020). Along with the anaerobic conditions that slow decomposition rates, the complex nature of marsh-derived C (Osburn et al. 2015) and the association of C with soil minerals (Sun et al. 2019); salt marshes contribute an estimated 6.5 Pg of soil C stock (Chmura et al. 2003; Bridgham et al. 2006; Duarte et al. 2013). Despite the importance of salt marsh C sequestration, these ecosystems are being lost to land use-change at an annual rate of 1-2% each year (Duarte et al. 2008), while SLR is also expected to cause widespread marsh loss. Modeling and meta-analysis have shown that SLR may completely submerge much of the existing salt marshes, decreasing blue C stocks (Valiela et al. 2018), unless enough

accommodation space is available for marsh migration (Schuerch et al. 2018). Consequently, it is critical to understand how SLR will alter soil C retention and stabilization mechanisms in current salt marsh soil C stocks.

Soil minerals stabilize C through physiochemical associations, but SLR may affect this process. In particular, Fe oxides, hydroxides, and oxyhydroxides (hereafter referred to collectively as Fe oxides) are common soil minerals that protect organic C via adsorptive processes (Saidy et al. 2015). A previous study illustrated that approximately 21% of all organic C in natural systems is directly bound to reactive Fe minerals (Lalonde et al. 2012). C-bearing Fe oxides have been extensively studied in noncoastal systems (Chen and Sparks 2015; Saidy et al. 2015; Sowers et al. 2018a; Wordofa et al. 2019; Huang et al. 2020) but there has been limited study into the importance of this C retention mechanism in blue C settings. Previously, Seyfferth et al. (Seyfferth et al. 2020) showed that the main Fe oxide found in salt marsh high marsh soils is ferrihydrite, which is a poorly crystalline Fe oxide with a high surface area that can form strong Fe-C associations (Gu et al. 1995). These reactive Fe oxides can be reductively dissolved by Fe-reducing bacteria under sub- to anoxic conditions, releasing mineral-associated C into the porewater along with reduced Fe (Fe^{2+}) (Riedel et al. 2013; Wordofa et al. 2019). Possible changes to C-bearing Fe oxides under SLR conditions include increased reductive dissolution and decreased mineral precipitation, thereby increasing the mobility and lateral transport of current C stocks from salt marsh soils.

Changes to the stability of C-bearing Fe oxides in tidal salt marshes may alter the mobility of soil C, affecting the lateral C flux. While the vertical C flux encompasses the flow of C into marsh vegetation and storage in the soil, the lateral C

flux is characterized as the import and export of C via tidal channels (Trifunovic et al. 2020; Santos et al. 2021). Until recently, the lateral flux has been ignored, leading to potential underestimation of net C flux from coastal wetlands (Santos et al. 2021). This underestimation may be important, particularly because evidence suggests the lateral C flux may exceed the vertical C flux in these ecosystems (Wang et al. 2016; Bogard et al. 2020; Czapla et al. 2020). While the uncertainty in the lateral C flux of tidal wetlands remains high (Cavallaro et al. 2018), the effect of SLR may add an additional layer of complexity. Changes to the lateral C flux may occur if SLR increases the mobility of previously mineral-stabilized soil C. This effect of SLR on the lateral C flux and current C stocks of marsh soils remains unresolved and is needed for proper representation in earth system models (Ward et al. 2020).

SLR may also affect the emission of greenhouse gases (GHGs) via multiple pathways (Capooci et al. 2019; Luo et al. 2019). An increase in the extent of inundation may alter the exchange of GHGs from marsh soils to the atmosphere by decreasing soil redox potentials and slowing respiration rates (Hackney 1987; Chambers et al. 2013; Capooci and Vargas 2022a). While respiration rates may be slower, C may be more bioavailable under flooded conditions due to decreased mineral protection under low redox conditions, increasing GHG flux even under anoxia (Huang et al. 2020). Furthermore, SLR may decrease methane (CH_4) emissions due to enhanced sulfate reduction and microbial competition for substrate (Poffenbarger et al. 2011). However, recent work has shown methanogenesis in tidal marshes is active at depth via a methylotrophic pathway in which sulfate-reducing bacteria do not compete with methanogens for substrate (Seyfferth et al. 2020). Methane fluxes are also often controlled by the balance between rates of

methanogenesis (production of CH_4) versus methanotrophy (consumption of CH_4) (Deborde et al. 2010), which may be impacted by SLR. Furthermore, tidal salt marsh soils have recently been attributed as acting as a net sink for nitrous oxide (N_2O) (Capooci and Vargas 2022b), though it is unclear how this process of nitrification in salt marshes will be affected by SLR. It is therefore important to understand how SLR will affect various GHG fluxes (i.e., carbon dioxide (CO_2), CH_4, N_2O) and the cumulative global warming potential (GWP) from salt marsh soils.

Our main goal was to investigate how SLR impacts C-bearing Fe oxides and GHG flux in salt marsh soils. This study focuses on soils from a high marsh area near a creek channel that currently experiences flooding only once every two weeks due to spring tides but is highly vulnerable to continuous inundation from SLR (Guimond et al. 2020). To isolate the impacts of SLR on C in marsh soils, we established a laboratory experiment using flow-through mesocosms subjected to two treatments: either to water-table fluctuation similar to established high marsh hydrology on a spring-neap tidal cycle (hereafter referred to as Control) or to continuous inundation (hereafter referred to as SLR). We hypothesize that (1) porewater DOC and lateral DOC export will be higher in the SLR treatment due to lower redox potential and more reductive dissolution of C-bearing Fe oxides, leading to greater DOC mobilization, and (2) increased DOC mobility will lead to greater microbial bioavailability and thus increase GHG emissions (i.e., CO_2, CH_4, N_2O) under SLR conditions. This study suggests that SLR will significantly impact the stability of existing soil C stocks in marsh soils by destabilizing Fe mineral-associated C and altering both the lateral C flux and vertical GHG fluxes.

4.2 Materials and Methods

4.2.1 Study Site and Soil Sampling

Soils were collected from the St. Jones National Estuarine Research Reserve, a temperate tidal salt marsh in the Mid-Atlantic region. This ecosystem has daily tidal influence from the nearby waterbodies, including the St. Jones River, which drains into Delaware Bay (Figure 4.1). The tidal creek has a salinity range of 5-18 ppt (Capooci et al. 2019). Vegetation consists primarily of *Spartina alterniflora*, with patches of S. patens and *S. cynosuroides*. Soils were collected in the high marsh area near a creek channel that is dominated by *S. cynosuroides*. The soils in this location are rarely continuously inundated and instead experience large spring-neap tidal oscillations. During spring tides, the soils are inundated but otherwise drain to as much as -25cm below the soil surface, causing wide ranges in porewater redox potentials from 0 to 700 mV (Seyfferth et. al 2020). Previous modeling efforts have suggested that this area is prone to continuous inundation under future SLR scenarios (Guimond et al. 2020).

To test how SLR will affect these soils, ten intact field moist soil cores (3cm diameter) were taken from the 0-8 cm depth in December 2019. Cores were taken with a semi-cylindrical gouge auger which has been shown to be effective at minimizing compaction (Smeaton et al. 2020). To preserve the low-oxygen conditions at the time of collection, each core was placed into individual gas-impermeable bags with oxygen scrubbers (Mitsubishi Anaero-Pack) during transport back to the laboratory on ice. The gas-impermeable bags with the soils were stored at 4°C for 25 days until the beginning of the experiment. While slight changes in temperature and holding times can possibly lead to changes in the microbial community, past work has shown that

these changes are minimal, (Lauber et al. 2010; Rubin et al. 2013), and the holding temperature (4°C) was not much lower than the temperature of the creek water (8°C) at the time of collection. Moreover, all soil cores were treated the same, so any slight changes that could have occurred would have been uniform across treatments.

Figure 4.1 Map of the study site location at the St Jones Reserve in Dover, Delaware. The coring location for this experiment is located close to a tidal channel. This high marsh location experiences a spring-neap flooding cycle characterized by a flooding event only every two weeks, and soils were saturated upon collection.

4.2.2 Soil Characterization

A subsample of a randomly selected soil core from both Control and SLR was taken before (pre-treatment) and after the experiment (post-treatment) to characterize changes in the solid phase due to treatment. Each subsample (n=4) was dried, ground,

and sieved to 2 mm inside an anoxic glove bag. These subsamples were further powdered and analyzed for total C (Vario EL Cube, Elementar) and total Fe with X-Ray fluorescence (Titan Handheld, Bruker). Furthermore, subsamples were used for X-ray diffraction (D8 XRD, Bruker) and Fe minerals were identified using software (Match!, Version 3.14). Fe extended X-ray fine structure (Fe EXAFS) were used to further characterize Fe mineralogy. Bulk Fe EXAFS were conducted at the National Synchrotron Light Source II on beamline 6BM. Fe K-edge spectra were obtained in transmission mode and three scans per sample were obtained and averaged in Athena (Ravel and Newville 2005). The averaged spectra were background subtracted, normalized, and fit with a spline function (k-weight=3). The normalized spectra were then fit using linear combination (k-range of 2-10 Å-1) to known standards of the minerals that were constrained by XRD. The minerals included in the EXAFS fits were jarosite (NaFe (SO4)(OH)), siderite (FeCO3), magnetite (FeO), green rust (Fe(OH)Cl) and a ferrihydrite (FeOOH)-galacturonic acid coprecipitate (hereafter referred to as Fh-C coprecipitate) from previous work (ThomasArrigo et al. 2019). The goodness of fit of the linear combination on the raw data was assessed using the reduced χ^2 and the R-value developed in Athena (Ravel and Newville 2005) and was also assessed by visually inspecting the raw data and linear combination fit data.

4.2.3 Flow-Through Soil Incubation

To test our hypotheses that SLR will alter marsh soil C, ten polyethylene soil flow-through mesocosms (7.5cm X 15cm) were constructed with inflow and outflow ports (Figure C.1a). The outflow port was screened with a nylon mesh to minimize soil loss. Before placing the ten soil cores into the flow-through mesocosms, 2cm (or ~300g) of acid-washed coarse sand was added to the bottom of the mesocosms to

avoid outflow clogging. We collected water from the nearby tidal channel at the study site to maintain the desired water levels in the mesocosms as performed in other salt marsh incubation studies (Capooci et al. 2019). The mesocosms were placed into an incubation system that was maintained at 24°C without light nor plants to avoid confounding effects to the main hypotheses. Ten flow-through mesocosms were used to simulate SLR (n=5) and Control (n=5) treatments, acknowledging that laboratory controlled mesocosms do not fully replicate field conditions, particularly the addition of sedimentation. After quality assurance and quality control of the experimental data, we decided to only use nine mesocosms for SLR (n=5) and Control (n=4) treatments. The total duration of the experiment was 66 days.

SLR mesocosms were continuously inundated 1cm above the soil surface, while the Control mesocosms went through a simulated spring-neap hydroperiod to represent current field site hydrodynamics. The simulation of a spring-neap oscillation was done by slowly flooding and draining the mesocosms over periods of two-weeks (Figure C.1b). Periods of flooding are hereafter referred to as “Control-Flood” while periods of draining are referred to as “Control-Ebb”. To maintain constant flow in all ten mesocosms, tidal channel water was cycled through at approximately 0.5ml/min using a peristaltic pump (Golander BT100s, Norcross, Georgia). Previous studies have shown the importance of maintaining hydraulic connectivity when performing hydrological manipulations in mesocosms (Petrakis et al. 2017; Northrup et al. 2018; Capooci et al. 2019). For the Control mesocosms, outflow was maintained at 0.5ml/min while inflow was altered slightly to achieve either incremental ebb or flood dynamics. Gas-permeable Tygon tubing was used for the tidal creek water inflow tubing to allow the input water to oxygenate before entering the mesocosms while

Viton tubing with a low gas permeability was used for the lateral export water to limit its exposure to the atmosphere. All flow-through mesocosms were open (i.e., not capped) to allow soil-atmosphere interactions, except during gas flux measurements described in the following section.

4.2.4 Measurement of Greenhouse Gas Fluxes

To test how simulated SLR impacts GHG dynamics, soil GHGs (i.e., CO_2, CH_4 , and N_2O) fluxes were measured every three days starting one day after mesocosms were flooded. We used the closed chamber approach with each flow-through mesocosm as has been done with other mesocosm experiments (Teasley et al. 2017; Capooci et al. 2019). Changes in concentrations of GHGs were measured every 5 seconds for 3 minutes per mesocosm with a Gasmet FTIR gas analyzer (DX4040, Gasmet Technologies, Finland) outfitted with gas impermeable tubing. Flux values were calculated using the following equation:

$$Soil\ GHG\ Flux = \frac{\Delta c}{\Delta t}\frac{V}{S}\frac{Pa}{RT}$$

where c is the mole fraction of CO2, CH4, or N2O in µmol mol-1, t is the observation time of 180 seconds, V is the total volume of the closed system, S is the surface area within the flow-through mesocosms, Pa is the atmospheric pressure inside the mesocosm, R is the universal gas constant, T is the surface water or surface soil temperature, and a linear fit was applied to calculate Δc/Δt using an in-house code (Limmer et al. 2018). We applied a linear fit as a conservative approach and to avoid bias induced by applying an exponential fit at near-zero fluxes or negative fluxes (Barba et al. 2018).

We applied a quality assurance and quality control (QA/QC) approach to calculate GHG fluxes described in previous studies (Petrakis et al. 2017; Barba et al.

2019; Capooci et al. 2019; Capooci and Vargas 2022a). Briefly, when the R^2 value of the calculated CO_2 flux was <0.8 we considered that the micrometeorological conditions inside the chamber were not appropriate to calculate an accurate flux. Consequently, calculations were removed for that measurement's CO_2, CH_4, and N_2O fluxes and replaced as not-a-number (i.e., NaN). When conditions inside the chamber were appropriate (R^2 value >0.8 for CO2), we kept flux calculations of all three GHGs under the assumption that appropriate micrometeorological conditions were achieved for that measurement. Out of 189 flux measurements taken, only 59 did not pass our QA/QC thresholds, were not used in further analyses, and demonstrate the importance of having a strict QA/QC protocol.

Global warming potentials (GWPs) for 20 and 100-year scenarios were calculated from the obtained flux values by multiplying the cumulative sum (g m^{-2} day^{-1}) of each daily average CH_4 or N_2O flux by the respective 20-year and 100-year GWP scenarios (86 and 34 for CH_4, 268 and 298 for N_2O) following previous studies (Myhre et al. 2014; Petrakis et al. 2017; Capooci et al. 2019; Capooci and Vargas 2022b) to convert CH_4 and N_2O to CO_2-equivalents of radiative forcing. Finally, we provided the sum of the CO_2, CH_4-CO_2-equivalents and N_2O-CO_2-equivelents to obtain the GWP of the GHG fluxes during our experiment.

4.2.5 Porewater and Export Water Collection

To capture porewater from the entire soil core throughout the experiment, Rhizon samplers with a nominal pore size of 0.2µm (Rhizosphere Research Products, product 19.21.01) were inserted into each soil core at a ~45° angle, ensuring that the entire sampling area was in contact with the soil, and these samplers remained in place throughout the entire experiment These methods have been used previously in a wide

range of mesocosm studies (Seyfferth and Fendorf 2012; Seyfferth et al. 2016; Teasley et al. 2017; Northrup et al. 2018; Capooci et al. 2019; Linam et al. 2022). Porewater was extracted using an evacuated bottle fitted to a needle and syringe, consistent with previous methods (Seyfferth and Fendorf 2012). Porewater sampling occurred every three days, starting after an equilibrium period of 18 days. Once porewater data collection started on day 18, GHG collection was done on the same days but before porewater measurements to ensure stable soil conditions for gas efflux.

Porewater was immediately aliquoted into prepared tubes within minutes of extraction to minimize sample oxidation. We placed 0.5ml into tubes containing ferrozine reagent for Fe^{2+} analysis by the colorimetric method (Stookey 1970) and 1.5ml was used for redox potential measurements (Orion 9179E Triode) and pH analysis (Orion Ross Ultra pH/ATC Triode) using calibrated probes. The remaining porewater sample were split for conductivity (Orion DuraProbe Conductivity Cell) and dissolved organic carbon (DOC) analysis. Conductivity was converted to salinity in part per thousand (ppt) using the conversion factor; salinity(ppt) = (conductivity(ms/cm)1.0878) x (0.4665). For DOC analysis, porewater was placed into acid washed glass vials, diluted with 5.0 mL of double deionized water, and acidified with 0.1mL of 6M HCl (pH <4.0) to drive off inorganic C and to inhibit microbial activity. DOC samples were frozen until analysis. In addition to porewater, 4.0mL of lateral export water was collected from the outflow port of the flow-through mesocosm approximately every 6 days starting after the 18-day equilibrium period. These lateral export water samples were filtered through 0.7µm glass fiber filters (Whatman GF/F) and prepared for DOC analysis as above. Porewater and lateral DOC

water samples were run on a TOC analyzer (Vario TOC Cube, Elementar) after sparging for 1 minute with CO_2-free air and calibrated against known standards.

4.2.6 Statistical Analysis

Repeated measurements analysis of variance (ANOVA) was performed when testing for significant differences between the Control and SLR treatments (α=0.05). In addition, Control was split into two groups of data: Control-Flood and Control-Ebb as previously described (Section 2.2). Splitting Control into two groups based on tidal stage allowed us to further investigate how water level change affected measured parameters. Structural Equation Models (SEMs) were also used to test for hypothesized relationships between porewater variables and lateral DOC export (Harlow 2002). This statistical method can be seen as a multiple regression approach in which interactions and nonlinearities are accounted for by a hypothesized model (Fan et al. 2016). We tested a hypothetical model based on a mechanism in which SLR will decrease soil redox potential, increase Fe reduction, thereby increasing the mobility and lateral flux of DOC (Figure C.2). Data used to parameterize this model includes both porewater (pH, redox, Fe^{2+}, DOC) and lateral export DOC for both treatments and for all available dates of the experiment. All data across the two-month experiment was used in the model. To assess the fit of our data to SEMs, we included the Comparative Fit Index (CFI), the Root Mean Square Error of Approximation (RMSEA) and the p-values. We also included these parameters for unrestricted (i.e., best fitting model) and independence models (i.e., worst fitting model). All statistical analyses were performed using JMP Pro 16 (Version 16.2).

4.3 Results

4.3.1 Soil Characterization

The total soil C and Fe concentrations were approximately 4% pre-treatment, with a C:Fe ratio of 1.00 (Table 4.1). Post-treatment, the C:Fe ratio increased by 14% in Control and 12% under SLR. Fe minerals were identified with XRD (jarosite, ferrihydrite, green rust, siderite, magnetite) and the spectra were similar between pre- and post-treatment in both Control and SLR samples (Figure C.3). Fe EXAFS analysis showed that Control and SLR pre-treatment soils were similar (Figure 4.2), demonstrating the homogeneity of the samples at the beginning of the experiment, and that jarosite made up the largest fraction of Fe minerals, followed by the Fh-C coprecipitate, green rust, siderite, and magnetite. However, post-treatment soils were affected by treatments where Fh-C increased by 54% under Control conditions while increasing by only 16% under SLR conditions. This indicates that Fh-C coprecipitates increased post-treatment 3.4 times more under Control conditions than they did under SLR conditions. Siderite increased under Control conditions but decreased for SLR. Jarosite decreased in both treatments. Green rust decreased under Control conditions but increased under SLR conditions. Magnetite increased under Control conditions but decreased under SLR conditions. The change in Fe mineralogy between Control and SLR treatments, particularly the Fh-C coprecipitate, have important implications for the stability of soil C under SLR conditions.

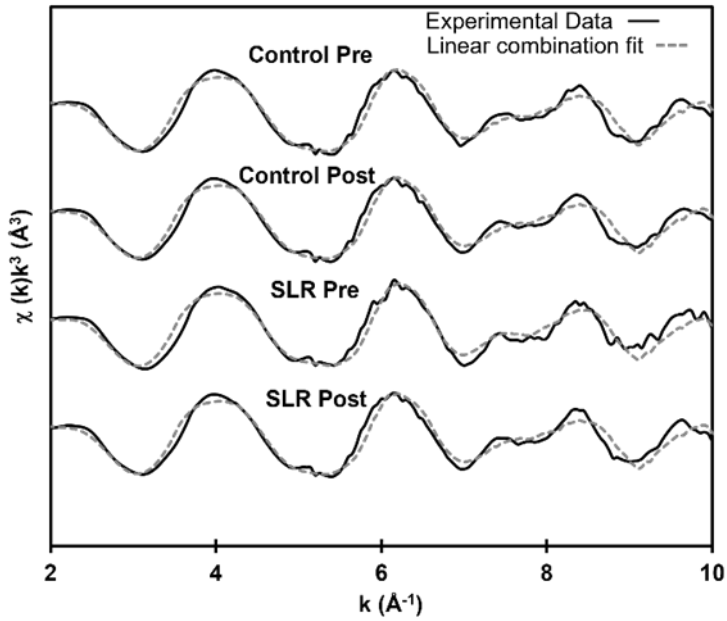

Figure 4.2 Normalized iron K-edge Extended X-Ray Absorption Fine Structure (EXAFS) spectra for Control and SLR pre and post treatment samples. Experimental data and linear combination model fits (k-range of 2-10 Å-1) are shown as solid and dashed lines, respectively.

Table 4.1 Total C and Fe for soil samples, along with linear combination fitting results of Fe EXAFS spectra from sediment used in the incubation study. FHY-GA = ferrihydrite-galacturonic acid coprecipitate; SID = siderite; JAR = jarosite; GR = green rust; MAG= magnetite. Reduced □2, and R values indicate the goodness of fit for EXAFS spectra. "Pre" indicates the sample was taken before the experiment while "post" indicates the sample was taken after the experiment.

				% mineral-species						
Sample	C (%)	Fe (%)	C:Fe Ratio	FHY-GA	SID	JAR	GR	MAG	Reduced χ^2	R value
Control Pre	3.68	3.71	1.00	24	16	36	18	6	0.38	0.08
Control Post	3.43	3.00	1.14	37	18	31	6	8	0.44	0.09
SLR Pre	4.01	4.02	1.00	25	17	37	16	6	0.31	0.07
SLR Post	4.33	3.86	1.12	29	14	35	17	5	0.32	0.07

4.3.2 Soil Greenhouse Gas Flux

Fluxes of GHGs (Figure 4.3) and the cumulative global warming potential (GWP) (Table 4.2) were affected by the experimental SLR treatment in different ways. The overall means were not statistically significant ($p>0.05$) for soil CO_2, CH_4 or N_2O fluxes because of the large temporal variability, but the cumulative sums of these GHG fluxes were different. Over the course of the experiment, both treatments were net sources of CO_2 while SLR had a lower cumulative soil CO_2 efflux by 29%. Both treatments were net sinks of CH_4 while SLR had a lower cumulative soil CH_4 flux by 225% under the 20-year GWP scenario and by 150% under the 100-year scenario. The Control treatment was a net sink of N_2O while the SLR treatment was a net source, which was an increase of approximately 900% under the 20-year and 100-year GWP scenarios. Even though N_2O and CH_4 have a much larger radiative forcing than CO_2, cumulative soil CO_2 efflux still comprised most of the net GWP in both treatments.

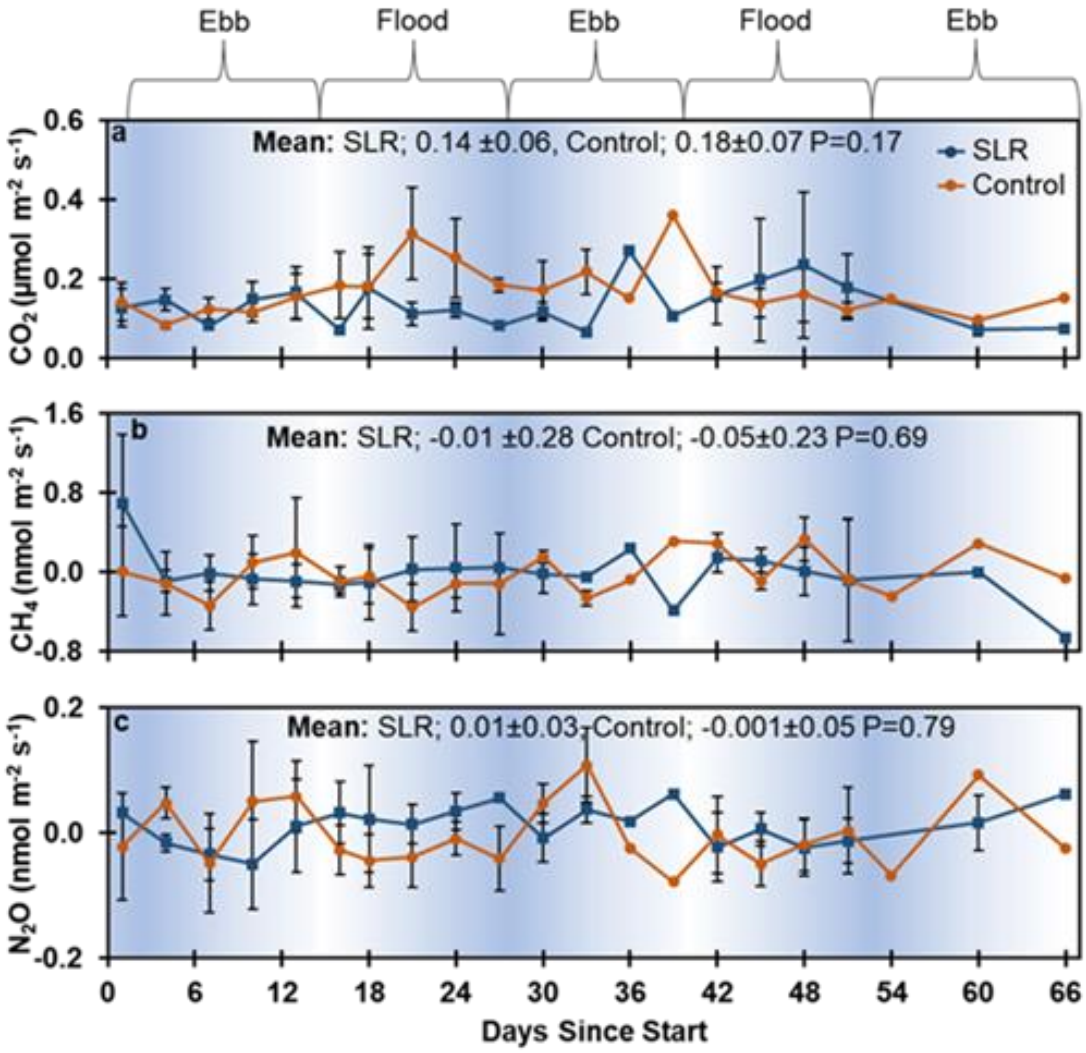

Figure 4.3 GHG timeseries indicating the averages of the replicate mesocosms for both SLR and Control treatments for (a) CO_2, (b) CH_4, and (c) N_2O. The error bars indicate the standard deviation among the replicates. P-value and means are a result of repeated measures ANOVA between SLR and Control across the entire 66-day experiment. The blue background indicates the relative water level of the Control treatment, with the brackets showing periods where the water level was increasing (flood) or decreasing (ebb). Not all timepoints had enough replicates (n<3) to calculate a standard deviation therefore not all points have error bars.

We further compared GHG flux by splitting Control treatments into Flood and Ebb stages and examined the means between SLR, Control-Ebb, and Control-Flood (Table 4.3). We did not find significant differences in the means of each GHG between treatments due to large temporal variability. The mean CO2 flux was always positive for Control-Flood and Control-Ebb; fluxes of N2O from Control-Ebb were positive while Control-Flood was negative; and CH4 flux was always negative for all scenarios. These results show the large temporal variability of GHG fluxes and reinforced the use of cumulative sums and GWP for this experiment.

Table 4.2 Global warming potential (GWP) of the cumulative GHG emissions for 20 and 100-year scenarios. Values indicate the GWP (± SD) for 20- and 100-year scenarios for each GHG

	CO_2 (g m^{-2})	**CH_4 ($CO_{2\,eq}$ (g m^{-2}))**		**N_2O ($CO_{2\,eq}$ (g m^{-2}))**		**Total ($CO_{2\,eq}$ (g m^{-2}))**	
		20-year	100-year	20-year	100-year	20-year	100-year
SLR	10.26±4.15	-0.13±0.58	-0.05±0.23	0.73±0.82	0.81±0.91	10.86±5.55	11.02±5.29
Control	13.73±1.22	-0.04±0.52	-0.02±0.21	-0.09±0.88	-0.10±0.98	13.6±2.62	13.61±2.41

Table 4.3 Summary of means for porewater, lateral DOC, and GHG flux. Values (± SD) with different superscripted letters are significantly different ($p<0.05$) based on repeated measures ANOVA analysis.

Parameter	SLR	Control-Flood	Control-Ebb
CO_2 (µmol m^{-2} s^{-1})	$0.14\pm(0.10)^{A*}$	$0.19\pm(0.10)^{A}$	$0.15\pm(0.07)^{A}$
N_2O (nmol m^{-2} s^{-1})	$0.01\pm(0.06)^{A}$	$-0.02\pm(0.06)^{A}$	$0.01\pm(0.08)^{A}$
CH_4 (nmol m^{-2} s^{-1})	$-0.02\pm(0.41)^{A}$	$-0.05\pm(0.40)^{A}$	$-0.01\pm(0.32)^{A}$
Porewater DOC (mM)	$1.7\pm(0.50)^{A}$	$1.3\pm(0.40)^{B}$	$1.0\pm(0.19)^{C}$
Lateral DOC (mM)	$0.63\pm(0.14)^{A}$	$0.60\pm(0.15)^{AB}$	$0.52\pm(0.14)^{B}$
Fe^{2+} (mM)	$0.15\pm(0.11)^{A}$	$0.09\pm(0.09)^{B}$	$0.07\pm(0.06)^{B}$
Redox (mV)	$214\pm(56)^{B}$	$205\pm(48)^{B}$	$263\pm(53)^{A}$
pH	$7.3\pm(0.32)^{A}$	$7.6\pm(0.24)^{B}$	$7.6\pm(0.31)^{B}$
Salinity (ppt)	$2.43\pm(0.88)^{A}$	$2.67\pm(0.76)^{A}$	$1.94\pm(0.87)^{B}$

4.3.3 Soil Porewater and Lateral Export Water

SLR significantly affected porewater biogeochemical variables, as well as the lateral DOC concentration (Figure 4.4). Porewater Fe^{2+} mean concentration was significantly higher in SLR treatments than Control treatments by a factor of approximately two, and both decreased over time reaching a new steady state equilibrium. When the Control treatment was split into periods of ebb stage versus flood stage, (SLR, Control-Ebb, Control-Flood), SLR had the highest mean Fe^{2+} concentration, followed by Control-Flood and Control-Ebb (Table 4.3). Higher Fe^{2+} levels corresponded with lower redox potential. SLR treatments had significantly lower redox potentials than the Control treatments. Control-Ebb had significantly higher mean redox potential than both Control-Flood and SLR which were not significantly different from each other. While the salinity was not significantly different between Control and SLR treatments, Control-Ebb was significantly lower

than SLR. In addition, salinity decreased over time and reached a new steady state equilibrium similar to the response of Fe^{2+}. Mean lateral DOC and porewater DOC levels were significantly higher under SLR conditions compared to Control. Porewater DOC concentrations are similar in concentration to DOC concentrations found at the field site (Seyfferth et al. 2020). In addition, porewater DOC mean concentrations in SLR, Control-Flood, and Control-Ebb are all significantly different from one another and decrease in concentration in that order.

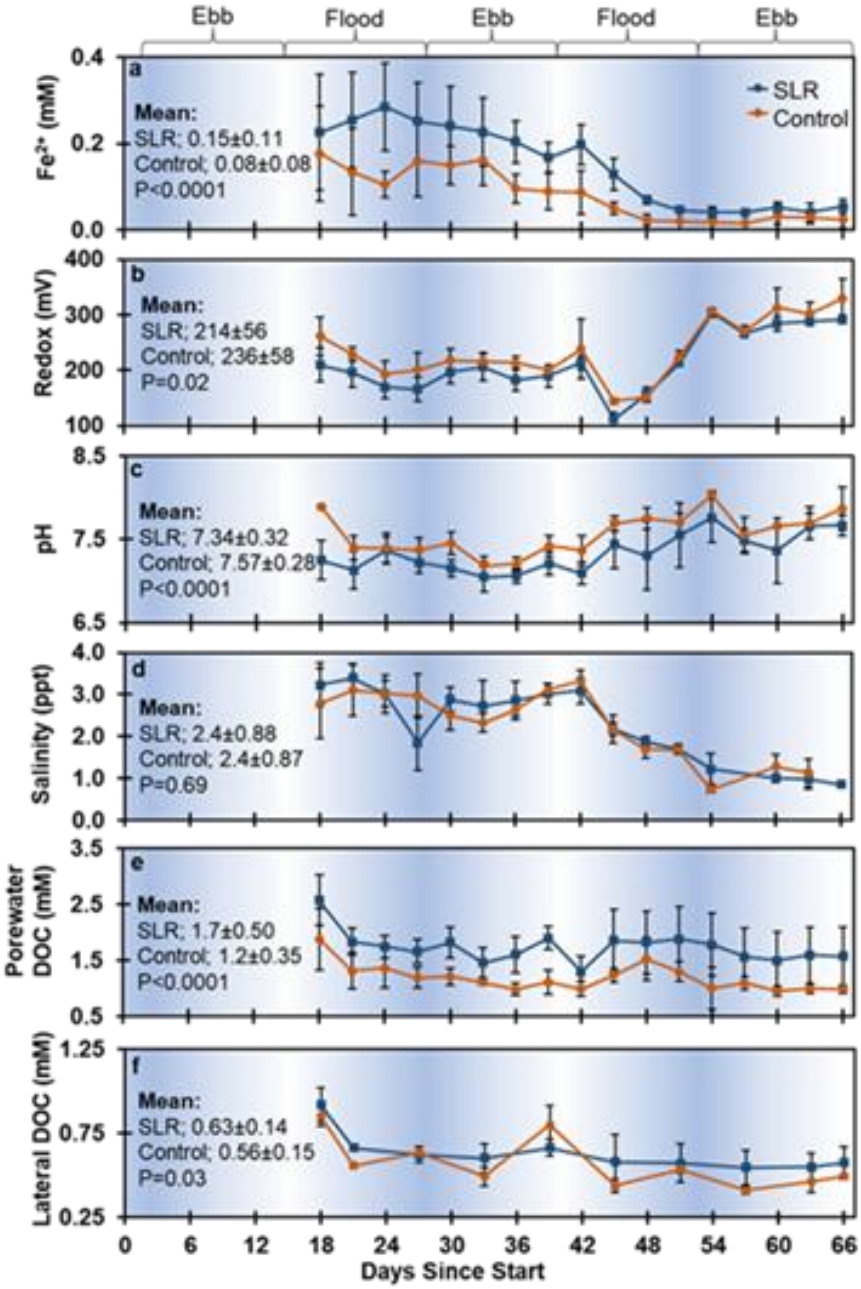

Figure 4.4 Timeseries for Fe^{2+} (a), Redox (b), pH (c), Salinity (d), Porewater DOC (e) and Lateral DOC (f). The error bars indicate the standard deviation among the replicates. P-value and means are a result of repeated measures ANOVA between SLR and Control treatments across the entire 66-day experiment. The blue background indicates the relative water level of the Control treatment, with the brackets showing periods where the water level was increasing (flood) or decreasing (ebb).

4.3.4 Porewater, Lateral Export Water, and GHG Relationships

Our data show that under increased flooding conditions due to SLR, the mobility and bioavailability of DOC may increase due to increased reductive dissolution of C-bearing Fe oxides. These results are supported by analyses exploring linear relationships and using SEMs. First, our results show positive, but weak, relationships between Fe^{2+} and lateral DOC in the SLR treatment (R^2=0.17, p=0.003) and in the Control-Flood (R^2=0.17, p=0.07), but not in Control-Ebb (R^2=0.10, p=0.18) (Figure 4.5). There was a strong significant linear relationship between porewater DOC and lateral export DOC for SLR (R^2=0.59, p<0.0001) but is weaker for the Control-Flood (R^2=0.28, p=0.01) treatment, while no such relationship exists for Control-Ebb (R^2=0.00008, p=0.97). In addition, the lateral export of DOC for SLR had a significant and positive relationship (R^2=0.56, p<0.0001) when analyzed against Control-Flood but does not when it is analyzed against Control-Ebb (R^2=0.11, p=0.16) (Figure 4.6). These results imply greater similarity between SLR and periods of Control-Flood than with periods of Control-Ebb for lateral DOC. In addition, we found statistically significant, but weak, relationships between soil CO_2 efflux and both lateral and porewater DOC, but only for SLR (Figure 4.5). No significant trends were observed between the other GHGs (i.e., CH_4, N_2O) and DOC variables. These results suggest that although linear relationships are apparent, there could be interacting or compounding effects among variables. Consequently, we tested a hypothesized model using a Structural Equation Model (SEM) approach.

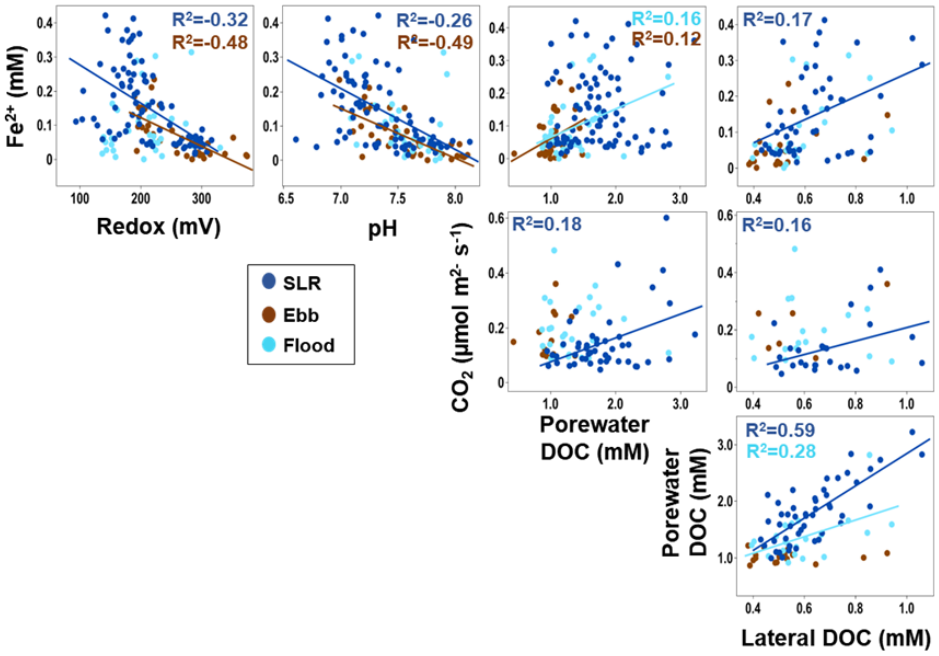

Figure 4.5 Linear trend matrix between variables. The data has been grouped into SLR, Control-Flood, and Control-Ebb. R^2 values and trend lines are reported only if the relationship was significant ($p<0.05$).

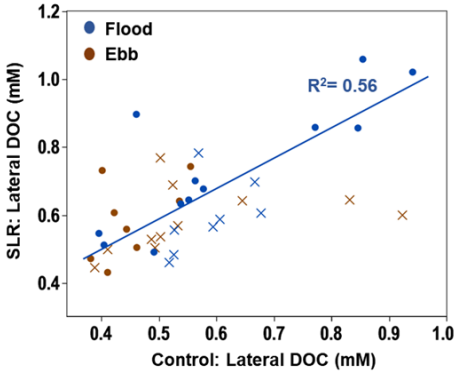

Figure 4.6 Plots of export DOC for SLR verse either Control-Flood or Control-Ebb. Timepoints represented by "X" are completely flooded Control timepoints, or completely drained Control timepoints. This represents how SLR is similar to Control-Flood lateral DOC export, but not Control-Ebb. R^2 and p-value are reported only if the relationship is significant ($p<0.05$)

An SEM was built to test the hypothesis that SLR increases lateral DOC export by increasing reductive dissolution of C-bearing Fe oxides (parameters included pH, redox, Fe^{2+} porewater DOC and lateral DOC; Figure C2). We independently tested the same hypothesized model using information derived from Control or SLR treatments (i.e., two independent SEMs were tested with information from either Control or SLR treatments). Our results show that different relationships among parameters are identified by the SEM approach (Figure 4.7). The strength of the model fit was greater for SLR treatment (Table 4.4), suggesting that our hypothetical model is better supported using data derived from a SLR scenario. Under Control conditions, pH and porewater redox potential significantly covary, but only pH is significantly and negatively related to Fe^{2+}, and then Fe^{2+} is positively related to porewater DOC but without a significant relationship with lateral fluxes of DOC (Figure 4.7a). In contrast, under SLR conditions, pH and redox significantly covary and both are negatively related to Fe^{2+}; consequently, Fe^{2+} and porewater DOC are positively related to lateral fluxes of DOC (Figure 4.7b). The SEM provides additional statistical evidence in support of our hypothesis that SLR will decrease redox, increase reductive dissolution of Fe, and increase lateral DOC export.

Table 4.4 Structural equation model (SEM) parameter output values. CFI = Cumulative Fit Index; RMSEA = Root Mean Squared Error Approximation; Prob>χ^2 = Significant ($p<0.05$) difference between experimental data and model output.

a Model Name	CFI	RMSEA	Prob>χ^2
Unrestricted Model	1.0	0.0	
Independence Model	0.0	0.29	<0.0001
Control Model	0.72	0.24	0.0004

b Model Name	CFI	RMSEA	Prob>χ^2
Unrestricted Model	1.0	0.0	
Independence Model	0.0	.35	<0.0001
SLR Model	0.98	0.07	0.22

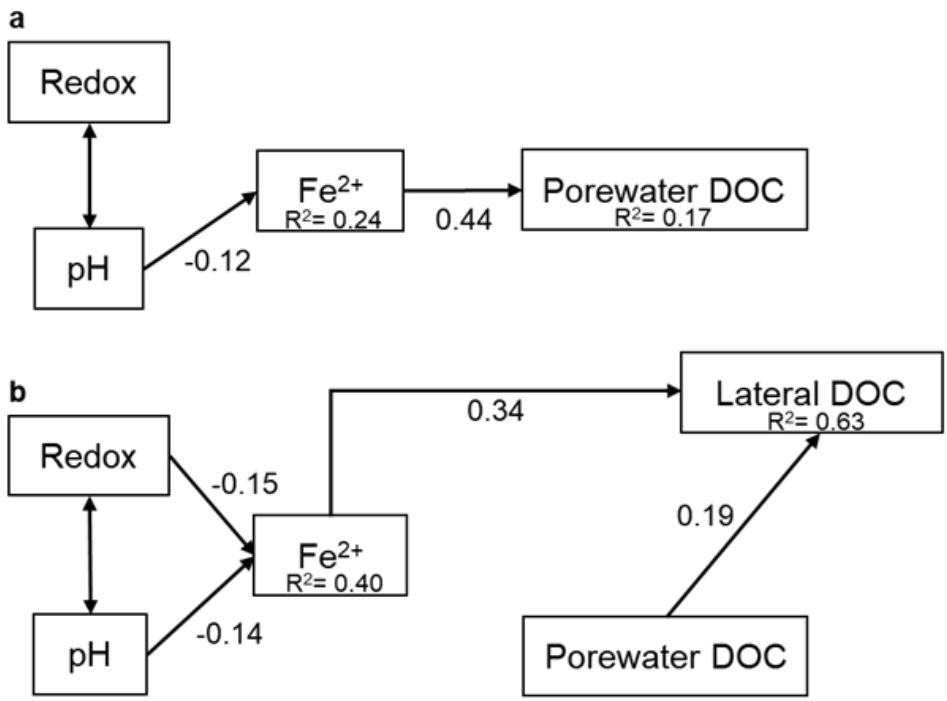

Figure 4.7 Structural equation model (SEM) diagram depicting relationships between measured variables for Control (a) and SLR (b) treatments. Values on the arrows are estimates for the relationships (i.e., Change in X of 1 unit causes this estimated amount of change in Y). R^2 values are also provided for each significant ($p<0.05$) regression Single-sided arrows represent a hypothesized regression in the direction of the arrow, while double-sided arrows indicate covariance between two variables. We tested the same hypothetical model using SEMs parameterized with information derived either from Control or SLR treatments and here we present the final models.

4.4 Discussion

4.4.1 Iron Mineral Control on DOC

Fe oxides are critical in stabilizing soil C in tidal marsh soils, as has been found for other ecosystems, but how the C-dense marsh soils will respond to SLR is still unresolved (Chen and Sparks 2015; Saidy et al. 2015; Sowers et al. 2018b; Wordofa et al. 2019; Adhikari et al. 2019; Huang et al. 2020). Here, our experimental data support the hypothesis that increased inundation under SLR conditions will lead to soil C loss from marsh soils via reductive dissolution of C-bearing Fe oxides. Under present-day conditions (simulated here by Control treatments), soils near tidal channels drain after each tidal cycle, allowing the soils to reoxygenate during low tides. This process re-oxidizes Fe^{2+}, forming reactive minerals such as ferrihydrite that can sequester DOC. These hydrodynamic conditions allow at least partial stabilization of porewater DOC onto newly formed Fe minerals by surface adsorption or coprecipitation, which can occur within less than 30 minutes of oxygen exposure (Sodano et al. 2017). While the difference in means between SLR and Control redox potential was small, SLR treatments had a significantly lower redox potential. We suscept even greater reducing conditions would have occurred with a longer experiment length. SLR treatments also had higher concentrations of porewater DOC Fe^{2+} (Fig. 4), which suggests enhanced reductive dissolution of C-bearing Fe oxides mediated by Fe reducing bacteria (Wordofa et al. 2019). Whereas dissolution and reoxidation of Fe^{2+} as ferrihydrite occurs periodically as Control soils are drained and flooded, prolonged inundation caused by SLR will deplete the soils of reactive ferrihydrite as it dissolves and making surface adsorption or coprecipitation of DOC with Fe oxides less likely. This is supported by our Fe EXAFS data, as post-treatment

SLR soils contained 3.4 times less Fh-C coprecipitate than post-treatment Control soils. Note that even though both treatments had decreasing porewater Fe^{2+} concentrations over time likely due to loss of reactive ferrihydrite minerals, this loss was more pronounced with SLR treatments. Thus, C destabilization appears to have been promoted under SLR treatments as reductive dissolution of C-bearing Fe oxides progressed because solution-phase DOC is more prone to microbial degradation (Huang et al. 2020) and/ or transport from the system.

4.4.2 SLR Conditions Increase DOC Export

Our data support the hypothesis that SLR conditions may increase the lateral export of DOC. On average, SLR treatments across the two-month study exported 12.5±33% more lateral DOC than Control treatments. While the differences between SLR and Control were small, it was significant, even in this relatively short-term experiment. Longer-term studies coupled with field investigations that include the added complexity of plant activity and sediment additions are warranted to determine if even larger changes could be observed as SLR progresses. For example, plants will add more C, but SLR will submerge plants and possibly increase C export. In our experiment, prolonged flooding led to greater DOC mobility and removal from the soil. The univariate linear analyses and the SEMs suggest that DOC builds up in the porewater under flooded conditions, is more likely to be exported from the soil, and that lateral transport of DOC may increase with SLR under future climate scenarios.

The fate of laterally exported C is difficult to determine, but pathways may include transport to adjacent estuaries or the coastal ocean where the C is either preserved outside the ecosystem or broken down and returned to the atmosphere as CO_2 or CH_4. Tidal creeks are hotspots for CO_2 and CH_4 flux, particularly during ebb

tide (Trifunovic et al. 2020) when the largest lateral transport of C from marsh soils to the tidal channel is expected (Xin et al. 2011). This suggests that a fraction of C, which is laterally transported, may be immediately returned to the atmosphere, and another fraction may be transported to coastal waters and buried in shelf sediments (Duarte 2017; Najjar et al. 2018). Understanding how SLR will affect the mechanisms and patterns of lateral C is critical because up to 80% of the net CO2 uptake in salt marshes could be laterally exported to adjacent waters (Santos et al. 2021). There are large uncertainties about how much C is exchanged laterally, returned to the atmosphere, or buried in coastal ecosystems as part of the global C cycle (Cavallaro et al. 2018). While the uncertainty of lateral C fluxes in tidal wetlands remains high (Cavallaro et al. 2018), our data show that patterns in hydrologic oscillation (spring-neap vs continuously flooded) can significantly alter DOC mobility and the lateral DOC flux from marsh soil. Therefore, changes and differences in hydrologic oscillation could be a source of uncertainty found in current lateral C flux estimates. We propose that future lateral C estimates should consider the effects of altered hydrologic oscillation on C transport, particularly in areas most vulnerable to SLR.

4.4.3 Soil Greenhouse Fluxes Altered by SLR

Our data do not support the hypothesis that soil GHG fluxes would increase under SLR conditions due to greater DOC bioavailability under flooded conditions. While we observed a positive and significant relationship between porewater DOC and soil CO_2 flux under experimental SLR conditions, this treatment overall had a lower cumulative GWP due mostly to decreased soil CO_2 efflux. Our data indicate that although prolonged flooding may increase DOC bioavailability as it becomes released from the mineral-phase, as was observed in other work (Huang et al. 2020), the

decreased oxygen during soil flooding limits aerobic microbial respiration and supports anaerobes that respire more slowly (Raich and Schlesinger 1992). Thus, the potential C losses by increased DOC during inundation were partially compensated for by decreased heterotrophic respiration and lower CO_2 diffusion because of flooding. In addition, increased lateral export under SLR conditions may have decreased the amount of labile DOC available for microbes, which could have decreased heterotrophic respiration. We conclude that while SLR could affect microbial and physical processes in different ways, the overall impact in our experiment is a decreased GWP due mainly to suppressed soil CO_2 efflux.

There is a discrepancy in the literature about how SLR will impact CH_4 fluxes from coastal wetlands (Capooci et al. 2019; Luo et al. 2019). Some studies suggest increased salinity will have inhibitory effects on CH_4 production (Poffenbarger et al. 2011), while increased inundation frequency may increase anaerobic conditions and thus increase methanogenesis (Mueller et al. 2020). Furthermore, automated measurements (i.e., hourly resolution) have shown the complexity of the influence of tidal flooding on the temporal patterns and pulse emissions (i.e., hot-moments) of soil trace gas fluxes in salt marshes (Capooci and Vargas 2022a). While our SLR treatment cumulatively emitted less soil CH_4 than Control, both treatments acted as net CH4 sinks, were not statistically different, and their CH_4 contributed little to the overall GWP. Methane consumption by soils (i.e., net CH_4 sink) may result from both anaerobic and aerobic oxidation of CH4 (Hoehler et al. 1994), both of which may have been occurring in our experiment. Aerobic oxidation of CH_4 requires oxygen and thus is more likely to have happened in the Control treatment. Anaerobic oxidation of CH_4 uses alternative electron acceptors in low oxygen conditions and may have occurred

more so in the SLR treatments. Sulfate-mediated anaerobic oxidation of methane is thought to be the primary means of CH_4 consumption in anoxic marine settings (Knittel and Boetius 2009; Smemo and Yavitt 2011), and some evidence suggests that sulfate-mediate anaerobic oxidation of CH_4 is also active in brackish coastal wetland sediments (Segarra et al. 2013). Other pathways that may be decoupled from sulfate-mediated oxidation of CH_4 include the use of Fe oxides as the terminal electron acceptor instead of sulfate (Segarra et al. 2013; Cai et al. 2018); both processes may have occurred in the SLR treatments here. Taken together, our data suggest that CH_4 oxidation is active in the surface soils collected for this experiment.

In this experiment we focused on current C stocks in soil, so we did not include plants to avoid confounding effects regarding inputs of organic matter and plant influences on CO_2 and CH_4 efflux. We isolated the effect of soils to test the main hypothesis of this study, but we recognize that addition of plants in the experiment would likely increase the fluxes of CO_2 and CH_4 due to higher C inputs from root exudation and leaf litter. It should also be considered that future SLR conditions would eventually lead to marsh cordgrass die-off and conversion to open water at our field site (Valiela et al. 2018; Guimond et al. 2020), which would lead to conditions more similar to our experimental mesocosms. Future experiments should consider long-term effects (e.g., year or multi-year) to test persistent effects of SLR on CH_4 and CO_2 dynamics in field-settings.

Fluxes of N_2O from salt marshes may also change under SLR conditions, and our data suggest that SLR alter soils from being an overall net sink to a net source of N_2O. While net differences between SLR and Control N_2O flux were not statistically significant, the cumulative emissions for SLR were positive, while for Control the

cumulative emissions were negative. The consumption of N_2O is primarily controlled by denitrification, while the production of N_2O is controlled by nitrification and the balance between those processes controls whether the ecosystem is a sink or source of N_2O (Foster and Fulweiler 2016; Maavara et al. 2019). Other work with salt marsh soils also showed a transition from a net sink to net source due to increased nitrate and ammonium loading (Moseman-Valtierra et al. 2011). The availability of nitrate and ammonium is a major factor controlling N_2O flux and their bioavailability could increase under SLR conditions. For example, saltwater intrusion increases the release of bioavailable nitrogen from mineral sorption sites (Widney et al. 2019). In addition, SLR conditions had lower soil redox potentials, possibly increasing the activity of anaerobic nitrifying microbes. While the cumulative emissions of N_2O transitioned from a sink to source under the SLR treatment tested here, N_2O contributed little to the overall GWP scenarios. Future studies that involve multi-year experiments on the effects of SLR are warranted to fully understand the effects of SLR on multiple GHGs from tidal salt marshes.

4.5 Conclusion

SLR is expected to alter C cycling in tidal salt marshes, particularly in vulnerable low-elevation coastal areas around the world. Fe oxides may stabilize a substantial amount of existing soil C stocks through physiochemical protection, but how SLR will affect their stability is unresolved. Our simulated SLR mesocosm experiment indicates that C-bearing Fe oxide minerals in marsh soils may be destabilized with increased inundation, releasing DOC to solution where it can be acted upon by soil microbes or be exported from the system. Our data suggest that the most reactive Fe minerals were consumed first and that SLR treatments reached a new

steady state over time, but always had higher porewater Fe^{2+} than Control treatments. By the end of the experiment, SLR treatments had >3x less C-bearing ferrihydrite than Control, which produced new ferrihydrite with each tidal oscillation that could sequester C and slow its release. However, despite SLR leading to more DOC release, the amount was small, and the low-oxygen conditions resulted in less energetically favorable microbial metabolisms that ultimately led to decreased GWP from SLR-treated soils.

As currently oxidized high marsh areas become further inundated from SLR, the soils may lose Fe oxides through reductive dissolution and limited periods of soil oxygenation, allowing the 6.5 Pg of soil C stock in tidal marsh soils to become more vulnerable to lateral transport and degradation. If soils become permanently reducing, the ability for redox sensitive minerals to hold onto freshly produced soil C may become increasingly diminished in the future, thereby decreasing soil C stocks, but increasing the lateral C flux. High surface area soil minerals that are prone to reduction (ferrihydrite) could be flushed from the system, drastically decreasing the C holding capacity of these efficient C sinks. It is possible that other coastal wetlands such as mangroves may also be susceptible to removal of mineral-associated C under SLR conditions. Management strategies that mitigate the effects of prolonged inundation due to SLR, and preserve natural tidal cycles, may help decrease this vulnerability of mineral-associated C in coastal wetlands. Future studies should further examine the vulnerability of mineral-associated C and changes to GHG flux under SLR conditions, particularly with long-term studies in a variety of coastal ecosystems.

REFERENCES

Adhikari D, Sowers T, Stuckey JW, et al (2019) Formation and redox reactivity of ferrihydrite-organic carbon-calcium co-precipitates. Geochim Cosmochim Acta 244:86–98. https://doi.org/10.1016/j.gca.2018.09.026

Alongi DM (2020) Carbon Balance in Salt Marsh and Mangrove Ecosystems: A Global Synthesis. Journal of Marine Science and Engineering 8:767. https://doi.org/10.3390/jmse8100767

Arias-Ortiz A, Masqué P, Garcia-Orellana J, et al (2018) Reviews and syntheses: ²¹⁰Pb-derived sediment and carbon accumulation rates in vegetated coastal ecosystems – setting the record straight. Biogeosciences 15:6791–6818. https://doi.org/10.5194/bg-15-6791-2018

Barba J, Cueva A, Bahn M, et al (2018) Comparing ecosystem and soil respiration: Review and key challenges of tower-based and soil measurements. Agricultural and Forest Meteorology. https://doi.org/10.1016/j.agrformet.2017.10.028

Barba J, Poyatos R, Vargas R (2019) Automated measurements of greenhouse gases fluxes from tree stems and soils: magnitudes, patterns and drivers. Sci Rep. https://doi.org/10.1038/s41598-019-39663-8

Bogard MJ, Bergamaschi BA, Butman DE, et al (2020) Hydrologic Export Is a Major Component of Coastal Wetland Carbon Budgets. Global Biogeochem Cycles 34:1–14. https://doi.org/10.1029/2019GB006430

Bridgham SD, Megonigal JP, Keller JK, et al (2006) The carbon balance of North American wetlands. Wetlands. https://doi.org/10.1672/0277-5212(2006)26[889:TCBONA]2.0.CO;2

Cai C, Leu AO, Xie G-J, et al (2018) A methanotrophic archaeon couples anaerobic oxidation of methane to Fe(III) reduction. The ISME Journal 12:1929–1939. https://doi.org/10.1038/s41396-018-0109-x

Capooci M, Barba J, Seyfferth AL, Vargas R (2019) Experimental influence of storm-surge salinity on soil greenhouse gas emissions from a tidal salt marsh. Science of the Total Environment 686:1164–1172. https://doi.org/10.1016/j.scitotenv.2019.06.032

Capooci M, Vargas R (2022a) Diel and seasonal patterns of soil CO2 efflux in a temperate tidal marsh. Science of The Total Environment 802:149715. https://doi.org/10.1016/j.scitotenv.2021.149715

Capooci M, Vargas R (2022b) Trace gas fluxes from tidal salt marsh soils: implications for carbon-sulfur biogeochemistry. Biogeosciences 19:4655–4670. https://doi.org/10.5194/bg-19-4655-2022

Cavallaro N, Shrestha G, Birdsey R, et al (2018) Second State of the Carbon Cycle Report. Washington, DC

Chambers LG, Osborne TZ, Reddy KR (2013) Effect of salinity-altering pulsing events on soil organic carbon loss along an intertidal wetland gradient: A laboratory experiment. Biogeochemistry 115:363–383. https://doi.org/10.1007/s10533-013-9841-5

Chen C, Sparks DL (2015) Multi-elemental scanning transmission X-ray microscopy-near edge X-ray absorption fine structure spectroscopy assessment of organo-mineral associations in soils from reduced environments. Environmental Chemistry 12:64–73. https://doi.org/10.1071/EN14042

Chmura GL, Anisfeld SC, Cahoon DR, Lynch JC (2003) Global carbon sequestration in tidal, saline wetland soils. Global Biogeochem Cycles 17:1111. https://doi.org/10.1029/2002GB001917

Czapla KM, Anderson IC, Currin CA (2020) Net Ecosystem Carbon Balance in a North Carolina, USA, Salt Marsh. J Geophys Res Biogeosci 125:1–16. https://doi.org/10.1029/2019JG005509

Deborde J, Anschutz P, Guérin F, et al (2010) Methane sources, sinks and fluxes in a temperate tidal Lagoon: The Arcachon lagoon (SW France). Estuarine, Coastal and Shelf Science 89:256–266. https://doi.org/10.1016/j.ecss.2010.07.013

Duarte CM (2017) Reviews and syntheses: Hidden forests, the role of vegetated coastal habitats in the ocean carbon budget. Biogeosciences 14:301–310. https://doi.org/10.5194/bg-14-301-2017

Duarte CM, Dennison WC, Orth RJW, Carruthers TJB (2008) The charisma of coastal ecosystems: Addressing the imbalance. Estuaries and Coasts 31:233–238. https://doi.org/10.1007/s12237-008-9038-7

Duarte CM, Losada IJ, Hendriks IE, et al (2013) The role of coastal plant communities for climate change mitigation and adaptation. Nat Clim Chang 3:961–968. https://doi.org/10.1038/nclimate1970

Fan Y, Chen J, Shirkey G, et al (2016) Applications of structural equation modeling (SEM) in ecological studies: an updated review. Ecol Process

Foster SQ, Fulweiler RW (2016) Sediment Nitrous Oxide Fluxes Are Dominated by Uptake in a Temperate Estuary. Frontiers in Marine Science 3:1–13. https://doi.org/10.3389/fmars.2016.00040

Gu B, Schmitt J, Chen Z, et al (1995) Adsorption and desorption of different organic matter fractions on iron oxide. Geochimica et Cosmochimica Acta 59:219–229. https://doi.org/10.1016/0016-7037(94)00282-Q

Guimond JA, Yu X, Seyfferth AL, Michael HA (2020) Using Hydrological-Biogeochemical Linkages to Elucidate Carbon Dynamics in Coastal Marshes Subject to Relative Sea Level Rise. Water Resour Res 56:1–16. https://doi.org/10.1029/2019WR026302

Hackney CT (1987) Factors Affecting Accumulation or Loss of Macroorganic Matter in Salt Marsh Sediments. Ecology 68:1109–1113. https://doi.org/10.2307/1938385

Harlow LL (2002) Using Multivariate Statistics (4th ed.) (Book). Structural Equation Modeling

Hoehler TM, Alperin MJ, Albert DB, Martens CS (1994) Field and laboratory studies of methane oxidation in an anoxic marine sediment: Evidence for a methanogen-sulfate reducer consortium. Global Biogeochemical Cycles 8:451–463. https://doi.org/10.1029/94GB01800

Huang W, Ye C, Hockaday WC, Hall SJ (2020) Trade-offs in soil carbon protection mechanisms under aerobic and anaerobic conditions. Global Change Biology 26:3726–3737. https://doi.org/10.1111/gcb.15100

Knittel K, Boetius A (2009) Anaerobic Oxidation of Methane: Progress with an Unknown Process. Annual Review of Microbiology 63:311–334. https://doi.org/10.1146/annurev.micro.61.080706.093130

Lalonde K, Mucci A, Ouellet A, Gélinas Y (2012) Preservation of organic matter in sediments promoted by iron. Nature 483:198–200. https://doi.org/10.1038/nature10855

Lauber CL, Zhou N, Gordon JI, et al (2010) Effect of storage conditions on the assessment of bacterial community structure in soil and human-associated samples. FEMS Microbiology Letters 307:80–86. https://doi.org/10.1111/j.1574-6968.2010.01965.x

Limmer MA, Mann J, Amaral DC, et al (2018) Silicon-rich amendments in rice paddies: Effects on arsenic uptake and biogeochemistry. Science of The Total Environment 624:1360–1368. https://doi.org/10.1016/j.scitotenv.2017.12.207

Linam F, Limmer MA, Tappero R, Seyfferth AL (2022) Rice husk and charred husk amendments increase porewater and plant Si but water management determines grain As and Cd concentration. Plant Soil. https://doi.org/10.1007/s11104-022-05350-3

Luo M, Huang J-F, Zhu W-F, Tong C (2019) Impacts of increasing salinity and inundation on rates and pathways of organic carbon mineralization in tidal wetlands: a review. Hydrobiologia 827:31–49. https://doi.org/10.1007/s10750-017-3416-8

Maavara T, Lauerwald R, Laruelle GG, et al (2019) Nitrous oxide emissions from inland waters: Are IPCC estimates too high? Global Change Biology 25:473–488. https://doi.org/10.1111/gcb.14504

Mcleod E, Chmura GL, Bouillon S, et al (2016) A blueprint for blue carbon: toward an improved understanding of the role of vegetated coastal habitats in sequestering CO2. Front Ecol Environ 9:552–560. https://doi.org/https://www.jstor.org/stable/41479959

Moseman-Valtierra S, Gonzalez R, Kroeger KD, et al (2011) Short-term nitrogen additions can shift a coastal wetland from a sink to a source of N2O. Atmospheric Environment 45:4390–4397. https://doi.org/10.1016/j.atmosenv.2011.05.046

Mueller P, Mozdzer TJ, Langley JA, et al (2020) Plant species determine tidal wetland methane response to sea level rise. Nature Communications 11:5154. https://doi.org/10.1038/s41467-020-18763-4

Myhre G, Shindell D, Huang J, et al (2014) Anthropogenic and Natural Radiative Forcing. In: Climate Change 2013 – The Physical Science Basis. Cambridge University Press, pp 659–740

Najjar RG, Herrmann M, Alexander R, et al (2018) Carbon Budget of Tidal Wetlands, Estuaries, and Shelf Waters of Eastern North America. Global Biogeochem Cycles 32:389–416. https://doi.org/10.1002/2017GB005790

Northrup K, Capooci M, Seyfferth AL (2018) Effects of Extreme Events on Arsenic Cycling in Salt Marshes. Journal of Geophysical Research: Biogeosciences 123:1086–1100. https://doi.org/10.1002/2017JG004259

Osburn CL, Mikan MP, Etheridge JR, et al (2015) Seasonal variation in the quality of dissolved and particulate organic matter exchanged between a salt marsh and its adjacent estuary. Journal of Geophysical Research G: Biogeosciences 120:1430–1449. https://doi.org/10.1002/2014JG002897

Petrakis S, Seyfferth A, Kan J, et al (2017) Influence of experimental extreme water pulses on greenhouse gas emissions from soils. Biogeochemistry 133:147–164. https://doi.org/10.1007/s10533-017-0320-2

Poffenbarger HJ, Needelman BA, Megonigal JP (2011) Salinity influence on methane emissions from tidal marshes. Wetlands 31:831–842. https://doi.org/10.1007/s13157-011-0197-0

Raich JW, Schlesinger WH (1992) The global carbon dioxide flux in soil respiration and its relationship to vegetation and climate. Chemical and Physical Meteorology 44:81–99. https://doi.org/10.3402/tellusb.v44i2.15428

Ravel B, Newville M (2005) ATHENA , ARTEMIS , HEPHAESTUS : data analysis for X-ray absorption spectroscopy using IFEFFIT. Journal of Synchrotron Radiation 12:537–541. https://doi.org/10.1107/S0909049505012719

Riedel T, Zak D, Biester H, Dittmar T (2013) Iron traps terrestrially derived dissolved organic matter at redox interfaces. Proceedings of the National Academy of Sciences 110:10101–10105. https://doi.org/10.1073/pnas.1221487110

Rubin BER, Gibbons SM, Kennedy S, et al (2013) Investigating the Impact of Storage Conditions on Microbial Community Composition in Soil Samples. PLoS ONE. https://doi.org/10.1371/journal.pone.0070460

Saidy AR, Smernik RJ, Baldock JA, et al (2015) Microbial degradation of organic carbon sorbed to phyllosilicate clays with and without hydrous iron oxide coating. European Journal of Soil Science 66:83–94. https://doi.org/10.1111/ejss.12180

Santos IR, Burdige DJ, Jennerjahn TC, et al (2021) The renaissance of Odum's outwelling hypothesis in "Blue Carbon" science. Estuar Coast Shelf Sci 255:107361. https://doi.org/10.1016/j.ecss.2021.107361

Schuerch M, Spencer T, Temmerman S, et al (2018) Future response of global coastal wetlands to sea-level rise. Nature 561:231–234. https://doi.org/10.1038/s41586-018-0476-5

Segarra KEA, Comerford C, Slaughter J, Joye SB (2013) Impact of electron acceptor availability on the anaerobic oxidation of methane in coastal freshwater and brackish wetland sediments. Geochimica et Cosmochimica Acta 115:15–30. https://doi.org/10.1016/j.gca.2013.03.029

Seyfferth AL, Bothfeld F, Vargas R, et al (2020) Spatial and temporal heterogeneity of geochemical controls on carbon cycling in a tidal salt marsh. Geochim Cosmochim Acta 282:1–18. https://doi.org/10.1016/j.gca.2020.05.013

Seyfferth AL, Fendorf S (2012) Silicate mineral impacts on the uptake and storage of arsenic and plant nutrients in rice (Oryza sativa L.). Environmental Science and Technology 46:13176–13183. https://doi.org/10.1021/es3025337

Seyfferth AL, Morris AH, Gill R, et al (2016) Soil Incorporation of Silica-Rich Rice Husk Decreases Inorganic Arsenic in Rice Grain. Journal of Agricultural and Food Chemistry 64:3760–3766. https://doi.org/10.1021/acs.jafc.6b01201

Smeaton C, Barlow NLM, Austin WEN (2020) Coring and compaction: Best practice in blue carbon stock and burial estimations. Geoderma 364:114180. https://doi.org/10.1016/j.geoderma.2020.114180

Smemo KA, Yavitt JB (2011) Anaerobic oxidation of methane: an underappreciated aspect of methane cycling in peatland ecosystems? Biogeosciences 8:779–793. https://doi.org/10.5194/bg-8-779-2011

Sodano M, Lerda C, Nisticò R, et al (2017) Dissolved organic carbon retention by coprecipitation during the oxidation of ferrous iron. Geoderma 307:19–29. https://doi.org/10.1016/j.geoderma.2017.07.022

Sowers TD, Adhikari D, Wang J, et al (2018a) Spatial Associations and Chemical Composition of Organic Carbon Sequestered in Fe, Ca, and Organic Carbon Ternary Systems. Environ Sci Technol 52:6936–6944. https://doi.org/10.1021/acs.est.8b01158

Sowers TD, Stuckey JW, Sparks DL (2018b) The synergistic effect of calcium on organic carbon sequestration to ferrihydrite. Geochem Trans 19:22–26. https://doi.org/10.1186/s12932-018-0049-4

Stookey LL (1970) Ferrozine-A New Spectrophotometric Reagent for Iron. Anal Chem 42:779–781. https://doi.org/10.1021/ac60289a016

Sun H, Jiang J, Cui L, et al (2019) Soil organic carbon stabilization mechanisms in a subtropical mangrove and salt marsh ecosystems. Science of The Total Environment 673:502–510. https://doi.org/10.1016/j.scitotenv.2019.04.122

Teasley WA, Limmer MA, Seyfferth AL (2017) How Rice (Oryza sativa L.) Responds to Elevated As under Different Si-Rich Soil Amendments. Environmental Science & Technology 51:10335–10343. https://doi.org/10.1021/acs.est.7b01740

ThomasArrigo LK, Kaegi R, Kretzschmar R (2019) Ferrihydrite Growth and Transformation in the Presence of Ferrous Iron and Model Organic Ligands. Environmental Science & Technology 53:13636–13647. https://doi.org/10.1021/acs.est.9b03952

Trifunovic B, Vázquez-Lule A, Capooci M, et al (2020) Carbon Dioxide and Methane Emissions From A Temperate Salt Marsh Tidal Creek. J Geophys Res Biogeosci 125:. https://doi.org/10.1029/2019JG005558

Valiela I, Lloret J, Bowyer T, et al (2018) Transient coastal landscapes: Rising sea level threatens salt marshes. Science of The Total Environment 640–641:1148–1156. https://doi.org/10.1016/j.scitotenv.2018.05.235

Wang ZA, Kroeger KD, Ganju NK, et al (2016) Intertidal salt marshes as an important source of inorganic carbon to the coastal ocean. Limnol Oceanogr 61:1916–1931. https://doi.org/10.1002/lno.10347

Ward ND, Megonigal JP, Bond-Lamberty B, et al (2020) Representing the function and sensitivity of coastal interfaces in Earth system models. Nature Communications 11:2458. https://doi.org/10.1038/s41467-020-16236-2

Widney SE, Smith D, Herbert ER, et al (2019) Science of the Total Environment Chronic but not acute saltwater intrusion leads to large release of inorganic N in a tidal freshwater marsh. Science of the Total Environment 695:133779. https://doi.org/10.1016/j.scitotenv.2019.133779

Wordofa DN, Adhikari D, Dunham-Cheatham SM, et al (2019) Biogeochemical fate of ferrihydrite-model organic compound complexes during anaerobic microbial reduction. Science of the Total Environment 668:216–223. https://doi.org/10.1016/j.scitotenv.2019.02.441

Xin P, Yuan L-R, Li L, Barry DA (2011) Tidally driven multiscale pore water flow in a creek-marsh system. Water Resour Res 47:. https://doi.org/10.1029/2010WR010110

Chapter 5

MARSH MIGRATION INTO FORESTS AND FARMS AFFECTS SOIL BIOGEOCHEMISTRY ALONG THE SALINITY GRADIENT

Abstract

Sea level rise (SLR) and increased storm intensity has caused the salinization of coastal soils due to a landward expansion of the intertidal zone in the low-lying Delmarva Peninsula, allowing salt marshes to migrate upland into forests and agricultural (ag) fields. Transitional zones along the marsh-forest and marsh-ag salinity gradients are visible above ground as ghost forests and crop die-off. While marsh migration affects the aboveground vegetation, it remains unclear how marsh migration affects belowground soil biogeochemistry along the salinity gradient. We hypothesized that as salt marshes move into upland zones, soil C concentration increases due to higher inundation and slower C mineralization rates. We further hypothesized that each transition zone will have unique soil biogeochemistry, characteristic of the extent of salinization. To investigate this, soil cores were taken along the salinity gradient in both marsh-forest and marsh-ag transects at 6 different sites (i.e., 3 marsh-ag and 3 marsh-forest) on the Delmarva Peninsula. Our results suggest significant ($p<0.05$) changes to soil C concentration as marshes move into forests and ag fields, with a range between 4-50 times more concentrated soil C in the marsh soils than their upland counterparts. The migrating marsh layer of soil is characteristic of a typical anaerobic wetland (i.e., low redox, high silt, high C), but is relatively thin and is underlain by typical upland aerobic soil (i.e., high redox, low silt,

low C), particularly in regions where marsh migration is fastest. In addition, unique biogeochemistry was apparent across the salinity gradient. Marsh end members support sulfate reduction; transitional zones support iron reduction; and upland end members support aerobic reduction with Fe reduction occurring at depth. In addition, the quality and quantity of chromophoric dissolved organic matter (CDOM) changed across the gradients, indicating differences in C cycling dynamics. These findings have important implications for coastal ecosystem function under rising sea level.

5.1 Introduction

Coastal wetlands are migrating upland into forests (Raabe and Stumpf 2016; Langston et al. 2017, 2022) and agricultural fields (Gedan and Fernández-Pascual 2019; Guimond and Michael 2021) due to a combination of fast processes associated with increased storm surge (Fagherazzi et al. 2019; Kearney et al. 2019) and slow processes associated with sea level rise (SLR) (Schieder et al. 2018) that are driving saltwater intrusion (Tully et al. 2019). The intrusion of saltwater and subsequent transition of upland terrestrial areas to more marine-like marsh habitat is controlled by key factors such as local rates of relative SLR (Schieder and Kirwan 2019), topographic slope (Kirwan et al. 2016a) , sedimentation rates (Kirwan et al. 2010) , ecosystem disturbance (Walters et al. 2021) , vegetation structure, and land use (Gedan et al. 2020; Jobe and Gedan 2021). A visible gradient in the extent of saltwater intrusion can be seen in the health of aboveground vegetation. In coastal forests, this manifests as decreasing tree foliage and sapling growth as trees become increasingly salt stressed towards the migrating marsh front (Smith and Kirwan 2021). The same salinity gradient exists along the marsh-ag transect as crop yield progressively declines with increased salt stress (Tully et al. 2019; Guimond and Michael 2021). These

transitional zones are a way to visualize the extent of inundation, saltwater intrusion, and subsequent ecosystem transition (Smith 2013). While climate change (i.e., increased storm surge and SLR) is altering aboveground vegetation in coastal forests and farms, its effects on belowground biogeochemistry along these salinity gradients are less clear as these alterations are not visible and have yet to be extensively studied across marsh-forest and marsh-ag transects.

The intrusion of saltwater into upland freshwater ecosystems can have a variety of effects on belowground soil biogeochemistry, which ultimately affects aboveground vegetation and ecosystem function. Soil salinization causes increased ionic strength, alkalinization, and sulfidation, all of which negatively affect vegetation not adapted for saline conditions (Tully et al. 2019). In particular, the primary productivity of freshwater vegetation is expected to decrease due to increased salt stress (McKee and Mendelssohn 1989; Willis and Hester 2004), likely changing the quality and quantity of fresh dissolved organic carbon (DOC) inputs to the soil. The optical properties of chromophoric dissolved organic matter (CDOM) may give an indication of DOC quality and at the marine-terrestrial interface, can give an indication of marine-like versus terrestrial-like derived DOC (Tzortziou et al. 2008, 2020; Osburn et al. 2015). In addition, microbial activity and communities may shift from increased inundation and soil salinity (Canavan et al. 2006; Weston et al. 2006) due to changes in redox potential, electrical conductivity, pH, and the availability of alternative electron acceptors such as Fe oxides and sulfate. Taken together, these soil processes could illuminate a biogeochemical fingerprint to the incremental effects of below-ground saltwater intrusion.

Marsh migration is also expected to increase soil C concentration. This is because marshes sequester soil C orders of magnitude more quickly than terrestrial systems. Blue C ecosystems (i.e., salt marshes, seagrasses, mangroves) have received much attention recently, as their protection and restoration have been considered important mitigators of climate change due to rapid soil C sequestration (Chmura et al. 2003; Duarte et al. 2013; Mcleod et al. 2016; Alongi 2018; Macreadie et al. 2021). While this is the case for mature and established blue carbon ecosystems, newly migrated marsh into upland forests have been shown to decrease overall C storage in the short term, namely due to a loss of aboveground C stocks in trees and shrubs (Smith and Kirwan 2021), ,while agricultural fields experiencing saltwater intrusion will likely increase their C storage (De La Reguera and Tully 2021) due to very low soil C inherent in US farm fields (Martens et al. 2004).

To more fully understand how marsh migration into forests and farms affects belowground soil biogeochemistry and coastal ecosystem soil C, we conducted an analysis of the soil and porewater at three forest and three ag locations where marsh migration is occurring along the coastline of the Delmarva Peninsula. We hypothesized that as marshes migrate upland, soil C concentration increases due to lower redox potential and slower microbial decomposition. We further hypothesized that points along the upland to lowland transects have a unique biogeochemical fingerprint, indicative of the extent of saltwater intrusion. Our findings have implications for better understanding how coastal ecosystem soil biogeochemistry will respond to a changing climate.

5.2 Methods and Materials

5.2.1 Field Sites

The 6 field sites are located along the Delmarva Peninsula and include 3 marsh-ag sites (hereafter referred to DE-ag, MD-ag, and VA-ag) and 3 marsh-forest sites (hereafter referred to as DE-forest, MD-forest and VA-forest) in each of the three states (Figure 5.1). At the ag sites, five points along the upland to lowland transect were identified and each was sampled separately (Figure 5.1). These ag-site transect points from upland to lowland were identified based on above-ground features and are hereafter referred to as “Ag”, “Margin”, “Transition”, “Phragmites”, and “Spartina”. At the forest sites, four points along the upland to lowland transect were identified and are hereafter referred to as “High Forest”, “Mid Forest”, “Low Forest”, and “Marsh” following previous identification and naming conventions (Smith and Kirwan 2021).

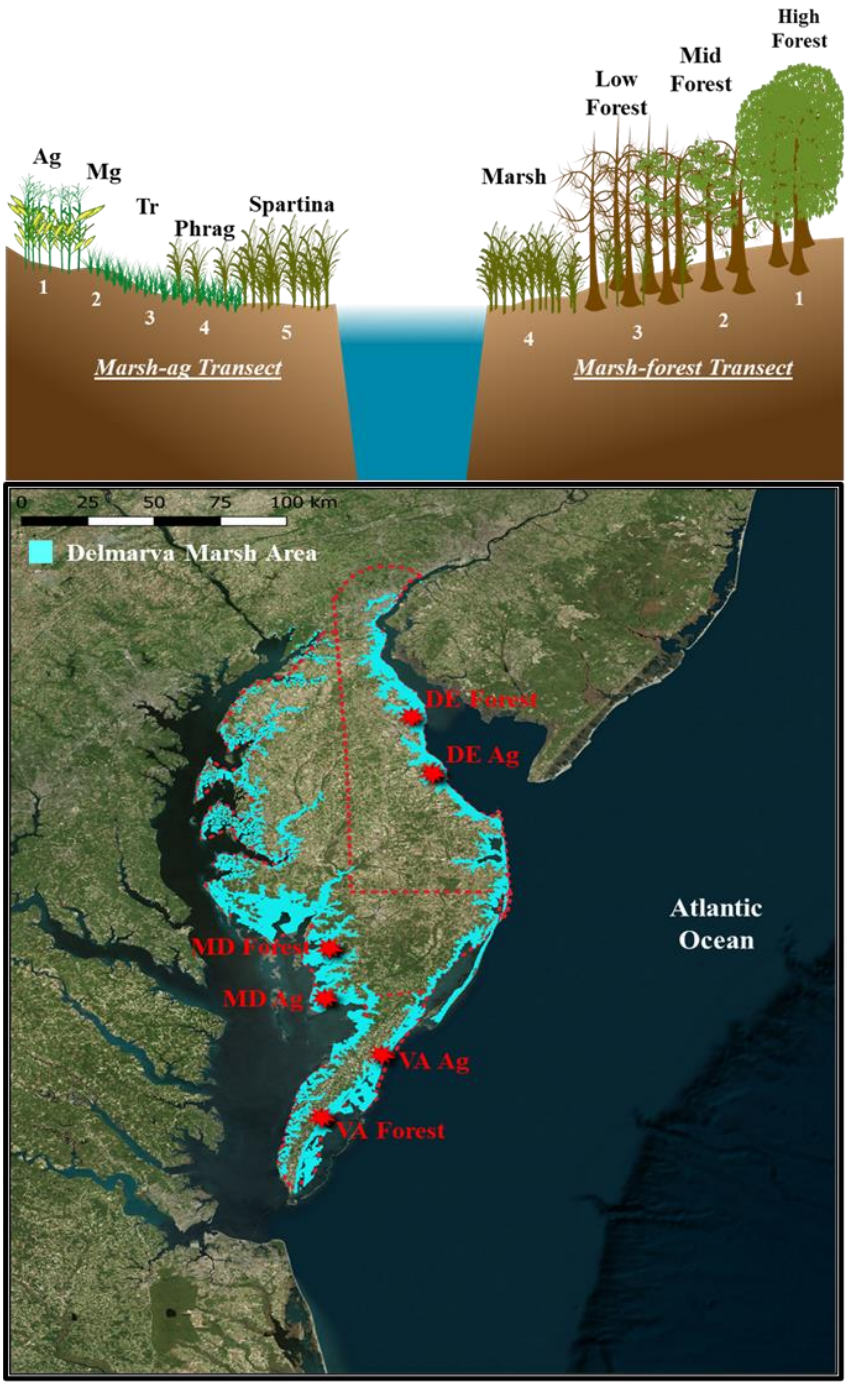

Figure 5.1 Map of the Delmarva Peninsula and locations of the Ag and Forest sites in each of the three Delmarva states (DE, MD, VA), as well as a conceptual diagram showing the transect points for both Ag (n=5) and Forest sites (n=4)

5.2.2 Soil Sampling and Analysis

Soil cores were collected at the 6 field sites at each of the transect points previously mentioned (Figure 5.1). Samples were collected in the summer and fall of 2021, as well as the summer of 2022. Soil cores (84 cm x 3 cm) were taken using a gouge auger which has been shown to minimize compaction (Smeaton et al. 2020). In the field, the cores were quickly sectioned into 12 cm increments (i.e., 7 increments per soil core), placed in 250 mL HDPE bottles, and sealed inside gas impermeable bags with oxygen scrubbers (AneroPack-Anero, Mitsubishi) for anoxic preservation during transport back to the lab. Once back in the lab, the 12 cm soil sections were immediately placed inside an anoxic glove bag containing 95% nitrogen and 5% hydrogen. A subsample of each soil section was left to dry inside the glove bag for elemental analysis. Once dried, the subsample was ground, sieved (2mm) and powdered for analysis of total C, H, N and S (Vario EL Cube, Elementar). The remaining field-moist soil was left inside the 250 mL HDPE vial, capped inside the glove bag, and centrifuged for extraction of porewater according to the following section.

5.2.3 Porewater Extraction and Analysis

Porewater was extracted from the individual 12 cm soil increments by centrifugation. Capped, anoxically preserved HDPE bottles containing field-moist soil sections were placed inside the centrifuge and spun at 2,000 *g* for 10 minutes. A fraction of the porewater was filtered with 0.45µm PTFE syringe filters while the remaining fraction was vacuum-filtered using glass fiber filters (0.7µm). The 0.45µm filtered porewater was analyzed for Fe^{2+} using the ferrozine colorimetric method (Stookey 1970), S^{2-} using the methylene blue method (Cline 1969), pH, redox

potential (relative to the standard hydrogen electrode), and salinity using calibrated electrodes (Orion Ross Ultra pH/ATC Triode, Orion 9179E Triode, Orion DuraProbe Conductivity Cell), and total elements with ICP-MS after acidification to 2% HNO_3 solution. The porewater filtered with 0.7 µm glass fiber was analyzed for dissolved organic carbon (DOC), dissolved inorganic carbon (DIC), and total nitrogen (TN) (Vario TOC Analyzer, Elementar). Optical properties of chromophoric dissolved organic matter (CDOM) were further characterized with ultraviolet-visible analysis (UV-VIS spectrometer, Aligent). Measurements were taken over the wavelengths of 200-730 nm with 2 nm steps. The instrument was calibrated using double deionized (DDI) water blanks. Absorbance indices (Abs_{254}, $SUVA_{254}$, S_r, E_2:E_3) were calculated using previously established equations (Hansen et al. 2016).

5.2.4 Statistical Analysis

Differences in biogeochemical variables between transect points at each site were assessed using one-way analysis of variance (ANOVA) with a post hoc Tukey HSD analysis (α=0.05). Bivariate linear regression was used to determine significant trends with depth and only the significant ($p<0.05$) correlations are reported. Other relationships among variables were analyzed using principal components analysis (PCA). Finally, a normal mixture cluster analysis was conducted to identify groupings of data based on statistically significant biogeochemical variables. All statistical analyses were done using JMP (Version 16.2).

5.3 Results

5.3.1 Solid-Phase Depth Profiles

Soil solid-phase data varied with depth in soil profiles (Figure 5.2). At the DE-ag site, the soil C at the Ag transect point decreased with depth (R^2=0.83, p=0.004), as did the C:H ratio (R^2=0.81, p=0.01). Soil S but not Soil C decreased with depth (R^2=0.31, p<0.0001) at the Marginal transect point. At Transition, soil C decreased with depth (R^2=0.93, p<0.0001), as did soil S (R^2=0.62, p=0.03) and the C:H ratio (R^2=0.84, p=0.003). At Phragmites, soil C decreased with depth (R^2=0.63, p=0.03). No significant trends in soil S or C with depth were observed at Spartina. The MD-ag site had several significant trends with depth in the solid phase data. Soil C decreased with depth across the entire site (R^2=0.67, p=0.02), as did the C:H ratio (R^2=0.84, p=0.004). At Marginal, soil C decreased with depth (R^2=0.64, p=0.03), as did the C:H ratio (R^2=0.66, p=0.03). At Transition, soil C decreased with depth, (R^2=0.61, p=0.04), as did the C:H ratio (R^2=0.58, p=0.04) while the sand:silt ratio increased with depth (R^2=0.93, p=0.04). At Phragmites, there were no significant trends with depth, but the surface soil C starts at ~40% C and drops to ~1% throughout the remainder of the soil core. Spartina had soil C which decreased with depth (R^2=0.83, p=0.004) while the C:N ratio increased with depth (R^2=0.74, p=0.01). At the VA-ag site, several transect points had significant trends with depth. Soil C decreased with depth at Ag (R^2=0.56, p=0.05) and Phragmites (R^2=0.57, p=0.05) while soil S decreased at Phragmites (R^2=0.60, p=0.04). At Transition, the sand:silt ratio decreased with depth (R^2=0.82, p=0.04).

At the DE-forest site, the High Forest soil C decreased with depth (R^2=0.69, p=0.02), while Mid Forest showed no significant trends with depth. Low Forest soil C

decreased with depth (R^2=0.97, p=0.002) and the sand:silt ratio increased with depth R^2=0.86, p=0.02). At the Marsh, there were no significant trends with depth. The MD-forest site also showed significant trends with depth. At the High Forest, soil C (R^2=0.61, p=0.04), soil S (R^2=0.61, p=0.04) and the C:H ratio (R^2=0.61, p=0.04) all decreased with depth. Mid Forest soil C decreased with depth (R^2=0.64, p=0.03), as did the C:H ratio (R^2=0.60, p=0.04). The Low Forest soil C decreased with depth (R^2=0.60, p=0.04) while the sand:silt ratio increased with depth (R^2=0.89, p=0.02). The Marsh had no significant trends with depth. The VA-forest site Marsh sand:silt ratio significantly increased with depth at the Marsh (R^2=0.75, p=0.03), as did redox (R^2=0.82, p=0.005).

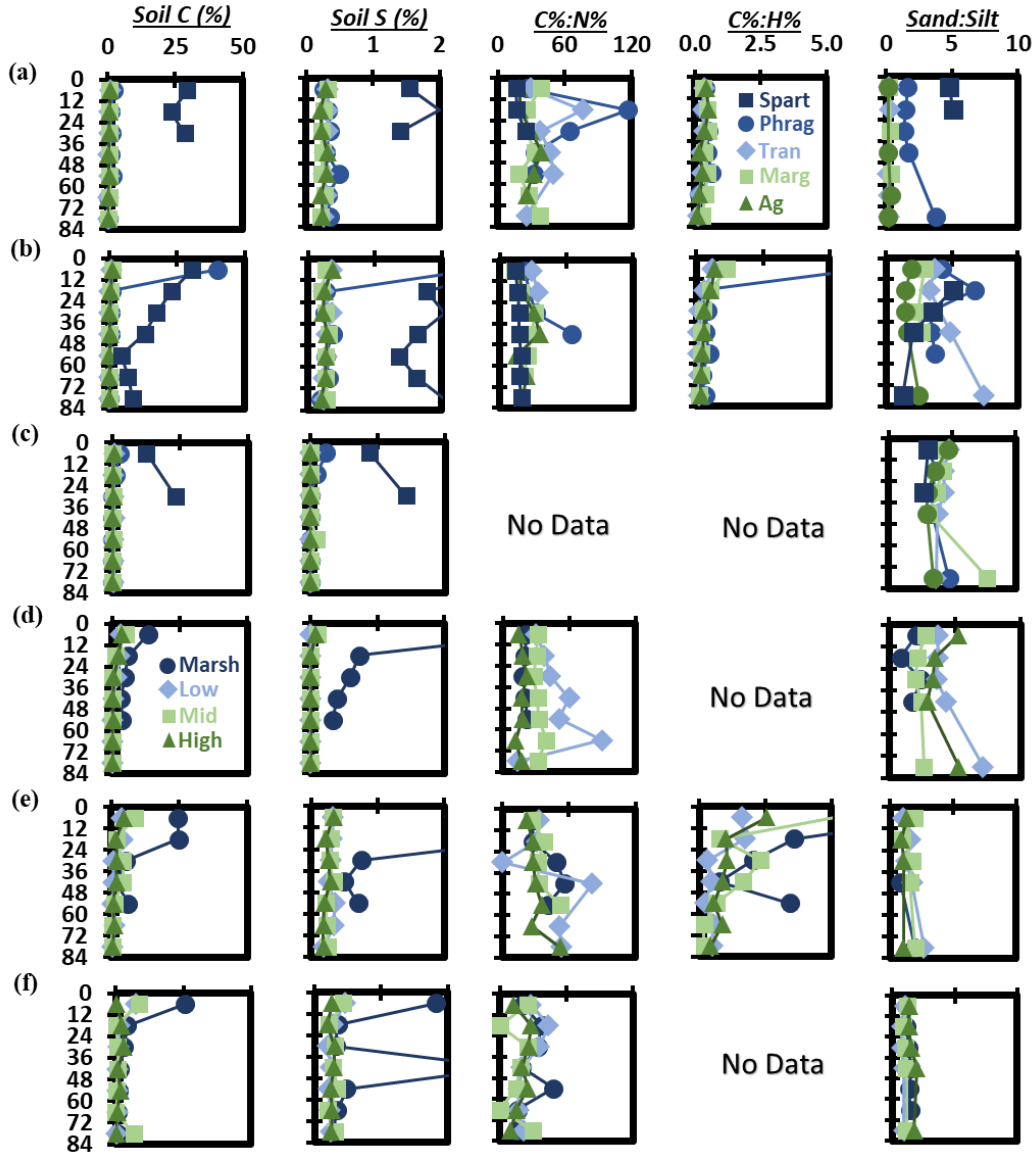

Figure 5.2 Depth profiles of the solid-phase data at (a) DE-ag, (b) MD-ag, (c) VA-ag, (d) DE-forest, (e) MD-forest, and (f) VA-forest.

5.3.2 Porewater Depth Profiles

Porewater data varied with depth in the soil profiles (Figure 5.3). At the DE-ag site, Ag DOC decreased with depth (R^2=0.69, p=0.02), as did salinity (R^2=0.72,

p=0.02). At Marginal, salinity decreased with depth (R^2=0.74, p=0.01). Transition DOC decreased with depth (R^2=0.59, p=0.04), as did redox (R^2=0.61, p=0.04), salinity (R^2=0.60, p=0.04) and E_2:E_3 (R^2=0.61, p=0.04). Phragmites and Spartina had no significant trends with depth. The MD-ag site showed significant trends with depth. At Ag, redox increased with depth (R^2=0.77, p=0.04) while pH decreased (R^2=0.93, p=0.01). At Marginal, DOC decreased with depth (R^2=0.85, p=0.01), as did pH (R^2=0.63, p=0.03), Fe^{2+} (R^2=0.79, p=0.02), DIC (R^2=0.96, p=0.02), TN (R^2=0.81, p=0.01) and $SUVA_{254}$ (R^2=0.89, p=0.01) while salinity increased with depth (R^2=0.90, p=0.001). At Transition, DOC decreased with depth (R^2=0.85, p=0.03), as did S^{2-} (R^2=0.79, p=0.04), pH (R^2=0.98, p=0.001) and $SUVA_{254}$ (R^2=0.83, p=0.03). Both redox (R^2=0.98, p=0.002) and salinity (R^2=0.89, p=0.02) increased with depth. At the Spartina location, E_2:E_3 (R^2=0.88, p=0.002) and TN (R^2=0.91, p=0.001) increased with depth, while S_r decreased with depth (R^2=0.70, p=0.02). The VA-ag site was dry during soil coring and therefore porewater was only recoverable from Phragmites and Spartina transect points. At Phragmites, pH increased with depth (R^2=0.98, p<0.0001). At Spartina, salinity increased with depth (R^2=0.96, p=0.006), as did $SUVA_{254}$ (R^2=0.99, p<0.04).

At the DE-forest site, High Forest soils were dry and porewater could not be recovered. Mid Forest DOC decreased with depth (R^2=0.84, p=0.01), as did redox (R^2=0.84, p=0.01), salinity (R^2=0.92, p=0.003), TN (R^2=0.74, p=0.03), and E_2:E_3 (R^2=0.80, p=0.01). At Low Forest, DOC (R^2=0.81, p=0.02) and S_r (R^2=0.80, p=0.04) decreased with depth while Fe^{2+} (R^2=0.70, p=0.04) and pH (R^2=0.79, p=0.02) increased with depth. At the Marsh, DOC (R^2=0.78, p=0.04) and E_2:E_3 (R^2=0.85, p=0.03) increased with depth while the salinity (R^2=0.77, p=0.04), DIC (R^2=0.98,

p=0.001), and $SUVA_{254}$ (R^2=0.73, p=0.004) decreased with depth**.** The MD-forest site also showed significant trends with depth. At High Forest, Fe^{2+} decreased with depth (R^2=0.65, p=0.03), as did salinity (R^2=0.77, p=0.01), while S^{2-} increased with depth (R^2=0.59, p=0.04). At Mid Forest, redox decreased with depth (R^2=0.77, p=0.01). At Low Forest, E_2:E_3 decreased with depth (R^2=0.68, p=0.02). In the Marsh, S_r decreased with depth (R^2=0.91, p=0.01). At the VA-forest, there were several significant trends with depth. The High Forest pH increased with depth (R^2=0.76, p=0.01) while E_2:E_3 decreased with depth (R^2=0.86, p=0.02). Mid Forest DOC decreased with depth (R^2=0.86, p=0.003), as did E_2:E_3 (R^2=0.83, p=0.01) while the salinity (R^2=0.77, p=0.01) and S_r (R^2=0.89, p=0.005) increased with depth. Low Forest redox increased with depth (R^2=0.83, p=0.004), as did the salinity (R^2=0.70, p=0.02). In the Marsh, Fe^{2+} increased with depth (R^2=0.69, p=0.02), as did the redox (R^2=0.82, p=0.01) and TN (R^2=0.61, p=0.04).

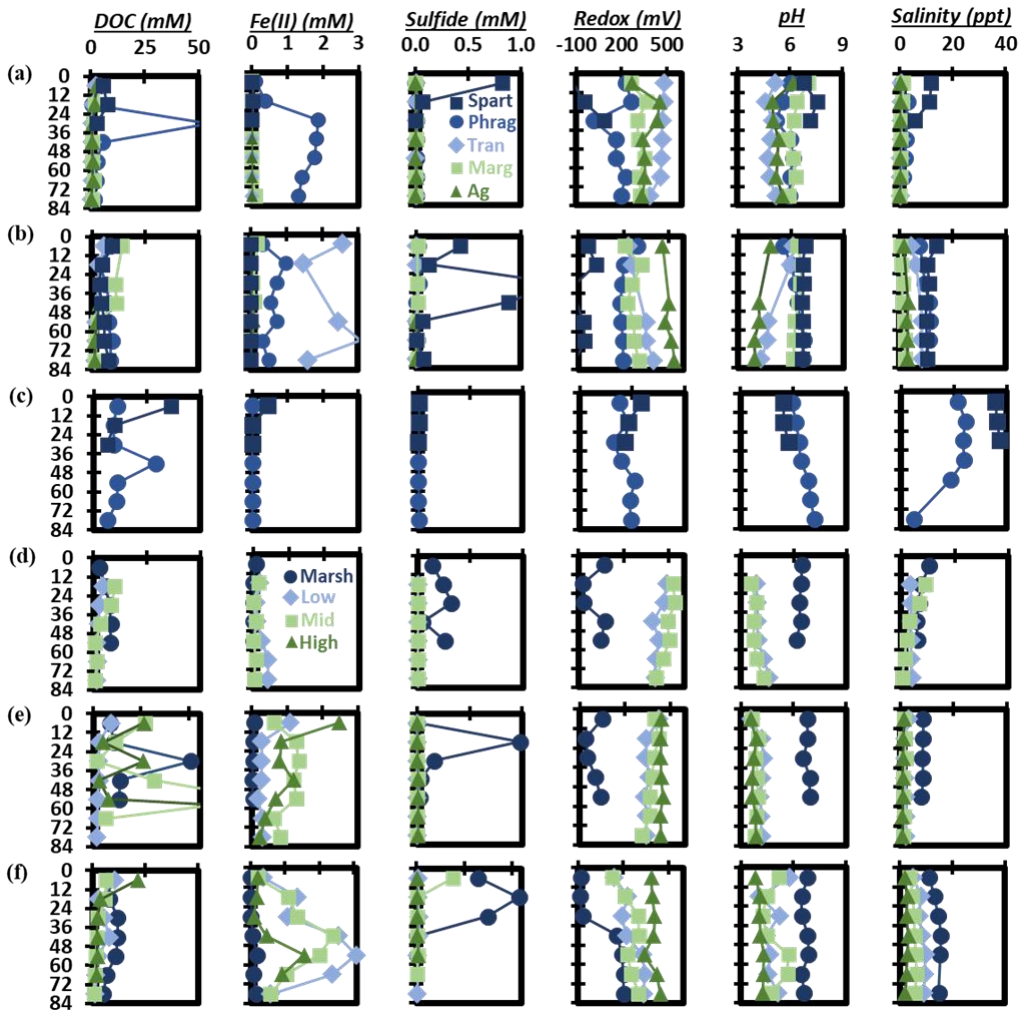

Figure 5.3 Depth profiles of the porewater data at (a) DE-ag, (b) MD-ag, (c) VA-ag, (d) DE-forest, (e) MD-forest, and (f) VA-forest.

5.3.3 Analysis of Variance Between Transects

5.3.3.1 Agricultural Sites

Significant ($p<0.05$) differences between points along the transects exist for many of the measured variables. At the DE-ag site (Table 5.1a), soil C is significantly higher at Spartina than all other transect points, which were statistically similar.

Spartina on average contains 23x more soil C than Phragmites, 47x more than Transition, 38x more than Margin and 49x more than Ag. Soil S is significantly higher at Spartina and is approximately 5x more concentrated than all other transect points. There were no significant differences in DOC between transect points due to the high variability with depth, though Phragmites has the highest mean, followed by Spartina. Transition had the lowest mean DOC concentration. DIC was significantly higher at Spartina by more than an order of magnitude while TN is also significantly higher at Spartina. Higher concentrations of S^{2-} were detected at the Spartina location, therefore S^{2-} is significantly higher at Spartina, while Fe^{2+} was higher in concentration at Phragmites and therefore Fe^{2+} is significantly higher at Phragmites. The redox potential was significantly highest at Transition, followed by Ag, Margin, Phragmites and was significantly lowest at Spartina. The pH was statistically different at all five transect points. Spartina had the highest pH, followed by Margin, Phragmites, Ag and Transition. The salinity was statistically similar at Ag, Margin and Transition, while Phragmites was significantly higher and Spartina was still significantly higher. The characterization of CDOM also differed between transect points. $SUVA_{254}$, a measure of aromaticity, was significantly highest at the Transition, and was significantly lowest at Ag and Phragmites. The E_2:E_3 ratio, which is inverse to molecular weight, was significantly lowest at Spartina, and significantly highest at Ag. The S_r, a measure of marine (higher number) vs terrestrial (lower number) DOC, was highest at Transition and lowest at Margin.

Table 5.1a Means (± SD) at the DE Ag site averaged across the 84 cm soil core. Letters indicate significant differences ($p<0.05$) between each transect point.

Variable	Ag	Margin	Transition	Phrag	Spartina
Soil C (%)	0.55(0.29)^{B}	0.71(0.15)^{B}	0.58(0.23)^{B}	1.17(0.68)^{B}	27.14(3.16)^{A}
Soil S (%)	0.26(0.04)^{B}	0.26(0.04)^{B}	0.30(0.03)^{B}	0.34(0.08)^{B}	1.66(0.31)^{A}
DOC (mM)	1.26(0.78)^{A}	1.89(1.73)^{A}	0.96(0.67)^{A}	10.28(7.49)^{A}	5.55(2.41)^{A}
DIC (mM)	0.12(0.25)^{B}	0.84(2.07)^{B}	0.01(0.01)^{B}	0.04(0.08)^{B}	9.70(3.83)^{A}
TN (mM)	0.13(0.11)^{B}	0.09(0.15)^{B}	0.34(0.34)^{B}	0.31(0.08)^{B}	1.42(0.48)^{A}
Sulfide (mM)	0.00(0.00)^{B}	0.00(0.00)^{B}	0.01(0.00)^{B}	0.01(0.00)^{B}	0.30(0.46)^{A}
Fe^{2+} (mM)	0.00(0.04)^{B}	0.00(0.00)^{B}	0.02(0.02)^{B}	1.24(0.71)^{A}	0.01(0.01)^{B}
Redox (mV)	363.94(63.4)^{B}	319.85(33.7)^{B}	460.60(12.6)^{A}	179.74(82.2)^{C}	-27.53(105.8)^{D}
pH	5.38(0.40)^{D}	6.30(0.38)^{B}	4.92(0.22)^{E}	5.87(0.13)^{C}	7.17(0.37)^{A}
Salinity (ppt)	0.21(0.57)^{C}	.49(0.50)^{C}	0.45(0.74)^{C}	1.77(0.33)^{B}	9.63(3.42)^{A}
$SUVA_{254}$	0.22(0.12)^{B}	0.29(0.13)^{AB}	0.41(0.18)^{A}	0.18(0.14)^{B}	0.35(0.07)^{AB}
E_2:E_3	6.15(1.19)^{A}	4.80(1.39)^{AB}	5.44(1.58)^{AB}	3.94(1.50)^{BC}	2.22(0.31)^{C}
S_r	3.78(2.01)^{AB}	2.16(0.94)^{B}	5.10(2.91)^{A}	2.44(2.43)^{B}	2.13(0.39)^{AB}

The MD-ag site showed significant differences between transect points (Table 5.1b). Spartina had significantly more soil C than all other transect points. Phragmites had an average soil C concentration over an order of magnitude higher than the upland areas but was not significantly different due to high variability across the depth profile. Soil S was significantly higher at Spartina than all other transect points. DOC was significantly highest at Phragmites and Marginal and was lowest at Ag and Transition. DIC was nondetectable at Ag and Transition while Spartina had

significantly higher DIC than both Phragmites and Marginal by an order of magnitude. The TN was significantly highest at Spartina and was statistically similar elsewhere. S^{2-} was essentially nondetectable at all transect points except at Spartina, while Fe^{2+} was significantly highest at Transition, followed by Phragmites and the remaining sites were close to nondetectable. The redox was significantly highest at Ag, followed by Margin and Transition which were statistically similar. Phragmites redox was significantly lower and Spartina was even lower. Spartina, Phragmites and Margin had significantly higher pH values, followed by Transition and Ag which had the lowest pH. The salinities at Spartina and Phragmites locations were statistically similar and significantly highest. Transition had a significantly lower salinity, followed by Margin and Ag whose salinities were statistically similar. $SUVA_{254}$ was only significantly different at Spartina which had the highest average value. Spartina location had the lowest E_2:E_3 ratio while Ag had the highest. The S_r was highest at Spartina and lowest at Margin and Phragmites.

Table 5.1b Means (± SD) at the MD Ag site averaged across the 84cm soil core. Letters indicate significant differences ($p<0.05$) between each transect point.

Variable	**Ag**	**Margin**	**Transition**	**Phrag**	**Spartina**
Soil C (%)	$0.46(0.35)^{B}$	$0.45(0.41)^{B}$	$0.25(0.29)^{B}$	$6.19(14.93)^{B}$	$15.00(9.45)^{A}$
Soil S (%)	$0.26(0.05)^{B}$	$0.27(0.03)^{B}$	$0.28(0.05)^{B}$	$0.60(0.86)^{B}$	$1.90(0.46)^{A}$
DOC (mM)	$2.02(1.02)^{B}$	$7.06(5.65)^{A}$	$2.65(1.78)^{B}$	$7.29(1.84)^{A}$	$5.77(2.09)^{AB}$
DIC (mM)	$0.00(0.00)^{B}$	$0.24(0.20)^{B}$	$0.00(0.00)^{B}$	$1.00(0.76)^{B}$	$11.27(2.65)^{A}$
TN (mM)	$0.27(0.20)^{B}$	$0.63(0.51)^{B}$	$0.23(0.11)^{B}$	$0.42(0.47)^{B}$	$2.41(0.93)^{A}$
Sulfide (mM)	$0.00(0.00)^{B}$	$0.01(0.01)^{B}$	$0.00(0.00)^{B}$	$0.01(0.01)^{B}$	$0.42(0.52)^{A}$

Fe^{2+} (mM)	0.04(0.05)^{C}	0.07(0.07)^{C}	2.23(0.68)^{A}	0.59(0.24)^{B}	0.01(0.01)^{C}
Redox (mV)	499.61(31.1)^{A}	264.41(39.6)^{B}	317.06(71.50)^{B}	205.06(38.9)^{C}	-71.54(50.9)^{D}
pH	4.21(0.37)^{C}	6.35(0.18)^{A}	5.14(0.84)^{B}	6.29(0.41)^{A}	6.68(0.07)^{A}
Salinity (ppt)	2.76(0.71)^{C}	1.29(0.67)^{C}	7.15(1.87)^{B}	9.93(1.47)^{A}	10.90(1.43)^{A}
$SUVA_{254}$	0.19(0.06)^{B}	0.31(0.10)^{AB}	0.25(0.12)^{B}	0.28(0.08)^{B}	0.41(0.12)^{A}
E_2:E_3	8.64(0.98)^{A}	4.81(0.97)^{B}	3.24(1.26)^{CD}	3.96(0.80)^{BC}	2.54(0.36)^{D}
S_r	1.01(0.20)^{B}	0.73(0.15)^{C}	1.06(0.35)^{B}	0.74(0.07)^{C}	2.16(0.19)^{A}

At the VA-ag site (Table 5.1c), both soil C and soil S concentration was significantly higher at Spartina than all other transect points. The porewater data are only available at Phragmites and Spartina due to dry conditions at the other transect points. The DOC concentrations at Phragmites and Spartina are not significantly different, but DIC is significantly higher at Phragmites than Spartina. The pH was significantly lower at Spartina, while the salinity was significantly higher. The remaining porewater variables showed no significant differences between Phragmites and Spartina.

Table 5.1c Means (± SD) at the VA Ag site averaged across the 84 cm soil core. Letters indicate significant differences ($p<0.05$) between each transect point.

Variable	Ag	Margin	Transition	Phrag	Spartina
Soil C (%)	0.36(0.22)^{B}	0.18(0.20)^{B}	0.68(0.18)^{B}	0.74(1.00)^{B}	17.9(7.5)^{A}
Soil S (%)	0.00(0.00)^{B}	0.01(0.04)^{B}	0.00(0.00)^{B}	0.05(0.09)^{B}	1.15(0.38)^{A}
DOC (mM)	No Data	No Data	No Data	12.45(7.57)^{A}	17.34(16.41)^{A}

DIC (mM)	No Data	No Data	No Data	1.56(1.03)^{A}	0.12(0.22)^{B}
TN (mM)	No Data	No Data	No Data	0.47(0.27)^{A}	0.59(0.40)^{A}
Sulfide (mM)	No Data	No Data	No Data	0.004(0.002)^{A}	0.004(0.0003)^{A}
Fe^{2+} (mM)	No Data	No Data	No Data	0.001(0.002)^{A}	0.15(0.25)^{A}
Redox (mV)	No Data	No Data	No Data	260.2(43.2)^{A}	294.7(48.4)^{A}
pH	No Data	No Data	No Data	6.55(0.47^{A})	5.54(0.16)^{B}
Salinity (ppt)	No Data	No Data	No Data	19.42(7.52)^{B}	36.50(0.90)^{A}
$SUVA_{254}$	No Data	No Data	No Data	0.07(0.05)^{A}	0.06(0.02)^{A}
E_2:E_3	No Data	No Data	No Data	No Data	No Data
S_r	No Data	No Data	No Data	No Data	No Data

5.3.3.2 Forest Sites

Differences between transect points were also apparent at the DE-forest site (Table 5.2a). The Marsh had significantly higher soil C than all upland transitions by approximately 6x. The Marsh also had significantly more soil S while at the forested sites, soil S was essentially nondetectable. The Low Forest had significantly less DOC than the Marsh, while the Marsh had the highest average DOC concentration. DIC was essentially nondetectable at the forested transitions and was significantly highest in the Marsh. TN in the forested transitions was approximately 0.5mM while the Marsh had approximately 3x that amount and was significantly higher. S^{2-} was only detectable in the Marsh while the forested transitions showed little sign of porewater S^{2-}. The Low Forest had significantly higher Fe^{2+} than any other location. The redox was similar at Mid and Low Forest while the Marsh was significantly lower. The pH and salinity at Mid and Low Forest were also statistically similar while the pH and salinity at the

Marsh was significantly higher. The $SUVA_{254}$ and S_r were statistically similar across transect points while the E_2:E_3 ratio was significantly highest at the Marsh.

Table 5.2a Means (± SD) at the DE Forest site averaged across the 84 cm soil core. Letters indicate significant differences ($p<0.05$) between each transect point.

Variable	High Forest	Mid Forest	Low Forest	Marsh
Soil C (%)	1.06(1.33)^{B}	1.09(1.77)^{B}	1.23(1.37)^{B}	6.13(4.16)^{A}
Soil S (%)	0.01(0.03)^{B}	0.02(0.04)^{B}	0.00(0.00)	1.13(1.38)^{A}
DOC (mM)	No Data	4.06(4.09)^{AB}	2.34(1.06)^{B}	6.41(2.26)^{A}
DIC (mM)	No Data	0.002(0.00)^{B}	No Data	3.09(1.80)^{A}
TN (mM)	No Data	0.42(0.47)^{B}	0.36(0.24)^{B}	1.54(0.59)^{A}
Sulfide (mM)	No Data	0.00(0.00)^{B}	0.00(0.00)^{B}	0.20(0.11)^{A}
Fe^{2+} (mM)	No Data	0.06(0.06)^{B}	0.24(0.14)^{A}	0.02(0.03)^{B}
Redox (mV)	No Data	488.67(46.8)^{A}	432.58(36.0)^{A}	9.8(74.9)^{B}
pH	No Data	3.85(0.24)^{B}	4.11(0.29)^{B}	6.35(0.13)^{A}
Salinity (ppt)	No Data	3.69(3.34)^{B}	3.66(0.12)^{B}	7.29(1.92)^{A}
$SUVA_{254}$	No Data	1.37(0.74)^{A}	1.55(1.41)^{A}	0.62(0.19)^{A}
E_2:E_3	No Data	1.57(0.11)^{B}	1.77(0.19)^{B}	2.52(0.28)^{A}
S_r	No Data	1.60(0.20)^{A}	1.52(0.13)^{A}	1.41(0.10)^{A}

At the MD-forest site (Table 5.2b), soil C was significantly highest at the Marsh while all other transect points had statistically similar soil C concentrations. Soil S trended similarly, where the Marsh had significantly more than all other transect points. While the average DOC concentration at the High Forest location was much higher than all other transect points, no transect points were statistically

different due to the high variability with depth. DIC was only detectable in the Marsh and High Forest, where the Marsh had significantly higher levels. TN was highest at the High Forest, but none of the transect points were statistically different. S^{2-} was only detectable at the Marsh location while Fe^{2+} was significantly highest at both the High and Mid Forest. The redox was significantly highest at the High Forest, followed by Mid and Low Forest which had statistically similar redox potentials. The Marsh had the significantly lowest redox. The pH was significantly lowest at the High and Mid Forest locations, followed by the Low Forest. The Marsh had the significantly highest pH. The salinities were all significantly different between transect points with the highest salinity at the Marsh, followed by Low, Mid, and High Forest. The $SUVA_{254}$ was significantly highest at the Mid Forest location, while the High Forest and marsh were significantly lower. The E_2:E_3 ratio was significantly highest at the Mid Forest, while the High Forest and Low Forest were significantly lower. S_r was not significantly different between any of the transect points.

Table 5.2b Means (± SD) at the MD Forest site averaged across the 84 cm soil core. Letters indicate significant differences ($p<0.05$) between each transect point.

Variable	High Forest	Mid Forest	Low Forest	Marsh
Soil C (%)	$1.76(1.40)^{B}$	$2.92(2.98)^{B}$	$1.60(1.55)^{B}$	$12.49(11.19)^{A}$
Soil S (%)	$0.24(0.06)^{B}$	$0.28(0.05)^{B}$	$0.30(0.06)^{B}$	$1.51(1.29)^{A}$
DOC (mM)	$43.60(73.69)^{A}$	$27.83(31.70)^{A}$	$3.50(2.53)^{A}$	$19.70(17.79)^{A}$
DIC (mM)	$0.68(0.166)^{B}$	$0.00(0.00)^{B}$	$0.00(0.00)^{B}$	$2.84(1.19)^{A}$
TN (mM)	$5.81(12.31)^{A}$	$0.35(0.15)^{A}$	$0.39(0.33)^{A}$	$0.63(0.13)^{A}$
Sulfide (mM)	$0.00(0.00)^{B}$	$0.00(0.00)^{B}$	$0.00(0.00)^{B}$	$0.24(0.42)^{A}$

Fe^{2+} (mM)	0.93(0.74)^{A}	1.01(0.31)^{A}	0.38(0.32)^{B}	0.04(0.02)^{B}
Redox (mV)	441.46(5.7)^{A}	376.54(34.2)^{B}	354.41(32.8)^{B}	-3.66(49.3)^{C}
pH	3.75(0.13)^{C}	3.86(0.12)^{C}	4.10(0.24)^{B}	6.81(0.16)^{A}
Salinity (ppt)	0.99(0.18)^{D}	1.41(0.31)^{C}	2.03(0.52)^{B}	8.30(0.32)^{A}
$SUVA_{254}$	0.26(0.23)^{B}	1.03(1.22)^{A}	0.55(0.10)^{AB}	0.23(0.13)^{B}
E_2:E_3	2.30(0.42)^{B}	3.78(1.52)^{A}	2.04(0.23)^{B}	2.95(0.57)^{AB}
S_r	2.11(0.53)^{A}	1.80(0.20)^{A}	2.26(0.36)^{A}	1.80(0.45)^{A}

At the VA-forest site (Table 5.2c), soil C was highest at the Marsh, but none of the transect points were statistically different from one another due to high variability with depth. Soil S was statistically highest at the Marsh location. DOC was significantly lower at Mid Forest than at the Marsh, which had the highest DOC concentration. DIC was essentially nondetectable at the forested transect points while DIC at the Marsh was significantly higher. TN was approximately twice as high at the Marsh than in the forested locations and was significantly higher in the Marsh. S^{2-} was significantly highest at the Marsh as well. Fe^{2+} was significantly highest at the Low Forest, significantly lower at the High Forest, and significantly lowest in the Marsh. The redox potential was significantly highest at High Forest, followed by mid and Low Forest which were statistically similar. The Marsh had a significantly lower redox potential than all other transect points. pH was significantly highest at the Marsh, followed by both Mid and Low Forest, while the High Forest was significantly lowest. The $SUVA_{254}$ was significantly highest at the Mid Forest, while the remaining transect points were all statistically similar. The E_2:E_3 ratio was significantly highest at the Marsh while the remaining transect points were all statistically similar. S_r showed no significant differences across any transect points.

Table 5.2c Means (± SD) at the VA Forest site averaged across the 84cm soil core. Letters indicate significant differences ($p<0.05$) between each transect point

Variable	High Forest	Mid Forest	Low Forest	Marsh
Soil C (%)	1.31(1.08)^{A}	2.45(3.52)^{A}	1.71(2.52)^{A}	5.24(9.04)^{A}
Soil S (%)	0.26(0.04)^{B}	0.30(0.08)^{B}	0.27(0.09)^{B}	0.93(1.03)^{A}
DOC (mM)	5.70(7.82)^{AB}	2.86(2.32)^{B}	4.60(3.47)^{AB}	8.85(2.73)^{A}
DIC (mM)	0.01(0.01)^{B}	0.00(0.01)^{B}	0.04(0.07)^{B}	3.87(2.98)^{A}
TN (mM)	0.34(0.18)^{B}	0.34(0.25)^{B}	0.16(0.21)^{B}	0.68(0.18)^{A}
Sulfide (mM)	0.01(0.01)^{B}	0.07(0.15)^{B}	0.02(0.01)^{B}	0.49(0.47)^{A}
Fe^{2+} (mM)	0.57(0.57)^{BC}	1.24(0.77)^{AB}	1.62(1.05)^{A}	0.07(0.07)^{C}
Redox (mV)	399.76(32.9)^{A}	246.5(64.5)^{B}	253.5(80.8)^{B}	73.83(143.7)^{C}
pH	4.13(0.16)^{C}	4.92(0.60)^{B}	4.83(0.58)^{B}	6.64(0.17)^{A}
Salinity (ppt)	2.65(0.47)^{D}	5.39(0.87)^{C}	8.19(1.61)^{B}	14.14(1.66)^{A}
$SUVA_{254}$	0.60(0.1)^{B}	0.86(0.22)^{A}	0.51(0.18)^{B}	0.50(0.09)^{B}
E_2:E_3	2.37(0.56)^{B}	2.03(0.32)^{B}	2.22(0.42)^{B}	3.11(0.51)^{A}
S_r	2.00(0.88)^{A}	2.47(1.31)^{A}	1.96(0.87)^{A}	1.53(0.22)^{A}

5.3.4 Relationships Between Variables

Principal components analysis (PCA) was used to simultaneously visualize relationships between all measured variables at all 6 sites (Figure 5.4). These results indicated several variables that trend well together across the entire dataset. An obvious grouping of variables includes DIC, sulfide, soil C, soil S, Ca, salinity, and pH. Because these variables trend in a similar direction, they have an overall positive relationship with one another. Porewater redox potential trended in the opposite

direction, indicating that redox potential generally trends negatively DIC, sulfide, soil C, soil S. Fe^{2+} and total Fe trend positively together which helps verify the quality of our Fe data. The sand:silt ratio trends in the opposite direction of the Fe variables, as does Si. DOC and Abs_{254} trend in the same direction which verifies the quality of our CDOM and absorbance data since Abs_{254} can be used to estimate DOC concentration. S_r trends in the opposite direction of Abs_{254}. This is likely because Abs_{254} tends to increase with terrestrial-like CDOM while S_r increases with marine-like CDOM.

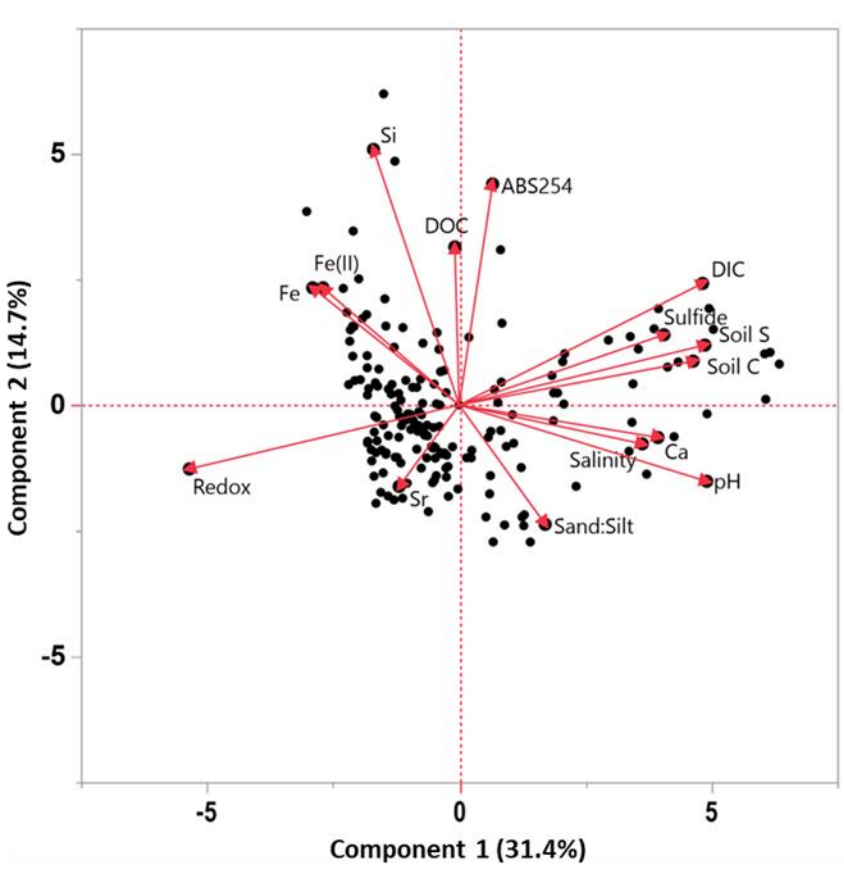

Figure 5.4 Principal Components Analysis (PCA) results, showing the relationships among variables across all six sites and across all transition zones.

5.3.4.1 Normal Mixture Clusters Analysis

Cluster analysis using the normal mixtures approach was conducted across the entire dataset. After finding the best fitting model by determining the correct number of clusters with the best fitting variables, there are three main clusters of data (Figure 5.5). Individual transect points are also indicated by different shapes within clusters. The three main clusters seem to represent lowland (Cluster 1), transition (Cluster 2) and upland (Cluster 3) do to associated mean cluster values for variables (Table 5.4). For example, Cluster 1 contains the highest salinity, pH, sulfide, soil C, soil S and lowest redox and E_2:E_3 (inverse to molecular weight) which are characteristics of highly reducing marsh soils. This is confirmed since most Cluster 1 data points are associated with the Marsh (Forest sites) and Spartina (Ag sites) transect locations. Cluster 2 has lower salinity, pH, sulfide, soil C, soil S, a higher redox and E_2:E_3 and the highest DOC and Fe^{2+}. Cluster 3 has the lowest salinity, sulfide, pH, soil C, soil S and the highest redox and E_2:E_3.

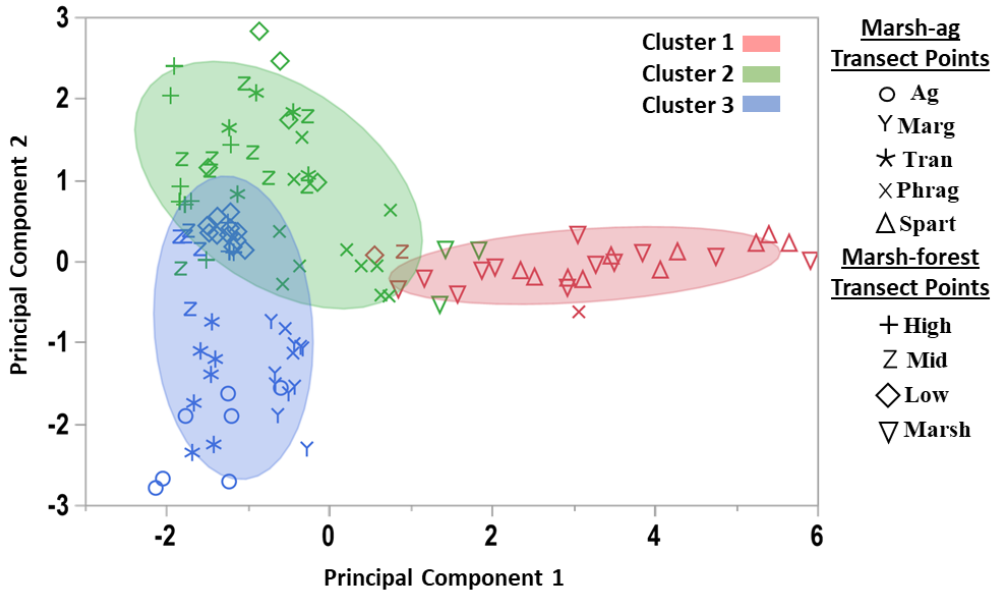

Figure 5.5 Normal mixture clusters analysis showing three main groupings of data.

Table 5.4 Mean values of the variables used to construct principal components in each cluster

Cluster #	Salinity	Redox	pH	Fe (II)	Sulfide	DOC	Soil C	Soil S	E_2:E_3
1	9.5	-1.6	6.6	0.05	0.4	7.5	14.5	1.6	2.7
2	5.4	274.7	5.0	1.3	0.01	16.0	1.3	0.3	2.9
3	1.6	375.6	4.9	0.12	0.005	2.7	0.8	0.2	4.1

5.4 Discussion

5.4.1 Soil C Increases with SLR in the Thin Marsh Layer

We hypothesized that as marshes migrate into upland areas, soil C concentration increases due to lower redox potential and slower microbial decomposition. Our results support this hypothesis, but we acknowledge that our

discrete soil core sampling design does not directly prove that marsh migration is occurring at our field sites, therefore we rely on previous studies in the area showing marsh migration (Kirwan et al. 2016b; Schieder and Kirwan 2019; Carr et al. 2020). We consistently found higher soil C concentrations in anaerobic lowland marsh areas than the oxidized upland forest and farms. Marshes on overage had 25x more soil C than their respective upland counterpart, with a range of between 4-50x higher soil C. Porewater redox potentials were significantly lower in the marsh than in upland soils and redox potential and soil C generally form a negative relationship (Figure 4). Reducing conditions in marsh soils causing increases in soil C is further confirmed by porewater sulfide concentrations that are positively correlated with soil C. These results indicate that as SLR causes marshes to migrate into upland forests and farms, soil C concentrations will drastically increase, though we found a relatively thin layer of marsh sediment in some of our marsh sites.

While marsh migration will increase soil C concentrations, the layer of marsh soil at the migration front seemed to be relatively thin compared to the buried forest soils underneath. This is particularly evident at the VA Forest site, where soils in the top half of the core have higher soil C and porewater sulfide, lower redox and a lower sand:silt ratio. Soil C drastically decreased from ~26% near the surface to 0.5% at 84 cm, porewater redox potential increased from -70 to 170mV, sulfide concentration decreased from ~1mM to nondetectable at 84 cm and the sand:silt ratio increased from ~1 to ~2. Furthermore, soil C decreased with depth and was close to significance (R^2=0.51, p=0.07) while redox and the sand:ratio ratio significantly ($p<0.05$) increased with depth. These deeper soils at the VA forest marsh are more characteristic of the upland forest soils (i.e., low soil C, oxygenated, high sand:silt ratio). We suspect that

the marsh layer is thin near the migration front, while established marshes nearer tidal creeks have thicker marsh soils, consistent with previous marsh modeling efforts (Guimond and Michael 2021). In addition, the spike in porewater redox potential with depth may be a result of oxygenated upland groundwater flowing into deeper sandier and more porous sediments, increasing C mineralization rates below the thin marsh layer, and decreasing soil C concentration at depth. Having both marsh soils and buried forest soils in the same soil core has implications for C stock estimates in migrating marsh areas. If the entire 84 cm soil C at the VA Forest site is considered in the estimate, the average soil C is 5.24%. If only the top half of the core is considered, this average soil C value increases to 8.6%, an increase of 65%. Therefore, long-term soil C estimates may be underestimated in recently migrated marsh if the buried upland soil underneath is included in the soil C estimate. While the thin marsh layer will be important to consider when conducting blue C assessments near transitional forests and farms, we suspect this process to be less important in areas with a higher slope between upland and lowland and a slower marsh migration rate, such as our MD and DE sites, as we saw less clear evidence for a thin marsh layer at these locations.

5.4.2 Biogeochemical Fingerprint Along the Salinity Gradient

We further hypothesized that transect points would have a unique biogeochemical fingerprint, indicative of the extent of saltwater intrusion. This is supported by our data because many of the transect points have statistically different biogeochemistry according to the ANOVA results (Tables 1 and 2). In addition, the cluster analysis shows that across all 6 sites, three unique groupings of data exist. These three clusters seem to represent lowland (Cluster 1) , transition (Cluster 2), and upland soils (Cluster 3). Lowland soil chemistry is characterized as salty, anaerobic,

and a neutral pH . Sulfate reduction is seemingly the main metabolic pathway due to elevated levels of porewater sulfide and soil S. Salty, low oxygen, and sulfidic soils enable marsh grasses to outcompete upland species not adapted to these soil conditions. Low oxygen and a less energetically favorable metabolic pathway allow these types of lowland soils to accumulate higher amounts of soil C.

The transitional location (Cluster 2) is categorized as intermediately salty, with a higher soil redox potential than the lowland areas. This soil chemistry allows for Fe reduction instead of sulfate reduction. This is supported by elevated levels of Fe^{2+} at many of our transitional locations across the 6 sites, as well as the transitional cluster having the highest Fe^{2+}. The transitional cluster also has the highest mean porewater DOC concentration which we suscept is due to more mobile and porewater associated DOC due to elevated Fe oxide reduction dominating these transect point locations. Fe oxides are known to control the transport of DOC in coastal ecosystems, where increased Fe reduction leads to higher mobility and lateral export of DOC (Fettrow et al. 2023).

The upland location is the least salty, has the highest redox and is the most acidic. Fe reduction still seems to occur at many of these upland locations, but particularly at depth at the forest sites. The upland cluster has the lowest mean DOC concentration, likely linked to low porewater DOC in many of the agricultural fields and higher microbial turnover rates due to high soil redox. Higher rates of upland DOC turnover is supported by a higher mean E_2:E_3 which indicates the upland cluster has some of the lowest molecule weight DOC. Low molecular weight DOC is associated with higher microbial degradation, likely linked to increased redox and aerobic degradation outcompeting anaerobes.

5.4.3 Implications for Coastal Forests and Farms

The transition of coastal forests and farms into migrating marsh is a critical dynamic caused by SLR that has many future implications. New evidence suggests that while some marsh area is lost to open water conversion, marsh expansion into forests has led to an overall increase in marsh area, particularly in the Chesapeake Bay region where our study took place (Schieder et al. 2018). Landward expansion of marshes is a survival strategy that allows coastal wetlands to escape drowning from SLR (Borchert et al. 2018), but marsh survival is at the expense of coastal forests. Coastal forests provide many ecosystem services such as timber, recreation, and biodiverse habitat for coastal species (Burkhard et al. 2012). As forests retreat and marshes migrate, forest ecosystem services would be replaced by coastal wetland ecosystem services. Coastal wetlands provide storm surge and flood protection to coastal communities, break down anthropogenic contaminants before reaching the ocean, habitat for coastal wildlife and fisheries (Barbier et al. 2011) and, as previously shown, store higher amounts of C in soils than forests (Table 2a,b,c).

Agricultural operations on the coast are highly susceptible to the negative impacts of SLR and storm surge. Most monocrops grown in the US cannot tolerate a soil salinity of higher than 2ppt (Tanji and Kielen 2002). We measured salinities higher than 2ppt at many of our ag sites. For example, at the MD-ag site, the porewater salinity in the Ag transect point was on average 2.7ppt across the 84cm core. It has become common for land managers and farmers to abandon fields along the coast due to decreases in yield caused by the effects of salinization (White and Kaplan 2017), allowing marshes to migrate into the abandoned field. While marsh migration can cause the loss of agricultural areas, bordering marsh can make farm fields more resilient to storm surge and SLR. This is because marshes can slow the

pace of the salt front in groundwater while also protecting fields against storm surge (Guimond and Michael 2021). This is supported by our data because there is a gradient of decreasing salinity from the Spartina Marsh to the Ag transect points at our ag field sites. If these transitional areas were not bordering the field, the salinity front would likely not be held outside the ag field. Preserving agricultural operations along the coast can be managed by protecting, restoring, and creating natural ecosystems that mitigate and buffer the negative effects of climate change.

5.5 Conclusion

Our results indicate that Marsh migration into forests and farms will significantly alter coastal soil C sequestration and biogeochemistry and subsequently change ecosystem functioning and dynamics. Marsh migration will significantly increase soil C concentrations in newly migrated marsh area by 4-50x compared to upland soils, particularly in agricultural fields that have low soil C. Newly migrated marsh area tends to have a thin marsh layer, with buried forest soils underneath. The thin marsh layer near transitional forests and farms will be important to consider when conducting C estimates with marsh migration since typical marsh soils (i.e., high soil C, low redox) may only represent a fraction of the entire soil profile, with typical upland soils (i.e., low soil C, high redox) underneath. If buried upland soils are incorporated into these C estimates, there may be a significant underestimation of marsh soil C storage. In addition, unique biogeochemistry exists in the upland, transition and lowland areas, indicative of the extent of SLR. These findings have important implications for identifying rapidly changing ecosystem function along the coastline with a changing climate. Future studies should incorporate assessments of

trace soil gas fluxes to understand the global warming or cooling potential of the migrating marsh.

REFERENCES

Alongi DM (2018) Kelp Forests. In: Springer Briefs in Climate Studies. pp 53–57

Barbier EB, Hacker SD, Kennedy C, et al (2011) The value of estuarine and coastal ecosystem services. Ecol Monogr

Borchert SM, Osland MJ, Enwright NM, Griffith KT (2018) Coastal wetland adaptation to sea level rise: Quantifying potential for landward migration and coastal squeeze. Journal of Applied Ecology 55:. https://doi.org/10.1111/1365-2664.13169

Burkhard B, Kroll F, Nedkov S, Müller F (2012) Mapping ecosystem service supply, demand and budgets. Ecol Indic 21:. https://doi.org/10.1016/j.ecolind.2011.06.019

Canavan RW, Slomp CP, Jourabchi P, et al (2006) Organic matter mineralization in sediment of a coastal freshwater lake and response to salinization. Geochim Cosmochim Acta. https://doi.org/10.1016/j.gca.2006.03.012

Carr J, Guntenspergen G, Kirwan M (2020) Modeling Marsh-Forest Boundary Transgression in Response to Storms and Sea-Level Rise. Geophys Res Lett 47:. https://doi.org/10.1029/2020GL088998

Chmura GL, Anisfeld SC, Cahoon DR, Lynch JC (2003) Global carbon sequestration in tidal, saline wetland soils. Global Biogeochem Cycles 17:1111. https://doi.org/10.1029/2002GB001917

Cline JD (1969) SPECTROPHOTOMETRIC DETERMINATION OF HYDROGEN SULFIDE IN NATURAL WATERS1. Limnol Oceanogr 14:454–458. https://doi.org/10.4319/lo.1969.14.3.0454

De La Reguera E, Tully KL (2021) Farming carbon: the link between saltwater intrusion and carbon storage in coastal agricultural fields. Agric Ecosyst Environ 314:

Duarte CM, Losada IJ, Hendriks IE, et al (2013) The role of coastal plant communities for climate change mitigation and adaptation. Nat Clim Chang 3:961–968. https://doi.org/10.1038/nclimate1970

Fagherazzi S, Anisfeld SC, Blum LK, et al (2019) Sea level rise and the dynamics of the marsh-upland boundary. Front Environ Sci 7:1–18. https://doi.org/10.3389/fenvs.2019.00025

Gedan KB, Epanchin-Niell R, Qi M (2020) Rapid Land Cover Change in a Submerging Coastal County. Wetlands 40:1717–1728. https://doi.org/10.1007/s13157-020-01328-y

Gedan KB, Fernández-Pascual E (2019) Salt marsh migration into salinized agricultural fields: A novel assembly of plant communities. Journal of Vegetation Science. https://doi.org/10.1111/jvs.12774

Guimond JA, Michael HA (2021) Effects of Marsh Migration on Flooding, Saltwater Intrusion, and Crop Yield in Coastal Agricultural Land Subject to Storm Surge Inundation. Water Resour Res 57:1–18. https://doi.org/10.1029/2020WR028326

Hansen AM, Kraus TEC, Pellerin BA, et al (2016) Optical properties of dissolved organic matter (DOM): Effects of biological and photolytic degradation. Limnol Oceanogr 61:1015–1032. https://doi.org/10.1002/lno.10270

Jobe JGD, Gedan K (2021) Species-specific responses of a marsh-forest ecotone plant community responding to climate change. Ecology 102:. https://doi.org/10.1002/ecy.3296

Kearney WS, Fernandes A, Fagherazzi S (2019) Sea-level rise and storm surges structure coastal forests into persistence and regeneration niches. PLoS One. https://doi.org/10.1371/journal.pone.0215977

Kirwan ML, Guntenspergen GR, D'Alpaos A, et al (2010) Limits on the adaptability of coastal marshes to rising sea level. Geophys Res Lett. https://doi.org/10.1029/2010GL045489

Kirwan ML, Temmerman S, Skeehan EE, et al (2016a) Overestimation of marsh vulnerability to sea level rise. Nat Clim Chang

Kirwan ML, Walters DC, Reay WG, Carr JA (2016b) Sea level driven marsh expansion in a coupled model of marsh erosion and migration. Geophys Res Lett 43:4366–4373. https://doi.org/10.1002/2016GL068507

Langston AK, Coleman DJ, Jung NW, et al (2022) The Effect of Marsh Age on Ecosystem Function in a Rapidly Transgressing Marsh. Ecosystems 25:252–264. https://doi.org/10.1007/s10021-021-00652-6

Langston AK, Kaplan DA, Putz FE (2017) A casualty of climate change? Loss of freshwater forest islands on Florida's Gulf Coast. Glob Chang Biol. https://doi.org/10.1111/gcb.13805

Macreadie PI, Costa MDP, Atwood TB, et al (2021) Blue carbon as a natural climate solution. Nat Rev Earth Environ 2:826–839. https://doi.org/10.1038/s43017-021-00224-1

Martens DA, Reedy TE, Lewis DT (2004) Soil organic carbon content and composition of 130-year crop, pasture and forest land-use managements. Glob Chang Biol 10:. https://doi.org/10.1046/j.1529-8817.2003.00722.x

McKee KL, Mendelssohn IA (1989) Response of a freshwater marsh plant community to increased salinity and increased water level. Aquat Bot. https://doi.org/10.1016/0304-3770(89)90074-0

Mcleod E, Chmura GL, Bouillon S, et al (2016) A blueprint for blue carbon: toward an improved understanding of the role of vegetated coastal habitats in sequestering CO2. Front Ecol Environ 9:552–560. https://doi.org/https://www.jstor.org/stable/41479959

Osburn CL, Mikan MP, Etheridge JR, et al (2015) Seasonal variation in the quality of dissolved and particulate organic matter exchanged between a salt marsh and its adjacent estuary. Journal of Geophysical Research G: Biogeosciences 120:1430–1449. https://doi.org/10.1002/2014JG002897

Raabe EA, Stumpf RP (2016) Expansion of Tidal Marsh in Response to Sea-Level Rise: Gulf Coast of Florida, USA. Estuaries and Coasts. https://doi.org/10.1007/s12237-015-9974-y

Schieder NW, Kirwan ML (2019) Sea-level driven acceleration in coastal forest retreat. Geology 47:1151–1155. https://doi.org/10.1130/G46607.1

Schieder NW, Walters DC, Kirwan ML (2018) Massive Upland to Wetland Conversion Compensated for Historical Marsh Loss in Chesapeake Bay, USA. Estuaries and Coasts 41:940–951. https://doi.org/10.1007/s12237-017-0336-9

Smeaton C, Barlow NLM, Austin WEN (2020) Coring and compaction: Best practice in blue carbon stock and burial estimations. Geoderma 364:114180. https://doi.org/10.1016/j.geoderma.2020.114180

Smith AJ, Kirwan ML (2021) Sea Level-Driven Marsh Migration Results in Rapid Net Loss of Carbon. Geophys Res Lett 48:. https://doi.org/10.1029/2021GL092420

Smith JAM (2013) The Role of Phragmites australis in Mediating Inland Salt Marsh Migration in a Mid-Atlantic Estuary. PLoS One 8:e65091. https://doi.org/10.1371/journal.pone.0065091

Stookey LL (1970) Ferrozine-A New Spectrophotometric Reagent for Iron. Anal Chem 42:779–781. https://doi.org/10.1021/ac60289a016

Tanji KK, Kielen NC (2002) Agricultural drainage water management in arid and semi-arid areas. FAO Irrigation and Drainage Paper 61

Tully K, Gedan K, Epanchin-Niell R, et al (2019) The invisible flood: The chemistry, ecology, and social implications of coastal saltwater intrusion. Bioscience

Tzortziou M, Neale PJ, Osburn CL, et al (2008) Tidal marshes as a source of optically and chemically distinctive colored dissolved organic matter in the Chesapeake Bay. Limnol Oceanogr 53:148–159. https://doi.org/10.4319/lo.2008.53.1.0148

Tzortziou M, Neale PJ, Osburn CL, Megonigal JP (2020) Tidal Marshes as a Source of Optically and Chemically Distinctive Colored Dissolved Organic Matter in the Chesapeake Bay Author (s): Maria Tzortziou , Patrick J . Neale , Christopher L . Osburn , J . Patrick Megonigal , Nagamitsu Maie and Rudolf Jaffé P. 53:148–159

Walters DC, Carr JA, Hockaday A, et al (2021) Experimental Tree Mortality Does Not Induce Marsh Transgression in a Chesapeake Bay Low-Lying Coastal Forest. Front Mar Sci 8:. https://doi.org/10.3389/fmars.2021.782643

Weston NB, Dixon RE, Joye SB (2006) Ramifications of increased salinity in tidal freshwater sediments: Geochemistry and microbial pathways of organic matter mineralization. J Geophys Res Biogeosci. https://doi.org/10.1029/2005JG000071

White E, Kaplan D (2017) Restore or retreat? saltwater intrusion and water management in coastal wetlands. Ecosystem Health and Sustainability 3:. https://doi.org/10.1002/ehs2.1258

Willis JM, Hester MW (2004) Interactive effects of salinity, flooding, and soil type on Panicum hemitomon. Wetlands. https://doi.org/10.1672/0277-5212(2004)024[0043:IEOSFA]2.0.CO;2

Appendix A

SUPPLEMENTAL INFORMATION FOR CHAPTER 2

Table A.1 The indices and peaks for UV-VIS/ EMMs analysis used in this study to determine molecular properties and source of DOC

Indices	Calculation	Characterization Information	Original Source
Abs_{254}	Absorption at 254 nm	Related to total CDOM concentration	
$SUVA_{254}$	Absorption at 254 nm divide by DOC concentration	Higher number is associated with greater aromaticity	Weishaar et all. 2003
S_r	Slope from $S_{275-295}$ divided by slope from $S_{350-400}$	Higher values indicates more marine-like	Helms et al. (2008)
E_2:E_3	Slope from $S_{250-365}$	Inversley related with DOM molecular weight	
Coble A	Ex260/ Em450	Terrestrial-like source, soil-humics	Cory et al 2010
Coble C	Ex340/ em450	Terrestrial-like source, soil-humics	Baker et al 2008
HIX	Area under em spectra from 435-480 m, divided by peak area 300-345 nm & 435-480 nm, at ex 254 nm	Higher values correspond with increased humic substances or degree of humification	Ohno (2002)
BIX	Ratio of em intensity at 380 nm divided by 430 nm at excitation 310 nm	Higher values correspond to with microbially-derived CDOM	Huguet et al 2009

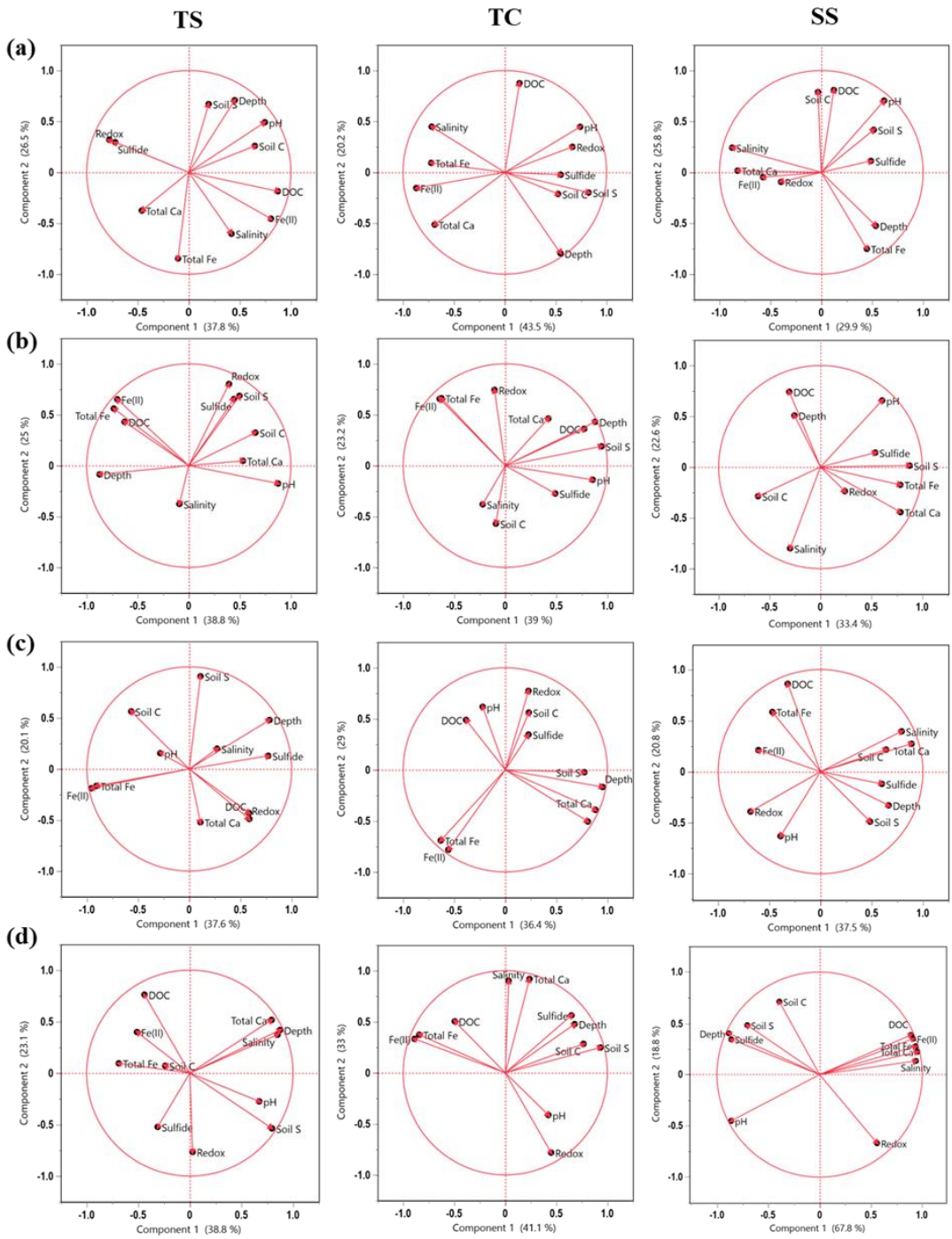

Figure A.1 Principal Components Analysis (PCA) to examine how the relationships among variables change between subsite and phenology: (a) senescence, (b) dormancy, (c) green-up and (d) maturity.

Appendix B

SUPPLEMENTAL INFORMATION FOR CHAPTER 3

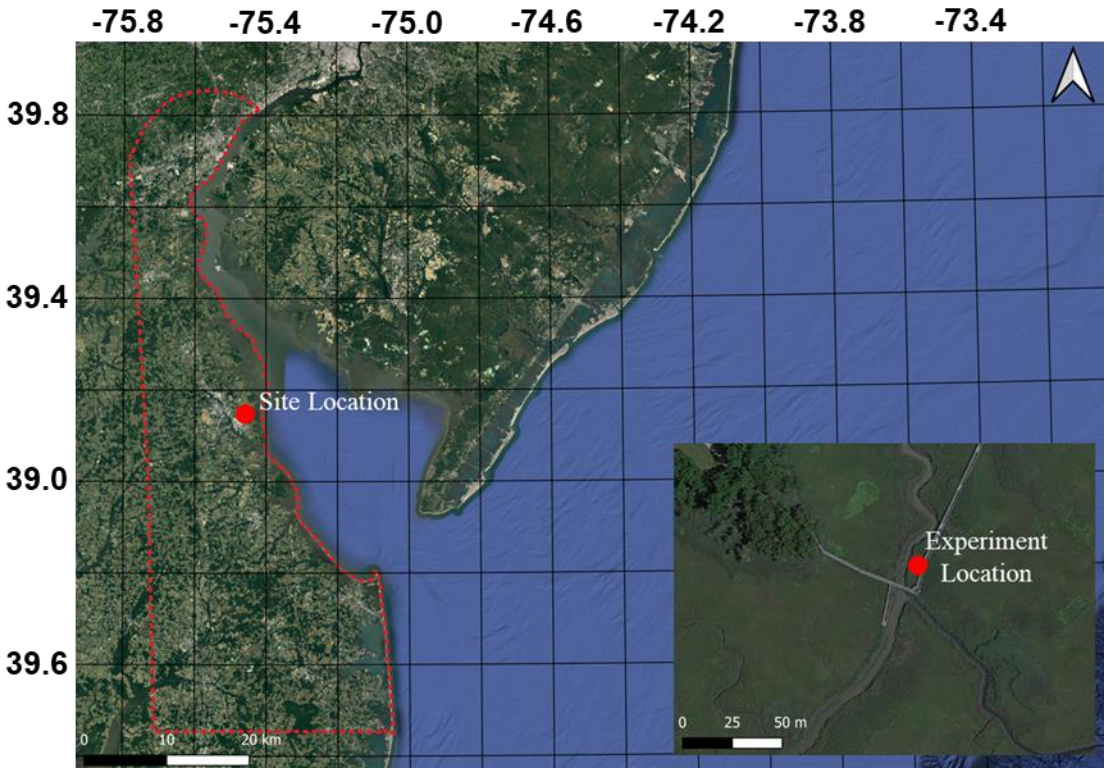

Figure B.1 Map of the study site location at the St Jones Reserve in Dover, Delaware. Our sampling location for this experiment is located along the tidal creek at the subsite TS found in Seyfferth et al. 2020.

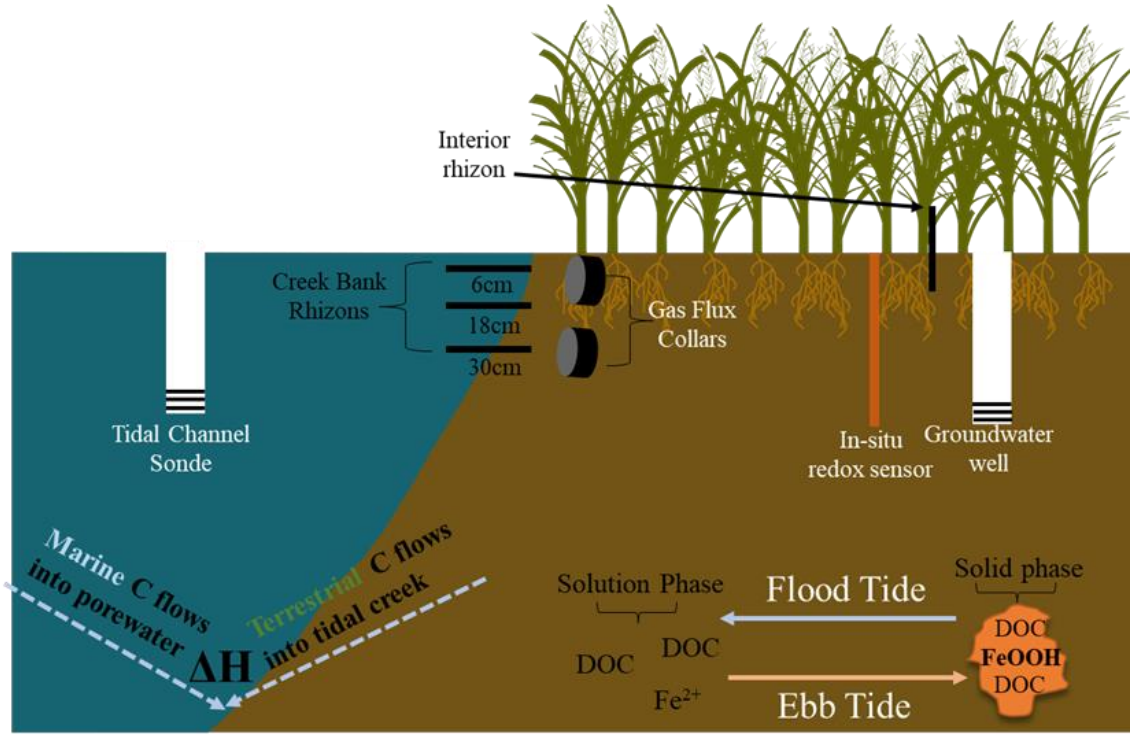

Figure B.2 Conceptual diagram of the experimental design and equipment setup. Rhizon samplers were inserted horizontally into the creek bank at 6, 18 and 30cm down the creek bank, while R-Int was inserted vertically to 10cm and further from the creek bank. Gas flux collars were inserted directly into the creek bank. A groundwater well and in-situ redox probe were installed near the creek. Our data show tidally driven mechanisms in which lateral carbon transport between near channel soil and the tidal creek (C) is chemically (Fe oxides) and physically (hydraulic gradient) controlled.

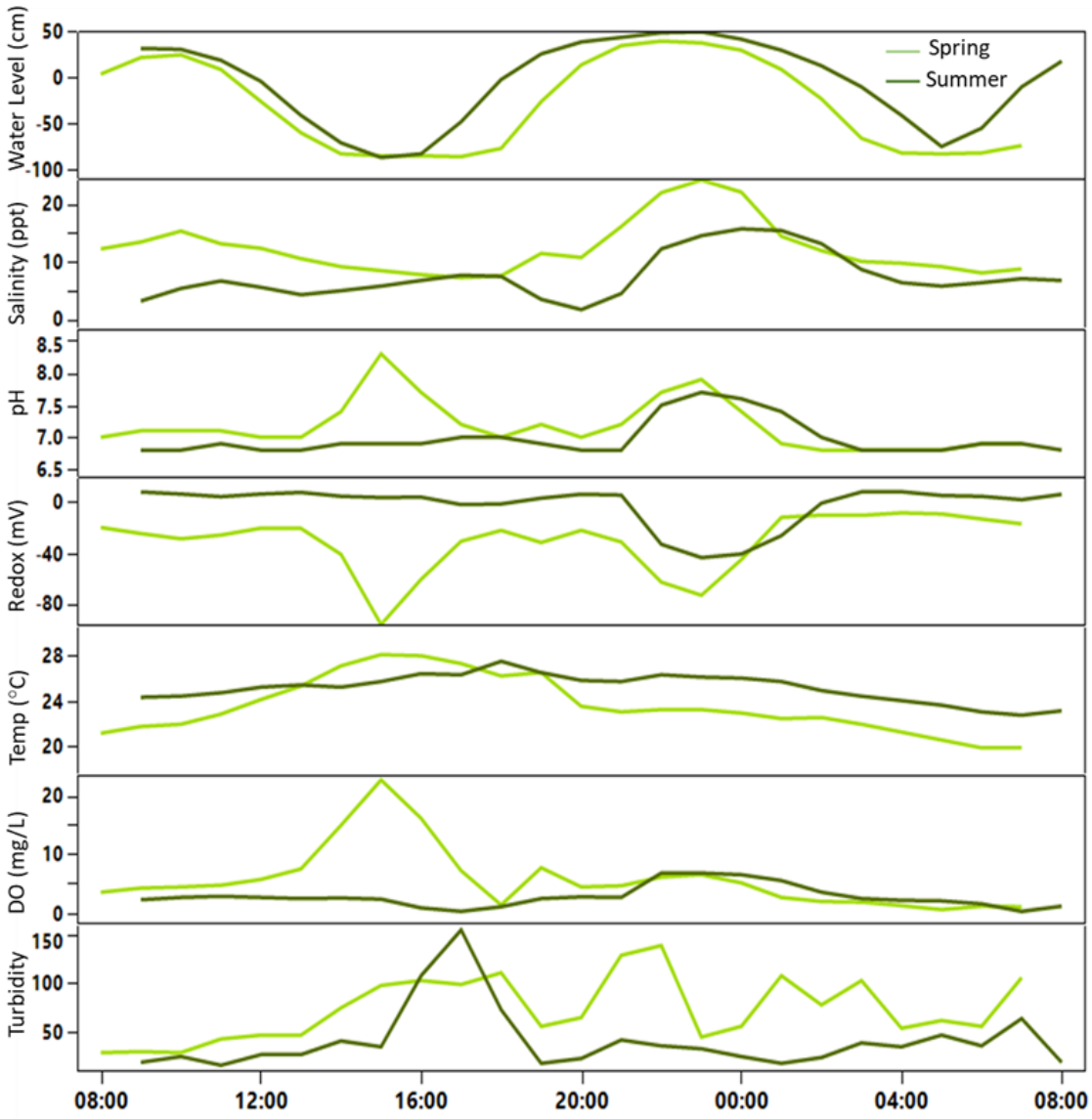

Figure B.3 Timeseries of surface water tidal channel data for both summer and spring 24-hour sampling events.

Table B.1 The indices and peaks for EEMs and UV-VIS analysis used in this study to determine molecular properties and source of DOC

Indices	**Calculation**	**Characterization Information**	**Original Source**
Abs_{254}	Absorption at 254 nm	Related to total CDOM concentration and aromaticity	Weishaar et al. 2003
$SUVA_{254}$	Absorption at 254 nm divide by DOC concentration	Higher number is associated with greater aromaticity	Weishaar et al. 2003
S_r	Slope from $S_{275-295}$ divided by slope from $S_{350-400}$	Higher values indicate more marine-like	Helms et al. 2008
E_2:E_3	Slope from $S_{250-365}$	Inversley correlated with DOM molecular weight	Helms et al. 2008
Coble A	Ex260/ Em450	Terrestrial-like source, soil-humics	Cory et al 2010
Coble C	Ex340/ em450	Terrestrial-like source, soil-humics	Baker et al 2008
HIX	Area under em spectra from 435-480 m, divided by peak area 300-345 nm & 435-480 nm, at ex 254 nm	Higher values indicate increase humic substances or degree of humification	Ohno 2002
BIX	Ratio of em intensity at 380 nm divided by 430 nm at excitation 310 nm	Higher values correspond to recently produced microbial derived C	Huguet et al 2009

Appendix C

SUPPLEMENTAL INFORMATION FOR CHAPTER 4

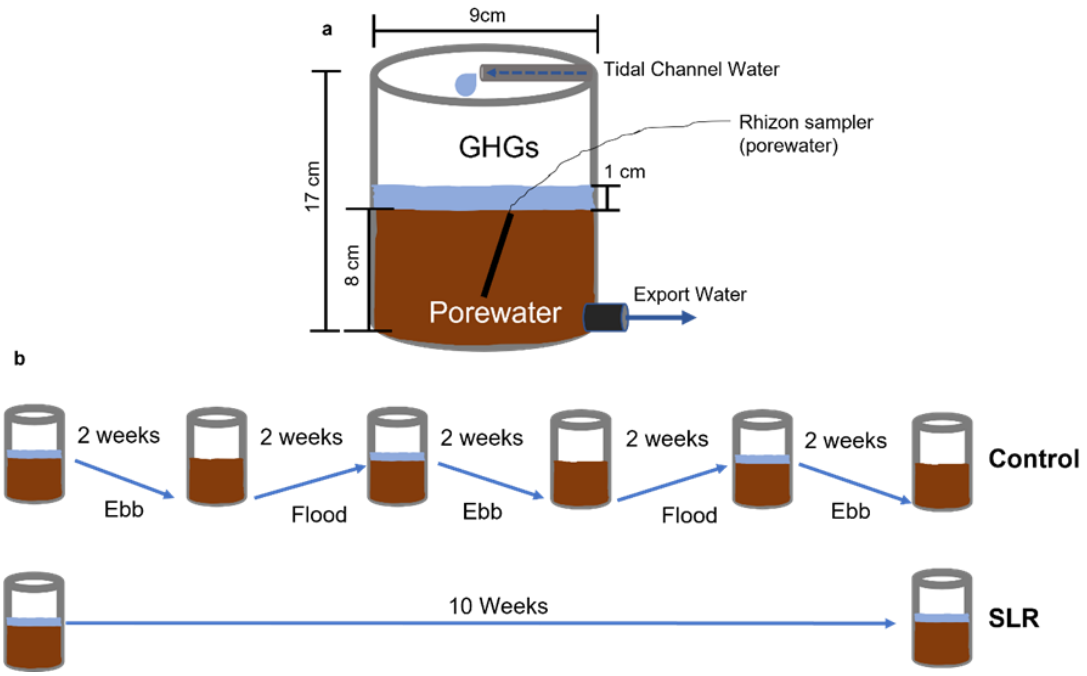

Figure C.1 Experimental setup of constructed flow-through mesocosms (a). Porewater was collected from Rhizon soil water samplers that were inserted into the center of the soil profile, completely below the soil surface. Export water was collected by sampling outflow water from the gas impermeable tubing. Flooding schedule for both treatments (b). SLR is consistently flooded at 1cm above surface throughout the entire 66-day experiment whereas Control started out flooded but was slowly drained over a period of 2 weeks and slowly reflooded over the same amount of time. Control went through multiple periods of flooding and drying to replicate spring-neap hydrology

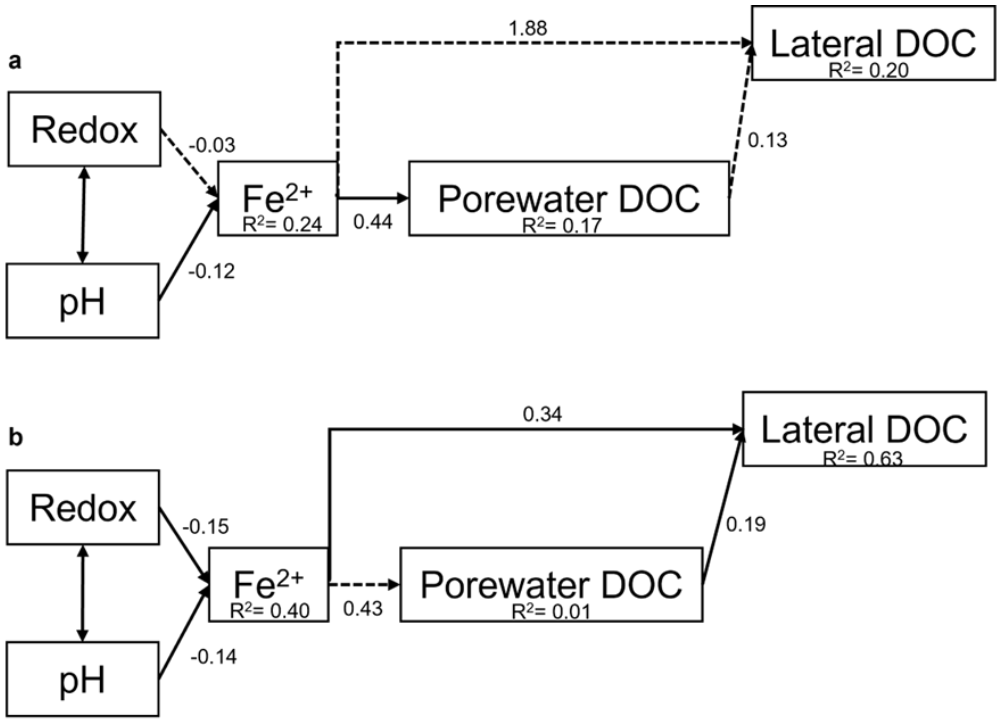

Figure C.2 Structural equation model (SEM) diagram depicting casual relationships between measured variables for Control (a) and SLR (b) conditions. Values on the arrows are predictive estimates for the relationships (i.e., Change in X of 1 unit causes this estimated amount of change in Y). R2 values are also provided for each regression. Single-sided arrows represent a hypothesized regression in the direction of the arrow, while double-sided arrows indicate covariance between variables. Solid arrows represent significant regressions ($p<0.05$) while dashed arrows represent insignificant regressions

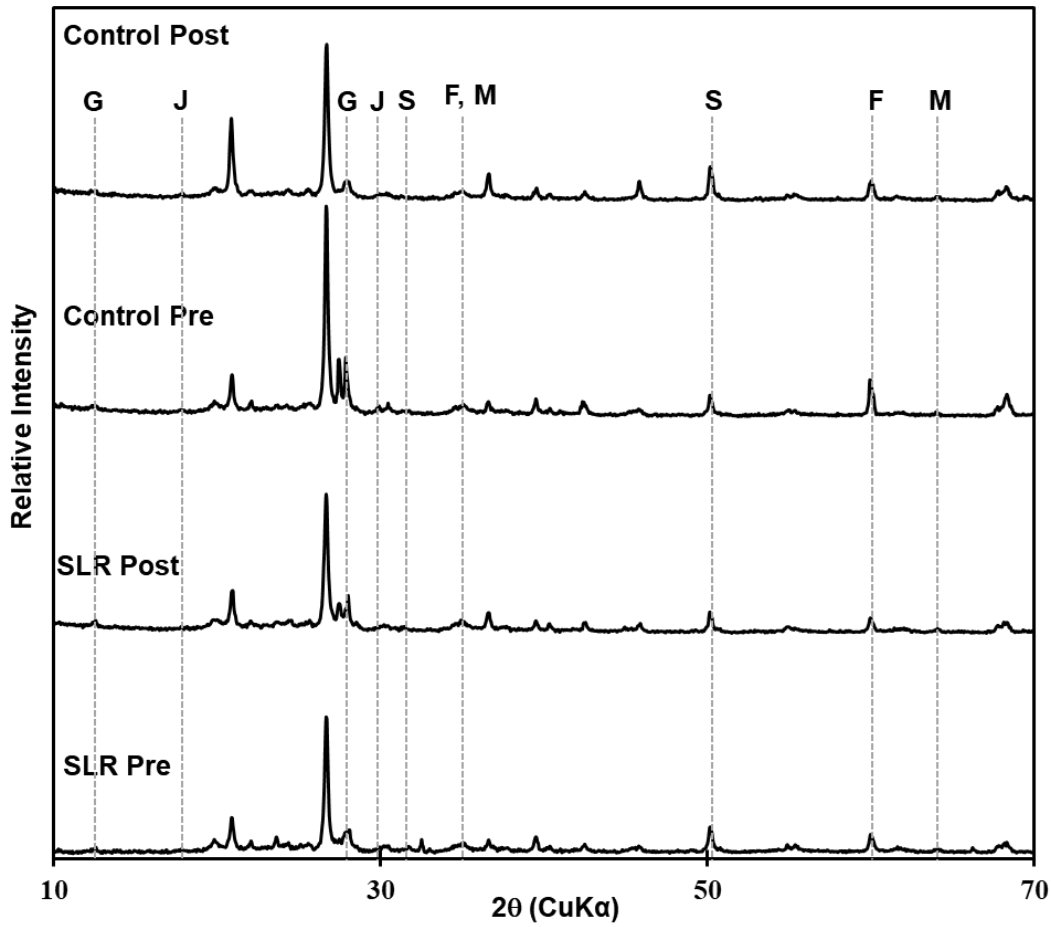

Figure C.3 X-Ray diffraction results for Control and SLR pre and post experiment samples. Measurements were taken from a 2□ range of 10-70 in order to confirm the presence of Fe oxides before EXAFS analysis. Peaks were assessed using Match! Software, but the two main peaks of each Fe mineral identified are present. G = green rust, J = jarosite, S = siderite, M = magnetite, and F = ferrihydrite

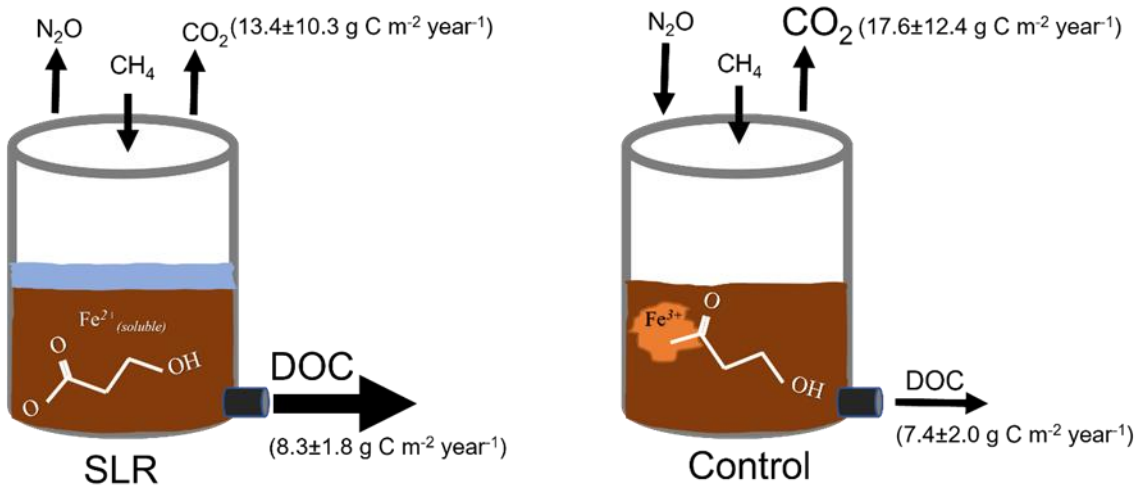

Figure C.4 Conceptual model of the carbon budget for the laboratory mesocosm flow-through experiment. SLR conditions caused greater porewater DOC followed by greater porewater lateral export. Greater DOC mobility was related to Fe oxide (dis)solution. The Global Warming Potential (GWP) of the soils were mainly from CO2, which was greatest under Control conditions

Appendix D

LATERAL C EXCHANGE BETWEEN A SALT MARSH TIDAL CREEK AND ADJACENT TIDAL RIVER AND OPEN-WATER BAY

D.1 Introduction

Tidal salt marshes are important reservoirs of carbon (C), as recent studies have identified that preserving and restoring these ecosystems and other blue C systems (i.e., mangroves, seagrass beds) are effective climate change mitigation strategies (Duarte et al. 2013; Howard et al. 2017; Crooks et al. 2018; Taillardat et al. 2018; Serrano et al. 2019; Macreadie et al. 2021). High C sequestration rates are due to a variety of factors including photosynthetically productive salt marsh cordgrass (Rocha and Goulden 2009), high sedimentation burial rates, (Arias-Ortiz et al. 2018), anoxic soil conditions from coastal inundation (Burdige 2007), and the contribution of allochthonous C from outside the ecosystem of origin (Saintilan et al. 2013; van de Broek et al. 2018). These factors contribute to a soil C storage rate orders of magnitude higher than other productive ecosystems including tropical rainforests (Chmura et al. 2003; Mcleod et al. 2016; Macreadie et al. 2019; Alongi 2020). This has led to recent efforts to better understand salt marsh C flux because estimates remain highly uncertain (Herrmann et al. 2015; Cavallaro et al. 2018). The vertical soil C storage rate in salt marshes ranges from 1-1100 g C m^{-2} $year^{-1}$ (Wang et al. 2021) in comparison to 1-10 g C m^{-2} $year^{-1}$ in tropical forests (Chmura et al. 2003; Mcleod et al. 2016; Macreadie et al. 2019).

Vertical soil C storage rates have been extensively studied in coastal wetland ecosystems, but there has been limited research into the lateral C flux (Santos et al. 2021). While vertical flux encompasses the flow of C into and out of marsh soils, the lateral C flux encompasses the flow of surface water C into and out of tidal wetlands during tidal oscillations, and recent studies have indicated that the lateral C flux may be similar in magnitude to or even exceed the vertical soil C flux (Mcleod et al. 2016; Wang et al. 2016; Santos et al. 2019; Bogard et al. 2020; Czapla et al. 2020). However, observational data is geographically sparse (Herrmann et al. 2015; Cavallaro et al. 2018; Najjar et al. 2018) and uncertainties in global lateral C flux estimates remain high at 31-78 Tg C year^{-1} (Duarte 2017). Therefore, further efforts to quantify lateral C flux from productive coastal ecosystems is required to improve estimates and to account for complex coastal surface water processes not currently represented in Earth System Models (Cole et al. 2007).

The fate of laterally-exported marsh C also remains unclear. Measurements of greenhouse gas flux from tidal creek surface waters indicate that a fraction of lateral C is respired by microbes and returned to the atmosphere (Barrón and Duarte 2015; Trifunovic et al. 2020), while other studies suggest that a fraction is stored outside the ecosystem of origin such as the coastal shelf and deep-sea sediments (Duarte 2017; Santos et al. 2021). Salt marshes have also been shown to be large contributors to both the dissolved inorganic carbon (DIC) and dissolved organic carbon (DOC) found in coastal ocean waters (Bauer et al. 2013). High concentrations of DIC exported from salt marshes to coastal waters ((Wang et al. 2016) could persist over geologic timescales (Maher et al. 2018), indicating that lateral C could be a source for long-term C storage in the ocean.

Understanding the flux and the fate of laterally exported salt marsh C will improve flux estimates and advance the accuracy of modeling efforts. While the flux is measured using surface water discharge and C concentration, the fate of C can be tracked using the characterization properties of DOC. Chromophorhic dissolved organic matter (CDOM) is defined as the light-reactive fraction of DOC. The optical signature of CDOM can give an indication of the molecular properties such as molecular weight, marine microbial source vs terrestrial plant source and the presence of soil humic substances (Tzortziou et al. 2008, 2011; Osburn et al. 2015). These measurements are now being attempted using new satellites and could drastically improve our understanding of how surface water C moves across the globe (Cao and Tzortziou 2021). Tracking the characteristics and source of lateral marsh C will improve our understanding of the dynamic exchange of solutes between the terrestrial-marine interface.

To improve our understanding of the lateral C flux across the marsh-aquatic interface, we conducted a 1-year long experiment to measure lateral C flux from a temperate tidal marsh across seasons while also observing the connection and flow of C between the salt marsh tidal creek, a nearby tidal river, and an adjacent open-water estuary. We hypothesized that the marsh tidal creek exports more C to the adjacent estuary during ebb tide than is imported into the marsh during flood tide. We further hypothesized that CDOM properties will allow us to observe changes in the source of C across tidal cycles (i.e., marine vs terrestrial derived C). Our results indicate mechanistic linkages between marsh tidal creeks and their adjacent rivers and bays which has implications for improving our understanding of the fate and estimate of the lateral C flux.

D.2 Methods and Materials

D.2.1 Study Site

The study was conducted primarily at a salt marsh located at the St. Jones Delaware National Estuarine Research Reserve in Dover, DE, U.S.A. Samples were taken in a tidal creek that has an average tidal amplitude of 1.5 m and salinity of 5-18 parts per thousand (ppt) (Capooci et al. 2019). Vegetation consists primarily of *Spartina alterniflora* with patches of *S. cynosuroides* and *S. patens*. Average precipitation is 117 cm y^{-1} with an average snowfall of 40 cm y^{-1} and an average yearly temperature range from 4.4 to 31.7°C, typical of a temperate Mid-Atlantic coastal climate. To relate tidal creek processes to larger scale flux, this study also took place at a larger connecting tidal river and at the adjacent bay (Figure E.1).

Figure D.1 Map of the study site with the four separate sampling locations (Tidal creek, groundwater, tidal river, DE bay).

D.2.2 Sampling Scheme

Four distinct phenophases were identified based on the greenness index (GI) identified in a pervious study at the field site (Trifunovic et al. 2020): a) Dormant for plant inactivity; b) Greenup for plant growth; c) Maturity for the plant growth peak; and d) Senescence for when plant activity slowed. Water samples were taken from the tidal creek during eight sampling campaigns to capture two sampling events for each phenophase (9/1/17, 11/9/17, 5/11/18, 8/6/18, 9/18/17, 11/3/17, 5/29/18, 8/15/18). Each campaign sampled over the course of a full tidal cycle, with measurements at both flood and ebb tide with a total of ~8 individual tidal creek samples per campaign.

Water samples were also taken from Scotton landing of the St. Jones River (hereafter referred to as tidal river), the Delaware Bay at Bowers Beach, DE (hereafter referred to as Bay), and drawn with a peristaltic pump from a groundwater well within a forest in the St. Jones Reserve (hereafter referred to as groundwater). These samples were taken at ebb and flood tide during the Dormant, Greenup, and Maturity phenophases on the dates of 4/27/2018, 5/29/2018, 6/29/2018, and 8/6/2018.

D.2.3 Analytical Measurements

All water samples were vacuum-filtered through 0.7-micron glass fiber filters. Samples taken from September 2017 to February 2018 were analyzed for total organic carbon (TOC) using an Elementar VarioMax CN Analyzer (Elementar Americas, Mt. Holly, NJ, U.S.A). Due to a technical issue with the Elementar, the rest of the samples taken from March 2018 to August 2018 were analyzed for TOC with a Shimadzu TOC-V CPH (Shimadzu, Kyoto, Japan). Both instruments were found to agree with TOC standard solutions and field and lab blanks were found to have minimal contamination. Particulate organic carbon (POC) was analyzed by burning glass fiber filters containing POC through the loss-on-ignition method using a Blue-M High Temperature Furnace model CW6680F (SPX Thermal Product Solutions, White Deer, PA, U.S.A) following standard procedures (Schulte and Hopkins 1996).

To assess the quality and source of chromophroic dissolved organic matter (CDOM) and fluorescent organic matter (FDOM) within the creek, excitation emission matrices and ultraviolet-visible (EEMs/ UV-VIS) measurements were taken with a Horiba Aqualog (Horiba, Kyoto, Japan). Protocols for emission wavelengths, instrument checks, and data processing were done following a previous study (Johnson et al. 2018). These included an excitation wavelength range from 240 to 700

nm at 4 nm increments, a manufacturer's excitation check, emission check, cuvette check, and Raman water scan before measurements, correction for inner filter effects and applied first- and second-order Rayleigh Masking. The EEMs/UV-VIS indices were calculated using R 3.4. Indices and peaks include the humification index (HIX), the fluorescence index (FI), the biological index (BIX), the spectral slope ratio (S_r) and the Coble C peak.

D.2.4 Ancillary Water Level Measurements

The water quality parameters (measured in ~15 min intervals) of salinity and water level were measured with a YSI 6600 sonde (YSI Inc., Yellow Springs, OH, USA) at both the tidal creek and tidal river. Water level values in the tidal creek and tidal river are recorded with respect to above (positive) or below (negative) mean sea level (NAVD83).

D.2.5 Statistical Analysis

To assess differences between the means of measured variables based on different groupings of data such as phenology, ebb/flood tide, location (i.e., tidal creek, tidal river, groundwater, DE Bay), one-way analysis of variance (ANOVA) was used with a post hox Tuckey HSD test (α=0.05). Linear correlations between variables were assessed and only significant ($p<0.05$) relationships are reported. All statistical analyses were assessed in JMP Pro 16 (Version 16.2).

D.3 Results

D.3.1 Dissolved Organic Carbon Concentration and Characterization

The concentration of dissolved organic carbon (DOC), particulate organic carbon (POC), dissolved inorganic carbon (DIC), total nitrogen (TN) and the optical properties of chromophoric dissolved organic matter (CDOM) was measured across the 1-year experiment (Figure E.2). Most of the measurements were taken in the tidal creek, with several samples taken in the groundwater upland of the tidal creek, in the tidal river connected to the tidal creek and the adjacent open water bay (DE Bay) to connect the flow of C between these various locations.

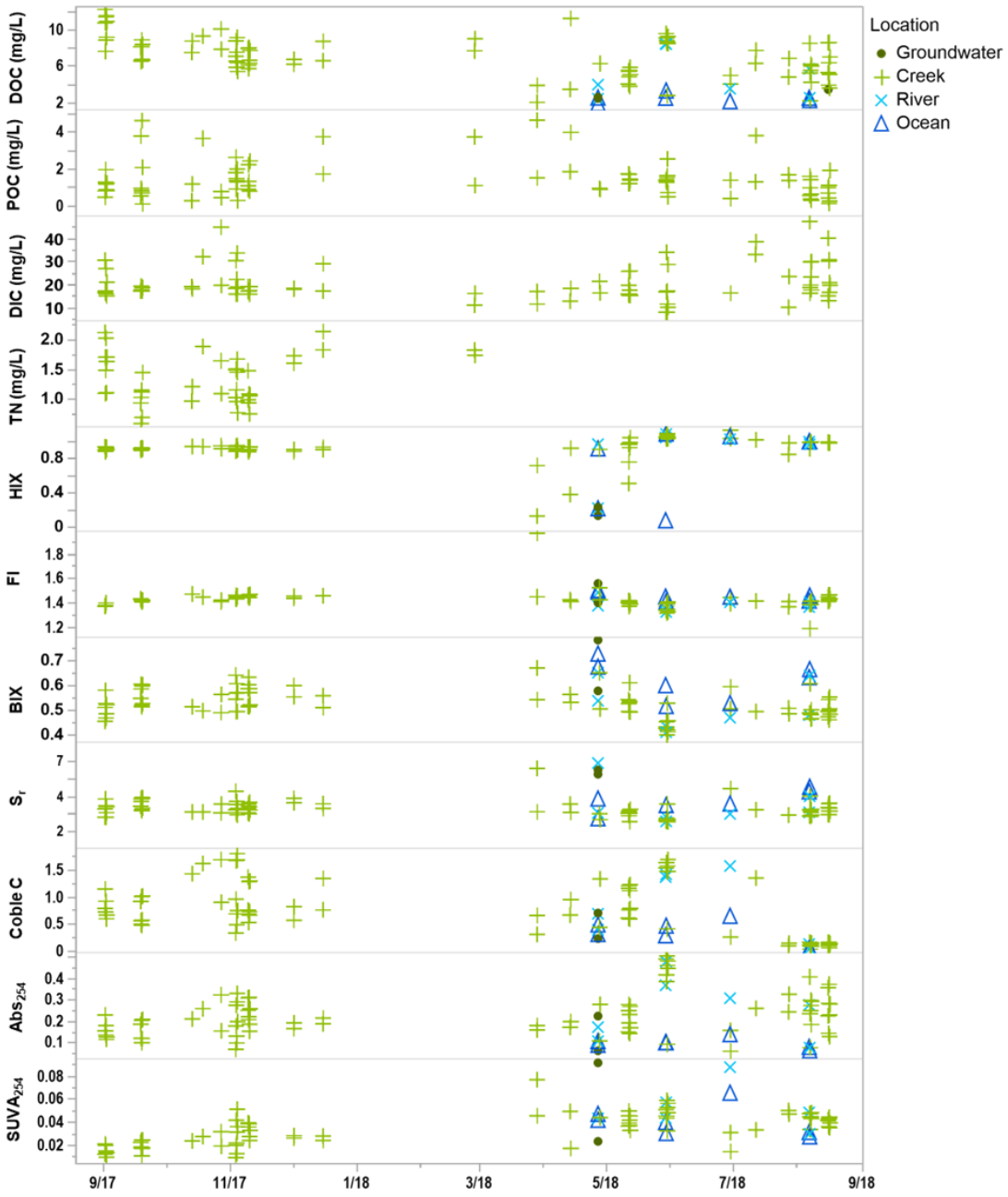

Figure D.2 Surface water (tidal river, tidal creek, bay) and groundwater data collected across the 1-year sampling campaign

Because samples were taken across all four phenology phases in the tidal creek and across tidal cycles, the means between phenology phases and between ebb/ flood stages of the creek was assessed (Table E.1). Tidal creek DOC concentrations were highest during senescence, followed by dormancy, green-up then maturity while tidal creek POC was highest during dormancy, followed by green-up, senescence and maturity. DIC was significantly highest during maturity, followed by senescence, dormancy and green-up. TN was only measured during dormancy and senescence and were not significantly different. Humification index (HIX) indicates the presence of soil humic substances and was highest during maturity and green-up, with a significantly lower humic signature during dormancy. The fluorescence index (FI) indicates microbial (higher values) vs terrestrial (lower values) sources of CDOM and is significantly higher during dormancy. The biological index (BIX) indicates recently produced microbial derived CDOM (higher values) and is highest during dormancy and lowest during green-up. The slope ratio (S_r) indicates low molecular weight marine (higher values) vs high molecular weight terrestrial (lower values) derived C. The S_r is significantly lower during green-up. The Coble C peak indicates terrestrial plant-like CDOM (higher values) and is significantly higher during green-up, followed by dormancy and senescence and is significantly lower during maturity. Abs_{254} and $SUVA_{254}$ indicates the presence of aromatic DOC and is highest during green-up and lowest during senescence.

Table D.1 Tidal creek ANOVA results based on the means (±SD) between phenology phases and between ebb/ flood

Variable	Dormancy	Green-up	Maturity	Senescence	Ebb	Flood

DOC (mg/L)	6.9(±1.9)^{B}	6.6(±2.3)^{BC}	5.8(±1.7)^{C}	8.9(±1.8)^{A}	7.8(±1.8)^{A}	6.1(±2.3)^{B}
POC (mg/L)	1.8(±1.1)^{A}	1.7(±1.1)^{AB}	1.0(±0.8)^{B}	1.4(±1.3)^{AB}	1.5(±1.1)^{A}	1.4(1.1)^{A}
DIC (mg/L)	19.6(±6.9)^{B}	18.0(±7.4)^{B}	24.5(±9.9)^{A}	20.3(±5.1)^{AB}	24.0(±8.6)^{A}	16.7(±3.9)^{B}
TN (mg/L)	1.3(±0.4)^{A}	No Data	No Data	1.3(±0.5)^{A}	1.5(±0.4)^{A}	1.1(±0.3)^{B}
HIX	0.9(±0.2)^{B}	1.0(±0.1)^{A}	1.0(±0.1)^{A}	0.9(±0.02)^{AB}	0.9(±0.1)^{A}	0.9(±0.2)^{A}
FI	1.5(±0.1)^{A}	1.4(±0.03)^{B}	1.4(±0.1)^{B}	1.4(±0.03)^{B}	1.4(±0.1)^{A}	1.4(±0.1)^{A}
BIX	0.6(±0.05)^{A}	0.5(±0.1)^{C}	0.5(±0.1)^{BC}	0.5(±0.04)^{AB}	0.5(±0.04)^{B}	0.6(±0.1)^{A}
S_r	3.5(±0.7)^{A}	2.8(±0.4)^{B}	3.3(±0.5)^{A}	3.5(±0.5)^{A}	3.1(±0.4)^{B}	3.6(0.7)^{A}
Coble C	0.9(±0.4)^{B}	1.2(±0.4)^{A}	0.2(±0.3)^{C}	0.8(±0.3)^{B}	1.0(±0.6)^{A}	0.6(±0.4)^{B}
Abs_{254}	0.2(±0.1)^{BC}	0.3(±0.1)^{A}	0.2(±0.1)^{B}	0.2(±0.1)^{C}	0.27(±0.1)^{A}	0.19(±0.1)^{B}
$SUVA_{254}$	0.03(±0.01)^{B}	0.05(±0.01)^{A}	0.04(±0.01)^{A}	0.02(±0.01)^{C}	0.04(±0.01)^{A}	0.03(±0.02)^{A}

Tidal creek DOC, POC and CDOM properties were also assessed based on ebb vs flood tide. There were significantly higher DOC concentrations in the tidal creek during ebb tide than flood tide, while POC remained statistically similar across tidal stage. DIC was significantly higher during ebb tide, as was TN. The BIX and S_r was significantly higher during flood tide while Coble C peak and Abs_{254} were significantly higher during ebb tide. There was no significant difference between ebb and flood for HIX, FI or $SUVA_{254}$.

These data were also assessed based on location (Table E.2). DOC concentrations were highest in the tidal creek, followed by the tidal river, groundwater, and the bay. POC and TN data was only collected in the tidal creek. The HIX was lowest in the groundwater, followed by the bay, tidal river and the tidal creek had the highest mean HIX. The FI was statistically similar across all for sampling

locations. The BIX was highest in the groundwater and bay and lowest in the tidal creek and tidal river. Likewise, the S_r was highest in the groundwater and bay and lowest in the tidal creek and tidal river. The Coble C peak was highest in the tidal creek, and lowest in the bay. Abs_{254} was significantly lower in the bay than in the tidal creek and river while $SUVA_{254}$ was significantly lower in the tidal creek than in the tidal river and groundwater.

Table D.2 ANOVA results based on the means (±SD) between sampling locations

Variable	Groundwater	Tidal Creek	Tidal River	Bay
DOC (mg/L)	2.8(±0.5)^{BC}	7.0(±2.2)^{A}	5.0(±2.6)^{B}	2.4(±0.4)^{C}
POC (mg/L)	No Data	1.5(±1.1)	No Data	No Data
DIC (mg/L)	No Data	20.7(±7.7)	No Data	No Data
TN (mg/L)	No Data	1.3(±0.4)	No Data	No Data
HIX	0.2(±0.1)^{C}	0.9(±0.1)^{A}	0.9(±0.3)^{AB}	0.8(±0.4)^{B}
FI	1.5(±0.1)^{A}	1.4(0.1)^{A}	1.4(0.1)^{A}	1.4(±0.03)^{A}
BIX	0.7(±0.1)^{A}	0.5(±0.1)^{B}	0.5(±0.1)^{B}	0.6(±0.1)^{A}
S_r	5.9(±0.2)^{A}	3.3(±0.6)^{B}	3.6(±1.4)^{B}	4.8(±2.7)^{A}
Coble C	0.5(±0.3)^{AB}	0.8(±0.5)^{A}	0.8(±0.7)^{AB}	0.3(±0.2)^{B}
Abs_{254}	0.1(±0.1)^{AB}	0.2(±0.1)^{A}	0.3(±0.1)^{A}	0.1(±0.02)^{B}
$SUVA_{254}$	0.1(±0.1)^{A}	0.03(±0.01)^{B}	0.05(±0.02)^{A}	0.04(±0.01)^{AB}

Finally, dissolved C and CDOM properties were assessed in the tidal river and bay based on ebb flood stages (Table E.3). No significant differences between ebb and

flood stages in the tidal river and bay existed in the dataset, but several important observations can be made based on the mean values. DOC mean values were higher during ebb tide in both the tidal river and bay, as is the HIX. The S_r is larger during flood tide in both the tidal river and bay.

Table D.3 ANOVA results based on the means (±SD) between ebb/ flood at the tidal river and bay

Variable	**Tidal River**		**Bay**	
	Ebb	**Flood**	**Ebb**	**Flood**
DOC (mg/L)	6.0(±2.2)^{A}	4.2(±2.9)^{A}	2.7(±0.5)^{A}	2.1(0.3)^{A}
POC (mg/L)	No Data	No Data	No Data	No Data
DIC (mg/L)	No Data	No Data	No Data	No Data
TN (mg/L)	No Data	No Data	No Data	No Data
HIX	1.0(±0.1)^{A}	0.8(±0.4)^{A}	1.0(±0.1)^{A}	0.6(±0.5)^{A}
FI	1.4(±0.03)^{A}	1.4(±0.05)^{A}	1.4(±0.1)^{A}	1.5(0.02)^{A}
BIX	0.5(±0.1)^{A}	0.6(±0.1)^{A}	0.6(±0.1)^{A}	0.6(±0.1)^{A}
S_r	2.9(±0.4)^{A}	4.1(±1.7)^{A}	3.6(±0.9)^{A}	5.8(±3.3)^{A}
Coble C	0.7(±0.7)^{A}	0.8(±0.7)^{A}	0.5(±0.4)^{A}	0.6(±0.5)^{A}
Abs_{254}	0.3(±0.2)^{A}	0.2(±0.1)^{A}	0.1(±0.01)^{A}	0.1(±0.03)^{A}
$SUVA_{254}$	0.05(±0.01)^{A}	0.05(±0.03)^{A}	0.03(±0.01)^{A}	0.04(±0.02)^{A}

D.3.2 Relationships Between Creek Water Level and Chemistry

Linear correlations ($p<0.05$) exist between several chemical variables measured in the tidal creek and the tidal creek water level (Figure 3). DOC tended to increase when the water level in the creek decreased, as did the Coble C peak, Abs_{254}, $SUVA_{254}$, DIC, and TN. This indicates that higher concentrations of terrestrially plant-derived, aromatic and nitrogen-rich DOC entered the tidal creek during lower tides, as did higher concentrations of DIC. The BIX and S_r increased as the creek level increased. This indicates that the amount of marine microbially derived DOC increased in the tidal creek during higher tides. No significant relationships between water level and chemical variables existed in the tidal river.

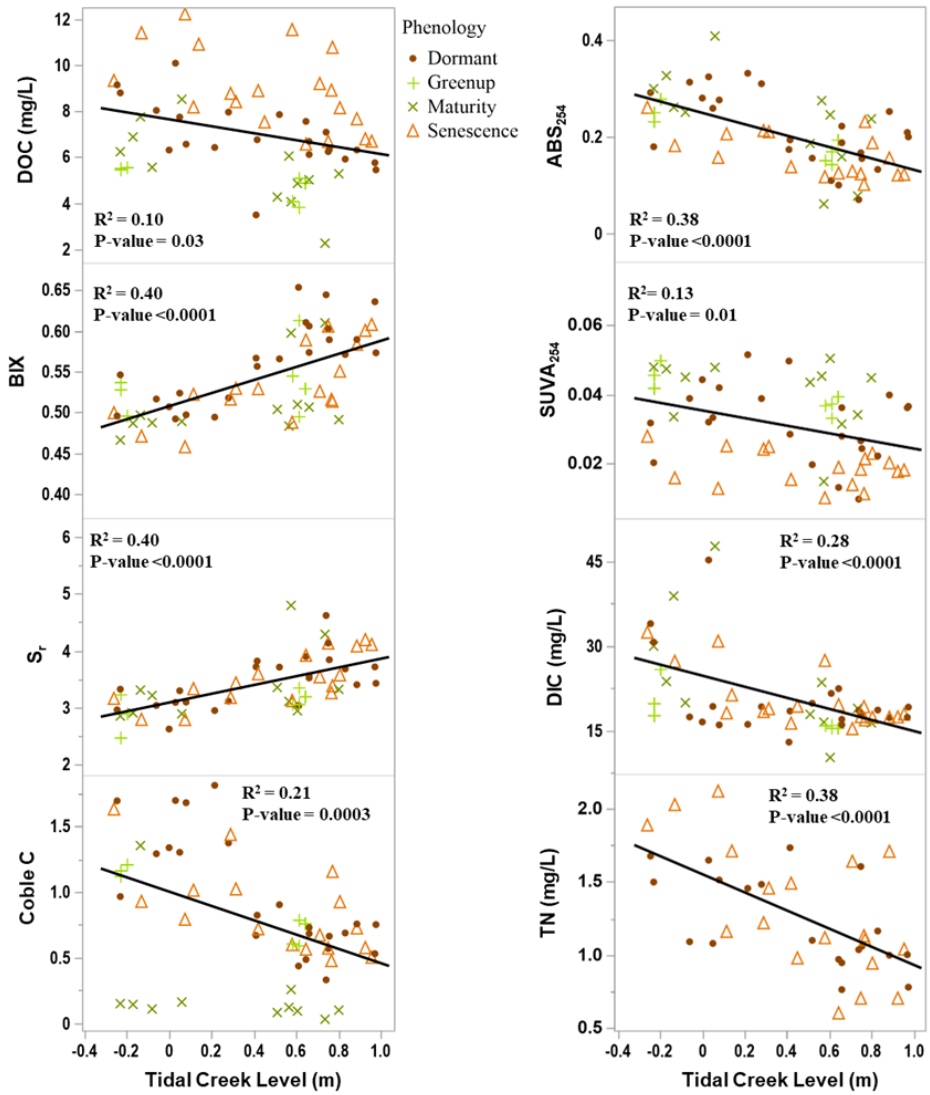

Figure D.3 Significant linear correlations between creek level and measured chemical variables in the tidal creek

D.4 Discussion and Conclusion

We hypothesized that there would be clear differences in tidal creek chemistry based on ebb-flood dynamics and connected to changes in source water from the tidal

river or DE bay. Our data support this hypothesis. We typically observed higher concentrations of terrestrial-like DOC and DIC in the tidal creek during ebb tide, likely linked to higher horizontal export of marsh-derived C during near channel groundwater flow towards the tidal creek. On the other hand, we found lower concentrations of DOC during flood tide that had a stronger marine-like signature, similar to the stronger marine-like signature observed in the DE bay. This indicates that the studied marsh exports higher quantities of C from the marsh during ebb tide, while flood tide brings in C from outside sources including the adjacent open-water bay. These findings have implications for better understanding lateral C flux in coastal ecosystems.

REFERENCES

Alongi DM (2020) Carbon Balance in Salt Marsh and Mangrove Ecosystems: A Global Synthesis. J Mar Sci Eng 8:767. https://doi.org/10.3390/jmse8100767

Arias-Ortiz A, Masqué P, Garcia-Orellana J, et al (2018) Reviews and syntheses:210Pb-derived sediment and carbon accumulation rates in vegetated coastal ecosystems –setting the record straight. Biogeosciences 15:6791–6818. https://doi.org/10.5194/bg-15-6791-2018

Barrón C, Duarte CM (2015) Dissolved organic carbon pools and export from the coastal ocean. 1725–1738. https://doi.org/10.1002/2014GB005056.Received

Bauer JE, Cai WJ, Raymond PA, et al (2013) The changing carbon cycle of the coastal ocean. Nature

Bogard MJ, Bergamaschi BA, Butman DE, et al (2020) Hydrologic Export Is a Major Component of Coastal Wetland Carbon Budgets. Global Biogeochem Cycles 34:1–14. https://doi.org/10.1029/2019GB006430

Burdige DJ (2007) Preservation of organic matter in marine sediments: Controls, mechanisms, and an imbalance in sediment organic carbon budgets? Chem Rev 107:467–485. https://doi.org/10.1021/cr050347q

Cao F, Tzortziou M (2021) Capturing dissolved organic carbon dynamics with Landsat-8 and Sentinel-2 in tidally influenced wetland–estuarine systems. Science of the Total Environment 777:. https://doi.org/10.1016/j.scitotenv.2021.145910

Capooci M, Barba J, Seyfferth AL, Vargas R (2019) Experimental influence of storm-surge salinity on soil greenhouse gas emissions from a tidal salt marsh. Science of the Total Environment 686:1164–1172. https://doi.org/10.1016/j.scitotenv.2019.06.032

Cavallaro N, Shrestha G, Birdsey R, et al (2018) Second State of the Carbon Cycle Report. Washington, DC

Chmura GL, Anisfeld SC, Cahoon DR, Lynch JC (2003) Global carbon sequestration in tidal, saline wetland soils. Global Biogeochem Cycles 17:1111. https://doi.org/10.1029/2002GB001917

Cole JJ, Prairie YT, Caraco NF, et al (2007) Plumbing the global carbon cycle: Integrating inland waters into the terrestrial carbon budget. Ecosystems 10:. https://doi.org/10.1007/s10021-006-9013-8

Crooks S, Sutton-Grier AE, Troxler TG, et al (2018) Coastal wetland management as a contribution to the US National Greenhouse Gas Inventory. Nat Clim Chang 8:1109–1112. https://doi.org/10.1038/s41558-018-0345-0

Czapla KM, Anderson IC, Currin CA (2020) Net Ecosystem Carbon Balance in a North Carolina, USA, Salt Marsh. J Geophys Res Biogeosci 125:1–16. https://doi.org/10.1029/2019JG005509

Duarte CM (2017) Reviews and syntheses: Hidden forests, the role of vegetated coastal habitats in the ocean carbon budget. Biogeosciences 14:301–310. https://doi.org/10.5194/bg-14-301-2017

Duarte CM, Losada IJ, Hendriks IE, et al (2013) The role of coastal plant communities for climate change mitigation and adaptation. Nat Clim Chang 3:961–968. https://doi.org/10.1038/nclimate1970

Herrmann M, Najjar RG, Kemp WM, et al (2015) Net ecosystem production and organic carbon balance of U.S. East Coast estuaries: A synthesis approach. Global Biogeochem Cycles 29:96–111. https://doi.org/10.1002/2013GB004736

Howard J, Sutton-Grier A, Herr D, et al (2017) Clarifying the role of coastal and marine systems in climate mitigation. Front Ecol Environ 15:42–50. https://doi.org/10.1002/fee.1451

Johnson ER, Inamdar S, Kan J, Vargas R (2018) Particulate Organic Matter Composition in Stream Runoff Following Large Storms: Role of POM Sources, Particle Size, and Event Characteristics. J Geophys Res Biogeosci 123:. https://doi.org/10.1002/2017JG004249

Macreadie PI, Anton A, Raven JA, et al (2019) The future of Blue Carbon science. Nat Commun 10:3998. https://doi.org/10.1038/s41467-019-11693-w

Macreadie PI, Costa MDP, Atwood TB, et al (2021) Blue carbon as a natural climate solution. Nat Rev Earth Environ 2:826–839. https://doi.org/10.1038/s43017-021-00224-1

Maher DT, Call M, Santos IR, Sanders CJ (2018) Beyond burial: lateral exchange is a significant atmospheric carbon sink in mangrove forests. Biol Lett 14:20180200. https://doi.org/10.1098/rsbl.2018.0200

Mcleod E, Chmura GL, Bouillon S, et al (2016) A blueprint for blue carbon: toward an improved understanding of the role of vegetated coastal habitats in sequestering CO2. Front Ecol Environ 9:552–560. https://doi.org/https://www.jstor.org/stable/41479959

Najjar RG, Herrmann M, Alexander R, et al (2018) Carbon Budget of Tidal Wetlands, Estuaries, and Shelf Waters of Eastern North America. Global Biogeochem Cycles 32:389–416. https://doi.org/10.1002/2017GB005790

Osburn CL, Mikan MP, Etheridge JR, et al (2015) Seasonal variation in the quality of dissolved and particulate organic matter exchanged between a salt marsh and its adjacent estuary. Journal of Geophysical Research G: Biogeosciences 120:1430–1449. https://doi.org/10.1002/2014JG002897

Rocha A v., Goulden ML (2009) Why is marsh productivity so high? New insights from eddy covariance and biomass measurements in a Typha marsh. Agric For Meteorol. https://doi.org/10.1016/j.agrformet.2008.07.010

Saintilan N, Rogers K, Mazumder D, Woodroffe C (2013) Allochthonous and autochthonous contributions to carbon accumulation and carbon store in southeastern Australian coastal wetlands. Estuar Coast Shelf Sci 128:84–92. https://doi.org/10.1016/j.ecss.2013.05.010

Santos IR, Burdige DJ, Jennerjahn TC, et al (2021) The renaissance of Odum's outwelling hypothesis in "Blue Carbon" science. Estuar Coast Shelf Sci 255:107361. https://doi.org/10.1016/j.ecss.2021.107361

Santos IR, Maher DT, Larkin R, et al (2019) Carbon outwelling and outgassing vs. burial in an estuarine tidal creek surrounded by mangrove and saltmarsh wetlands. Limnol Oceanogr 64:996–1013

Schulte EE, Hopkins BG (1996) Estimation of soil organic matter by weight loss-on-ignition. In: Soil Organic Matter: Analysis and Interpretation

Serrano O, Lovelock CE, B. Atwood T, et al (2019) Australian vegetated coastal ecosystems as global hotspots for climate change mitigation. Nat Commun 10:4313. https://doi.org/10.1038/s41467-019-12176-8

Taillardat P, Friess DA, Lupascu M (2018) Mangrove blue carbon strategies for climate change mitigation are most effective at the national scale. Biol Lett 14:. https://doi.org/10.1098/rsbl.2018.0251

Trifunovic B, Vázquez-Lule A, Capooci M, et al (2020) Carbon Dioxide and Methane Emissions From A Temperate Salt Marsh Tidal Creek. J Geophys Res Biogeosci 125:. https://doi.org/10.1029/2019JG005558

Tzortziou M, Neale PJ, Megonigal JP, et al (2011) Spatial gradients in dissolved carbon due to tidal marsh outwelling into a Chesapeake Bay estuary. Mar Ecol Prog Ser 426:41–56. https://doi.org/10.3354/meps09017

Tzortziou M, Neale PJ, Osburn CL, et al (2008) Tidal marshes as a source of optically and chemically distinctive colored dissolved organic matter in the Chesapeake Bay. Limnol Oceanogr 53:148–159. https://doi.org/10.4319/lo.2008.53.1.0148

Van de Broek M, Vandendriessche C, Poppelmonde D, et al (2018) Long-term organic carbon sequestration in tidal marsh sediments is dominated by old-aged allochthonous inputs in a macrotidal estuary. Glob Chang Biol 24:2498–2512. https://doi.org/10.1111/gcb.14089

Wang F, Sanders CJ, Santos IR, et al (2021) Global blue carbon accumulation in tidal wetlands increases with climate change. Natl Sci Rev 8:. https://doi.org/10.1093/nsr/nwaa296

Wang ZA, Kroeger KD, Ganju NK, et al (2016) Intertidal salt marshes as an important source of inorganic carbon to the coastal ocean. Limnol Oceanogr 61:1916–1931. https://doi.org/10.1002/lno.10347

Appendix E

Permission to Include Material Published in Biogeochemistry

Chapter 4 of this thesis was previously published with permission from Biogeochemistry (Springer Nature). Rights Link. "Authors have the right to reuse their article's Version of Record, in whole or in part, in their own thesis. Additionally, they may reproduce and make available their thesis, including Springer Nature content, as required by their awarding academic institution. Authors must properly cite the published article in their thesis according to current citation standards". The DOI for this work is: https://doi.org/10.1007/s10533-023-01024-z